Novel pathogenic mechanisms of porcine reproductive and respiratory syndrome virus: intercellular transmission and persistence

by

Rui Guo

B.S., Yangzhou University, 2010
M.S., Yangzhou University, 2013

AN ABSTRACT OF A DISSERTATION

submitted in partial fulfillment of the requirements for the degree

DOCTOR OF PHILOSOPHY

Department of Diagnostic Medicine & Pathobiology
College of Veterinary Medicine

KANSAS STATE UNIVERSITY
Manhattan, Kansas

2018

Abstract

Porcine reproductive and respiratory syndrome virus (PRRSV) causes a tremendous economic loss in swine industry worldwide. The capabilities to evade host immune responses and to establish persistent infection are the two hallmark features of PRRSV infection. In this dissertation, the research was mainly focused on investigating the novel mechanisms underlying PRRSV transmission and persistence.

In chapter 2, the research was focused on an alternative pathway of PRRSV intercellular transmission. Our data showed that intercellular nanotube connections can be utilized for cell-to-cell spreading the core infectious viral machinery (viral RNA, certain replicases and structural proteins) of PRRSV. Live-cell movies tracked the intercellular transport of a recombinant PRRSV that expressed green fluorescent protein (GFP)-tagged nsp2 in a receptor-independent manner. The cytoskeleton proteins F-actin and myosin-IIA were identified as co-precipitates with PRRSV nanotube associated proteins. Drugs inhibiting actin polymerization or myosin-IIA activation prevented nanotube formations and viral clusters in virus-infected cells. These data lead us to propose that PRRSV utilizes the host cell cytoskeletal machinery inside nanotubes for efficient cell-to-cell spread. This form of virus transport represents an alternative pathway for virus spread, which is resistant to the host humoral immune response.

In chapter 3, we further showed that PRRSV infection could induce the formation of nanotubes between infected and uninfected cells following a ROS-dependent nanotube formation model. Co-culturing PRRSV-infected cells with uninfected cells rescued PRRSV-induced cell death. Mitochondrion was observed transferring from uninfected to PRRSV-infected cells. Importantly, impaired formation of nanotube or defective mitochondrion was unable to rescue infected cells from apoptosis/necrosis. Certain PRRSV proteins were detected to associate with

mitochondria and transport from infected to uninfected cells through TNTs. Our results suggest that TNTs-transfer of functional mitochondria rescued PRRSV-infected cells from apoptosis/necrosis in the early stage of infection. On the other hand, mitochondria could be utilized as a cargo to transport viral materials for spreading the infection.

In chapter 4, a novel mechanism s of PRRSV persistent infection has been studied. In this study, a cellular model of persistent infection was established. Strand-specific quantitative RT-PCR and RNase I treatment analysis showed that double-stranded RNA (dsRNA) conformation existed in persistently infected cells. This data has been further confirmed *in vivo* by performing two independent PRRSV persistence studies. Immunohistochemistry analysis showed that viral dsRNAs were detected aggregating inside the germinal centers of tonsils and lymph nodes from PRRSV persistence pigs, but RNA array analysis further showed that dsRNA in lymphoid tissues had limited ability to stimulate host antiviral responses during persistent infection stage. These results suggest that the PRRSV dsRNA functions as a mediator for viral persistence. The viral dsRNA persistence in germinal centers of lymphoid tissues may reveal a novel mechanism for PRRSV to escape antiviral immune responses.

In summary, this study investigated two novel pathogenic mechanisms of PRRSV infection, which could provide insights on the development of effective control strategies.

Novel pathogenic mechanisms of porcine reproductive and respiratory syndrome virus: intercellular transmission and persistence

by

Rui Guo

B.S., Yangzhou University, 2010
M.S., Yangzhou University, 2013

A DISSERTATION

submitted in partial fulfillment of the requirements for the degree

DOCTOR OF PHILOSOPHY

Department of Diagnostic Medicine & Pathobiology
College of Veterinary Medicine

KANSAS STATE UNIVERSITY
Manhattan, Kansas

2018

Approved by:

Major Professor
Ying Fang

Abstract

Porcine reproductive and respiratory syndrome virus (PRRSV) causes a tremendous economic loss in swine industry worldwide. The capabilities to evade host immune responses and to establish persistent infection are the two hallmark features of PRRSV infection. In this dissertation, the research was mainly focused on investigating the novel mechanisms underlying PRRSV transmission and persistence.

In chapter 2, the research was focused on an alternative pathway of PRRSV intercellular transmission. Our data showed that intercellular nanotube connections can be utilized for cell-to-cell spreading the core infectious viral machinery (viral RNA, certain replicases and structural proteins) of PRRSV. Live-cell movies tracked the intercellular transport of a recombinant PRRSV that expressed green fluorescent protein (GFP)-tagged nsp2 in a receptor-independent manner. The cytoskeleton proteins F-actin and myosin-IIA were identified as co-precipitates with PRRSV nanotube associated proteins. Drugs inhibiting actin polymerization or myosin-IIA activation prevented nanotube formations and viral clusters in virus-infected cells. These data lead us to propose that PRRSV utilizes the host cell cytoskeletal machinery inside nanotubes for efficient cell-to-cell spread. This form of virus transport represents an alternative pathway for virus spread, which is resistant to the host humoral immune response.

In chapter 3, we further showed that PRRSV infection could induce the formation of nanotubes between infected and uninfected cells following a ROS-dependent nanotube formation model. Co-culturing PRRSV-infected cells with uninfected cells rescued PRRSV-induced cell death. Mitochondrion was observed transferring from uninfected to PRRSV-infected cells. Importantly, impaired formation of nanotube or defective mitochondrion was unable to rescue infected cells from apoptosis/necrosis. Certain PRRSV proteins were detected to associate with

mitochondria and transport from infected to uninfected cells through TNTs. Our results suggest that TNTs-transfer of functional mitochondria rescued PRRSV-infected cells from apoptosis/necrosis in the early stage of infection. On the other hand, mitochondria could be utilized as a cargo to transport viral materials for spreading the infection.

In chapter 4, a novel mechanism s of PRRSV persistent infection has been studied. In this study, a cellular model of persistent infection was established. Strand-specific quantitative RT-PCR and RNase I treatment analysis showed that double-stranded RNA (dsRNA) conformation existed in persistently infected cells. This data has been further confirmed in vivo by performing two independent PRRSV persistence studies. Immunohistochemistry analysis showed that viral dsRNAs were detected aggregating inside the germinal centers of tonsils and lymph nodes from PRRSV persistence pigs, but RNA array analysis further showed that dsRNA in lymphoid tissues had limited ability to stimulate host antiviral responses during persistent infection stage. These results suggest that the PRRSV dsRNA functions as a mediator for viral persistence. The viral dsRNA persistence in germinal centers of lymphoid tissues may reveal a novel mechanism for PRRSV to escape antiviral immune responses.

In summary, this study investigated two novel pathogenic mechanisms of PRRSV infection, which could provide insights on the development of effective control strategies.

Table of Contents

List of Figures ix
List of Tables xi
Acknowledgements xii
Chapter 1 - Literature Review 1
1.1 Overview of porcine respiratory and reproductive syndrome: 1
1.2 The causative agent- PRRSV: 2
1.3 PRRSV persistent infection 9
1.4 Tunneling nanotubes (TNTs) as an alternative pathway for virus spread 14
1.5 Purpose of this research 18
1.6 References 19
Chapter 2 - Porcine reproductive and respiratory syndrome virus utilizes nanotubes for intercellular spread 37
2.1 Introduction 38
2.2 Materials and Methods 39
2.3 Results 45
2.4 Discussion 52
2.5 References 57
Chapter 3 - Intercellular transfer of mitochondria rescues virus-induced cell death but facilitates cell-to-cell spreading of porcine reproductive and respiratory syndrome virus 78
3.1 Introduction 79
3.2 Materials and Methods 82
3.3 Results 88
3.4 Discussion 95
3.5 References 99
Chapter 4 - Double-stranded viral RNA persists *in vitro* and *in vivo* during prolonged infection of porcine reproductive and respiratory syndrome virus 119
4.1 Introduction 120
4.2 Materials and Methods 122
4.3 Results 128

4.4 Discussion 134
4.5 References 138
Chapter 5 - Conclusion 161
Publisher's Permission for Reproducing Published Materials 165

List of Figures

Figures in Chapter 1

Figure 1.1 Life cycle of PRRSV replication.. 34
Figure 1.2 Stages of PRRSV infection.. 35
Figure 1.3 Formation of tunneling nanotubes connecting among cells. 36

Figures in Chapter 2

Figure 2.1 Detection of intercellular nanotubes containing PRRSV GP5 and N protein. 64
Figure 2.2 Intercellular nanotubes contain viral proteins in PRRSV-infected cells.. 66
Figure 2.3 Detection of PRRSV RNA in the intercellular nanotube connections. 67
Figure 2.4 Intercellular spreading of PRRSV infection in cells with the presence of virus-neutralizing antibody. 69
Figure 2.5 Live cell images demonstrating intercellular transport of PRRSV GFP-tagged nsp2 through nanotubes.. 71
Figure 2.6 Intercellular transport of the GFP-nsp2 protein in co-cultured MARC-145 and HEK-293T cells.. 72
Figure 2.7 Co-precipitation of PRRSV proteins with cytoskeleton F-actin and myosin IIA.. 75
Figure 2.8 Inhibitors of F-actin and myosin IIA affect the intercellular spread of PRRSV.. 77

Figures in Chapter 3

Figure 3.1 PRRSV-infected cells release ‘call-for-help’ signals (ROS, S100A4) and increased formation of nanotubes. 107
Figure 3.2 Confocal cell image demonstrating intercellular mitochondria transportation from uninfected to infected cells through tunneling nanotubes..... 109
Figure 3.3 Microtubulins were associated with nanotubes containing mitochondria..... 110
Figure 3.4 Kinetics of cell death in GFP-PRRSV-positive cells. 111
Figure 3.5 Mitochondria transfer through nanotubes rescued necrosis/apoptosis in PRRSV infected cells.. 112
Figure 3.6 Ethidium bromide and uridine treated cells carrying defective mitochondria were unable to rescue PRRSV-infected cells from necrosis. 114

Figure 3.7 Co-culture of PUC stem cells rescued GFP-PRRSV infected PAMs from apoptosis 116
Figure 3.8 Localization of PRRSV proteins and mitochondria in the TNTs. MARC-145 cells were initially infected with PRRSV. 118

Figures in Chapter 4

Figure 4.1 Establishment and characterization of the *in vitro* cell model system for PRRSV persistence.. 150
Figure 4.2 PRRSV persistent cells with increased population containing only viral dsRNA. ... 152
Figure 4.3 Detection of viral dsRNA in serum and lymphoid tissues from PRRSV-infected pigs. 155
Figure 4.4 Analysis of viral load in serum and TBLN samples from PRRSV-infected pigs at 70 dpi.. 156
Figure 4.5 RNA array analysis of swine immune gene expression in TBLN samples from PRRSV-infected pigs at 10 dpi versus 52 dpi.. 158
Figure 4.6 Comparison of immune gene expression profiles in TBLN samples from different treatment groups of pigs. 160

Figures in Chapter 5

Figure 5.1 A proposed model for PRRSV intercellular spread.. 164

List of Tables

Table 2.1 List of antibodies used in this study. 62

Table 4.1 192 genes in swine immune gene RNA array 144

Table 4.2 DEGs consistently identified in two independent pig studies 147

Acknowledgements

I express my sincere gratitude to my major advisor, Dr. Ying Fang for her mentoring during my Ph. D study. Her patience, motivation, enthusiasm, and immense knowledge guided me in all the time of research. I am grateful that she gave me tremendous freedom and trust in conducting my research projects, provided me opportunities to attend various professional conferences, and always encouraged me to think independently and to work smart.

I would like to thank my committee members, Dr. John Tomich, Dr. Gary Anderson, Dr. Jianfa Bai, and Dr. William Wilson, for their precious suggestions on my research and tremendous support of my career.

I would like to thank our collaborators, Dr. Thomas Gallagher, Dr. Crystal J. Jaing, Dr. Celena A. Carrillo, Dr. Raymond R. R. Rowland, Dr. Megan Niederwerder, Dr. Duane Davis, Dr. Gourapura J. Renukaradhya, and Dr. Jodi McGill. This work would not have been possible without the advice and support from you!

I would like to thank Dr. M.M. Chengappa, Dr. T.G. Nagaraja, and other faculty member and staff in the College of Veterinary Medicine, who helped me in fulfilling the requirements of my Ph.D degree. Special thanks to Joel Sanneman for the best confocal microscopy training I ever had.

I express my thanks to all of the lab members in Dr. Ying Fang's laboratory, including Pengcheng Shang, Dr. Yanhua Li, Sailesh Menon, Russel Ransburgh, Xingyu Yan, Dr. Yongning Zhang, Fangfeng Yuan, Longchao Zhu, Tori Matta and William Patterson. I'd like also thank to all my friends who have given me tremendous help in my life.

I deeply thank my parents, Jianming Guo and Jufang Qin and parents-in-law, Laizhong Wang and Peizhen Wang for their trust, encouragement, and patience. I also dedicate this Ph.D. thesis to my lovely daughter, Gwen who is the pride and joy of my life.

This last word of acknowledgment I have saved for my soul mate and dearest wife Yin Wang, who has been with me all these years and has made them the best years of my life.

Chapter 1 - Literature Review

1.1 Overview of porcine respiratory and reproductive syndrome:

Porcine respiratory and reproductive syndrome (PRRS) was first documented in North America in 1987 (1). At the beginning, PRRS was named as "mystery swine disease" due to the absence of a recognized cause (2, 3). In early 1991, a disease with similar clinical symptoms was observed in the Netherlands (4). The causative agent, designated “Lelystad virus”, was isolated and subsequent research demonstrated the fulfillment of Koch’s postulates (4). Shortly after the isolation of Lelystad virus (LV), a virus showing resembling clinical signs was isolated in USA and designated American Type Culture Collection VR-2332 (ATCC VR-2332) (5, 6). In 2006, highly pathogenic (HP) PRRS virus (PRRSV) strains were isolated in China and Southeast Asia (7, 8), which resulted in severe losses, affecting millions of pigs with high (~20%) mortality, and currently, it is still causing severe problems in the swine industry in China. Most recently, another highly pathogenic East European subtype 3 PRRSV, Lena, was isolated in Eastern Europe (9). During last two decades, this disease has become one of the most economically significant swine diseases worldwide. It has been estimated to cost the US swine industry at least $600 million annually (10).

Clinical signs vary and depend on a number of factors including virus virulence, ages of exposed pigs, infection phase, herd size and management practice. Generally, for breeding age gilts, sows, and boars, clinical signs include a period of anorexia, fever, lethargy, depression, and occasionally respiratory distress or vomiting. Reproductive deficiency is the most common sign including an increase in premature farrowing, abortions, stillborn, and mummified fetuses. For young pigs, primary clinical signs include high fever, depression, lethargy, stunting due to systemic disease, and pneumonia. Sneezing, fever and lethargy are followed by expiratory

dyspnea and stunting (11). Infection with HP-PRRSV strains is associated with more severe clinical signs, pulmonary lesions and aberrant host immune responses (12, 13).

The phase of the disease can be divided into three distinct stages: acute infection, persistent infection, and extinction. During the acute infection phase, the causative agent PRRSV mainly propagates in macrophages and dendritic cells in lungs and the upper respiratory tract, resulting in viremia by 6–12 h post-infection. One of the typical characteristics of acute infection is long-lasting serum viremia, which may last for several weeks after the initial infection. The disease then progresses into the asymtomatic persistent infection stage, during which virus is no longer detected in blood and lungs and pigs no longer exhibit obvious clinical signs. At this stage, viral replication is primarily localized in lymphoid organs, including tonsil and lymph nodes (14-16). Evidence showed that virus replication in lymph nodes resulted in the efficient transmission of virus to naïve pigs via oral-nasal secretions and semen (17). After persistent infection phase, virus replication gradually declines until the virus disappears in the host, which represents the final stage of infection. However, given the typical swine production setting that pigs are normally kept for 250 days, PRRS is a "life-long" disease for most of the infected pigs.

1.2 The causative agent- PRRSV:

PRRSV belongs to the family *Arteriviridae*, order Nidovirales (18-20). PRRSV has two species, currently named as PRRSV-1 and PRRSV-2. Other members of the family *Arteriviridae* include lactate dehydrogenase-elevating virus (LDV), equine arteritis virus (EAV), and simian hemorrhagic fever virus (SHFV) (18-20).

PRRSV is an enveloped positive-stranded RNA virus with diameter about 50-60 nm. The single stranded viral genome is encapsulated by nucleocapsid proteins, and surface glycoproteins

and membrane proteins are inserted into the lipid-bilayered envelope, which surround the nucleocapsid to form virion particles. The PRRSV genomic RNA molecule is about 15 kb in length and contains eleven known open reading frames. The replicase gene consists of the large ORFs 1a and 1b, which are situated in the 5'-proximal three quarters of the polycistronic genome. They encode two long nonstructural polyproteins, pp1a and pp1ab, with expression of the latter depending on a -1 ribosomal frame shift signal in the ORF1a/ORF1b overlap region. Following their synthesis from the genomic mRNA template, the pp1a and pp1ab replicase polyproteins are processed into at least 14 nonstructural proteins (nsps), including nsp1α/β, nsp2-nsp12 (18). Our lab recently identified a novel ORF (TF) (21, 22), which is translated via an efficient -2 ribosomal frameshift mechanism, resulted in the expression of a transframe protein, nsp2TF. At the same frameshifting site, -1 ribosomal frame shift also occurs, yielding a truncated nsp2 protein (nsp2N). The 3' end of the genome encodes four membrane-associated glycoproteins (GP2a, GP3, GP4 and GP5), three unglycosylated membrane proteins (E, ORF5a and M) and a nucleocapsid protein (N) (19).

1.2.1 Restricted host tropism and receptors of PRRSV

PRRSV has a very restricted tropism for host cells. Among many different cell lines tested, only the African green monkey kidney cell line MA-104 and derivatives such as MARC-145 are fully permissive to PRRSV infection in vitro (23). In infected pigs, PRRSV mainly infects subsets of swine macrophages that are present in lungs and lymphoid organs. Virus–receptor interaction plays a profound role in determining the host and cell tropism and therefore constitutes an interspecies barrier (24), which contributes to the restricted host range of PRRSV. Entry of PRRSV into macrophages has been shown to occur via pH-dependent, receptor

mediated endocytosis (25). PRRSV receptors have been studied intensely during the last two decades. At least 6 putative cell surface molecules have been shown to be associated with PRRSV attachment and entry, including heparan sulphate, vimentin, CD151, CD163 (scavenger receptor for hemoglobin-haptoglobin complex), CD169 (Siglec-1; also known as sialoadhesin), and DC-SIGN (dendritic cell-specific intercellular adhesion molecule-3-grabbing non-integrin; also known as CD209)(26). Recently a cytoskeleton protein, non-muscle myosin heavy chain 9 (MYH-9), has been identified to be associated with PRRSV attachment and cell to cell spread through intercellular nanotubes (27, 28). Among these molecules, CD163 and CD169 have been studied most extensively as putative receptors for PRRSV. An intact N-terminal domain of CD169 was considered as a primary determinant of the permissiveness of cultured porcine alveolar macrophages for infection by PRRSV (29). However, CD169 gene knocked out pigs didn't show increased resistance to PRRSV infection, suggesting that CD169 is not essential for PRRSV infection in pigs (30). By screening a cDNA expression library of PAM cells, CD163 was identified as another important molecule for PRRSV infection and further biochemical analysis showed that the loop 5–6 region of scavenger receptor cysteine-rich domain 5 (SRCR5) of CD163 is responsible for primary viral ligand binding (31). Recently, CD163 knock out and CD163/SRCR5 knock out pigs has been generated by CRISPR/Cas9 editing technology. In comparison to CD169-KO pigs, CD163-KO or CD163/SRCR5-KO pigs have been shown to be fully resistant to PRRSV infection (32, 33), which confirmed that SRCR5 domain of CD163 is the key factor that mediates PRRSV entry. Due to the importance of SRCR5 in PRRSV infection, the crystal structure of porcine CD163 SRCR5 has been solved recently (34). Comparing to the known crystal structures of other SRCR superfamily members such as human CD5 SRCR3, porcine CD163 SRCR5 has a shorter N-terminal region and displayed inverted

loop flexibility (34). This identical structure may contribute to the receptor specificity of pCD163 for PRRSV infection. Furthermore, cells transfected with CD163 cDNA possessing a swap between SRCR 5 and the human CD163LI (hCD163LI) homolog are not permissive to PRRSV-1 infection (35). Interestingly, a recent study shows replacement of SRCR domain 5 with a synthesized hCD163L1 SRCR domain homolog in pigs by gene editing conferred resistance of pigs to PRRSV-1 but not to PRRSV-2, suggesting the distinct difference in CD163 recognition between PRRSV-1 and PRRSV-2 (36). This evidence suggests that CD163 is the likely receptor for PRRSV to infect pigs, and the virus-pCD163 interaction could play an important role in determining PRRSV host and cellular tropism.

A transgenic study showed that CD163 from different species (human, monkey, dog, and mouse) can confer the susceptibility of PRRSV-2 in non-permissive cell lines, like porcine kidney cells, feline kidney cells, and baby hamster kidney cells (31). On the other hand, the restricted host tropism of PRRSV might not only depend on virus-pCD163 interaction but also on other downstream cellular factors, such as induced antiviral signaling pathways. Canine DH82 cells support PRRSV internalization and viral gene expression, but progeny virus cannot be generated from this cell line, indicating an inhibition in late stages of viral replication (31). Thus, receptor-independent mechanisms may also contribute to PRRSV restricted host tropism. A recent study for myxoma virus indicated that the myxoma virus protein M156 specifically inhibited the antiviral protein kinase R (PKR) from rabbits but not PKR from other mammals resulted in its restricted-tropism to rabbits (37). In that line of thought, PRRSV may have similar mechanisms.

1.2.2 Life cycle of PRRSV

PRRSV shares the similar life cycle as other nidoviruses (**Fig. 1.1**). Binding to the receptor triggers clathrin-mediated endocytosis, after which viral membrane fuses with the endosomal membrane to release the viral genomic RNA into the cytoplasm. Subsequently, viral genomic RNA is translated into the replicase pp1a and pp1ab. These polyproteins are then cleaved by internal viral proteinases and membrane-associated non-structural proteins interact together to assemble a replication and transcription complex (RTC). The RTC then engages to synthesize the full-length minus-strand RNA and subgenomic (sg)-length minus-strand RNAs. Subsequently, the full-length minus-strand RNA serves as the template for genome replication to synthesize the full-length plus-strand RNA, while the sg minus-strand mRNAs serve as templates for the synthesis of plus-strand sg mRNAs. This nested set of sg mRNAs is required to express the structural proteins. The newly synthesized genomes are then assembled together with structural proteins at the endoplasmic reticulum (ER) and released into the extracellular environment via exocytosis to infect other naïve cells (18, 19).

1.2.3 PRRSV-host immune system interactions

In general, PRRSV infection elicits poor host immune responses. The overall quantity of innate immune cytokines in PRRSV-infected pigs is significantly lower than that in pigs infected with other viruses (44). High concentrations of activated interferon-α (IFNα), tumor necrosis factor-α (TNFα), and interleukin-1 (IL-1) were secreted in lungs of the swine influenza virus infected pigs, resulting in clinical symptoms and effective eradication of the virus during the acute infection phase. In contrast, low level of IFNα was detected during the whole course of PRRSV infection, which has been noted in various strains infected pigs (45, 46). Previous in vitro studies further demonstrated that PRRSV infection was fully armed to significantly dampen

and delay the type I interferon responses (47, 48). A dual-luciferase gene reporter assay showed that numerous viral proteins, especially the non-structural proteins, acted as antagonists of host type I interferon responses; nsp1α/β, nsp2, nsp4 and nsp11 were shown to act as antagonists of IFN-β promoter activation (38-42, 49). However, since most of these observations are based on the eukaryotic cell over-expression system, further *in vivo* studies are needed to confirm whether PRRSV can also exploit the same mechanisms to antagonize host anti-viral responses.

Due to the weak innate immune response, activation of adaptive immunity is therefore inhibited, which in turn results in a delayed and insufficient production of neutralizing antibodies. In contrast to the weak neutralizing antibody responses, PRRSV infection results in the early and lasting production of virus-specific antibodies; nsp1α, nsp1β, nsp2 and nsp7 induced production of specific antibodies that were able to be detected as early as 14 days post-infection (dpi) and lasting to at least 202 dpi (50, 51). Antibody responses against all glycoproteins, M and N proteins were also described (50, 52, 53). Various neutralizing epitopes were mapped to the ectodomains of GP5 and GP4 (19, 54). However, synthetic peptides designed based on mapped neutralizing epitopes from PRRSV GP5 did not induce neutralizing antibodies, suggesting that additional residues or structural features are critical for neutralizing antigenicity. Currently, the exact neutralizing epitopes remain unclear.

Adaptive cell mediated responses have been observed as early as 2 weeks post infection (46, 52). Pigs infected with PRRSV developed a delayed hypersensitivity against the virus (55) indicating a dampened response with CD4 T helper cells. IFNγ producting T cells also showed a delayed response (56-58). Till now, limited evidence showed that effective CD8+ cytotoxic T cells (CTLs) were involved in controlling PRRSV acute infection; and weak PRRSV specific

CTL response was only observed after clearance of viremia (59). No apparent correlation of lymphoid tissue viral levels and PRRSV-specific CD8+ T-cell frequencies was found.

To efficiently antagonize the host anti-viral response, PRRSV also evolves strategies to utilize host immunosuppressive modulatory system. PRRSV N protein has been shown to be able to upregulate Foxp3+ T-regulatory cells (Tregs) and induce the IL-10 secretion (60). Enhanced expression of TGF-β protein in lymphoid organs and lung was also reported after PRRSV infection (61, 62). Indeed, increasing evidence shows that the coordinated immunosuppressive function of PRRSV is likely mediated by IL-10, TGF-β, and Tregs (60, 62-65).

1.2.4 PRRSV-induced cell death

Apoptosis is a highly regulated mechanism of cell death with highly characteristic morphological changes, including cell shrinkage, plasma membrane blebbing, chromatin condensation and DNA fragmentation (66). Apoptosis can be induced by the virus-infected cell as a response to viral replication, which has been shown to act as an important innate defense mechanism that interrupts replication of intercellular pathogens (67). In PRRSV, it was reported that the virus has ability to stimulate anti-apoptotic pathways in macrophages and MARC-145 cells during the early stage of infection, and PRRSV infection caused cell death by apoptosis later in the infection (68). Although there are still debates relating to whether PRRSV induces apoptosis by itself or by other host factors (bystander cells). But it is at least clear that within both infected tissue cultured cells and animals, apoptotic cells are observed and contribute to the pathology in hosts (69). Besides apoptosis, necrosis and necrosis-like apoptosis were also observed in infected cells (69-74). Different from apoptosis, necrosis is a passive cell death due to depletion of cellular resources. Cells undergoing necrosis are characterized by increased ion permeability of the plasma membrane, cellular swelling and osmotic lysis, which lead to

extensive tissue damage and an intense inflammatory response (66). Necrosis or necrosis-like apoptosis was observed at the late event during PRRSV replication (71). Treatment of macrophages with a pan-caspase inhibitor further showed that the observed necrosis was secondary to apoptosis at 12 and 24 hpi. The release of intracellular contents from these necrotic infected cells may activate inflammatory responses and production of cytokines, which then induce apoptosis in bystander cells (71).

1.3 PRRSV persistent infection

1.3.1 Definition of PRRSV persistence

For most of RNA viruses, the virus replicates rapidly and is shed into the environment and spreads to new susceptible individuals during the acute phase of infection. In a typical response to an acute viral infection it is expected that a virus will be effectively cleared by innate and adaptive immune responses within a few weeks of infection (75). Therefore, any infection that persists longer than this may be considered as persistence, even if it does not cause the life-long infection with continuous production of infectious viral progeny like HIV or HSV. The capacity to establish and maintain an asymptomatic persistent infection is one of the hallmarks of PRRSV infection. After the initial infection, virus can persist in infected pigs for several months (76). But, PRRSV persistence is not a steady-state persistent infection; the virus production decays with time and will eventually extinct in most of the infected pigs. With the current swine production setting, pigs are maintained for 250 days. In the view of this, PRRSV persistent infection can be regarded as “life-long” infection. In general, PRRSV persistence refers to the period between viremia disappearance and extinction within the host (**Fig. 1. 2**) (76).

1.3.2 Clinical and experimental reports of PRRSV persistence

During PRRS persistent stage, the virus becomes undetectable in blood and replicates continuously with a low level in lymphoid organs, including tonsil and lymph nodes for several months (76). Previous experimental studies indicate that virus can be detected in tonsils for up to 150 days and in semen for 90 days after initial infection by RT-PCR (15). Continuous virus replication in regional lymph nodes accounts for the efficient transmission of virus to naive pigs via oral-nasal secretions and semen (17). Other transmission experiments also showed infection transmission from a sow infected 99 days earlier to other susceptible individuals in the same pen (77). Virus isolation and RT-PCR are commonly used for detecting persistently infected pigs. Allende et al. in a bioassay with materials of PRRSV-2 infected pigs showed that tonsils of 40% of pigs contained sufficient infectious virus to be transmitted at 150dpi (15). Non-viremic pigs have been shown to be able to transmit the virus to naive sentinels up to 62dpi. Likewise, non-viremic sows were able to transmit infection by contact with naive sows between 49 and 86dpi (78). When infecting 2-week-old piglets with PRRSV-2, Wills et al. detected viral RNA in serum and to nsils in about 3.5% of pigs at 251dpi (79). With regards to the ability of persistently infected pigs to transmit the virus to susceptible animals, it is worth noting that certain circumstances resulting in stress such as farrowing, regrouping etc., might induce a reactivation of viral replication and shedding. Albina et al. demonstrated reactivation of PRRSV shedding after corticosteroid treatment at 15 weeks after the initial seroconversion of the animal (45). In summary, the circulating infectious PRRSV within herds could transmit from persistently infected pigs to naive susceptible individuals, which make it more complicated to prevent and control PRRSV in the swine industry.

PRRSV infection causes more severe outcomes in newborn pigs, which is partially because of the immature immune system of piglets. In comparison to the ineffective immune

responses in infected young pigs, finishing pigs with PRRSV persistence in the lymphoid tissues were detected exhibiting higher titers of circulating homologous PRRSV neutralizing antibody (46). A recent study determined the NA titers in sows from commercial herds documented with a history of PRRSV outbreaks occurring every year from 2006 to 2012 (80). Results showed that the mean reciprocal 50% neutralization titer reached 512, and the highest individual titer was 2187 (80). Reasons why those sows produced such high titers of neutralizing antibodies to PRRSV are unknown, but could be associated with multiple exposures to the persistent circulating viruses in the herds. The maintenance of the infection within a farm is basically due to the combination of animals with long-term infection (such as persistently infected sows) and the continual availability of susceptible pigs. The latter can be added to the population by replacement, by birth of piglets from seronegative sows, or by loss of maternal immunity in young pigs. As a result, PRRSV can circulate in the farm for several years (81).

1.3.3 Potential mechanisms for PRRSV persistence

Theoretically, to establish persistent infections within host cells, viruses have to meet at least two conditions: (1) avoiding elimination by the host immune response; (2) being able to maintain their genomes within at least some infected cells (75). The compromised immune response is one of the proposed causes for PRRSV persistence, which provides an ideal environment for viral persistence. The delayed and dampened protective immune response results in ineffective in elimination of the virus from the circulatory system and lymphoid tissues. During the persistent infection stage, PRRSV RNA was detected in lymphoid tissues together with minimal or no expression of structural viral antigens (82). Several hypotheses for explaining PRRSV RNA persistence have been proposed based on previous findings with other viruses. Similar to LDV, PRRSV may maintain its genome in a subpopulation of renewable

macrophages with lower replication efficiency to avoid host surveillance (83). Viral genomic RNAs may also persist in immunoprivileged sites, such as the male reproductive tract (17, 82), which is observed during infection with other arteriviruses, such as EAV and LDV (84), or nervous system, which serves as targets for herpes simplex virus (HSV) latency (85, 86). Similarly, PRRSV antigens have been detected in central nervous system in numerous studies; immunohistochemistry (IHC) results showed that PRRSV antigens were present in the mononuclear cells in perivascular regions and in microglia-like cells of the brain (87). Recently, B cell follicle or germinal centers (GC) in lymphoid tissue has been proposed as an additional immune privileged site for viral persistence (88, 89). Studies showed that HIV RNA persisted in the GC, while HIV-specific CD8+ T cells are most predominant in T cell zones outside of B cell follicles in lymph node and spleen tissues (88-91). Likewise, in LDV persistently infected mice, large amounts of viral RNA were detected aggregating in the GCs (83). Evolutionarily, it is reasonable for GCs to be immune privileged sites in order to prevent unwanted CD8+ cell cytolytic activity within follicles, which might lead to decreased ability of B cells to make antibodies (92).

Viral double-stranded RNAs (dsRNAs) have been shown to act as a potential genomic reservoir and be associated with persistent infection of several positive stranded RNA viruses (93-95). For instance, the poliovirus dsRNA persists in the mouse L cells and is capable of launching an infection from those cells (96). Hepatitis C virus dsRNA is maintained as the predominant form in the HCV-infected liver (95). Coxsackievirus dsRNA persists in myofibers and other non-dividing cells which survive from the initial cytolytic infection for extended times without producing detectable levels of infectious virus (93). The stability of dsRNA within cells could promote long term persistence; intracellular viral dsRNA has been shown experimentally

to be more stable than single-stranded RNA, which decays within hours (97). For arteriviruses, dsRNAs have been proposed to function as an intermediate product of replication (98). Therefore, PRRSV RNA may persist within lymphoid tissues in a more stable duplex form.

Apart from compromised immune response and viral RNA persistence, another hypothesis is associated with antigenic drift in the ectodomain of GP5, which could account for the selection of clones that are resistant to neutralizing antibody or change the tropism of the virus for a different population of cells (99, 100).

1.3.4 *In vitro* cells models of viral persistence

In vitro cell culture model systems provide insight to elucidate mechanisms of viral persistence *in vivo*. They are useful tools for investigating virus and cell co-evolution (84, 101, 102), for determining virulence factors (103, 104), and for studying virus-host interaction. Since the capacity to establish persistence is the common feature of members in order Nidovirales, numerous *in vitro* persistent infection models have been established, including severe acute respiratory syndrome-associated coronavirus (105, 106), human coronaviruses OC43 and 229E (107, 108), murine hepatitis virus(101, 109), bovine coronavirus(110, 111), lactate dehydrogenase-elevating virus (112) and equine arterivirus (113). EAV can establish persistent infection in stallions, which serve as principal reservoir of EAV and account for the dissemination of EAV in equine populations. The mechanisms of EAV persistence remain unclear. Using a EAV persistently infected cell culture system, Zhang and colleagues identified the mutations in structural proteins are important for the establishment of persistent infection. Interestingly, they found that a single mutation in GP (Pro98→ Leu) was able to establish persistent infection in Hela cells (113). Using persistently-infected DBT cells, Chen et al. showed that polymorphism and mutations resulting in intra-leader ORFs were not required for

MHV persistence. In contrast, MHV persistence was significantly associated with an A to G mutation at nt 77 in the 5' end untranslated region (UTR) of the genomic RNA (109). From the aspect of viral-host co-evolution, the same group further demonstrated that MHV persistence in vitro is mediated by the epigenetic selection for resistant host cells which express low level of viral receptor. Besides, MHV persistence also requires the subsequent co-evolution of viral quasispecies which display altered binding capacity for receptors and recognize an entirely new receptor protein(s) for entry into these resistant cells (109).

1.4 Tunneling nanotubes (TNTs) as an alternative pathway for virus spread

1.4.1 TNT formation and its structural components

TNTs were first described in 2004 as a new type of cell-to-cell connection. This specific structure appears to be a thin membranous bridge connecting two cells over long distances and serves as a pathway for cellular components transferring. TNTs are range from 50 to 200 nm in diameter and up to several cell diameters long contained cytoskeleton components including F-actin and/or microtubule (**Fig. 1. 3**). After the initial discovery of TNTs in 2004, it has gained increased attention. The mechanisms of TNTs formation have been intensely studied. Live cell imaging showed that TNTs are transient structures, lasting for minutes to several hours, and formed by two potential mechanisms. For the first mechanism, cells protrude a filopodia, which makes contact to the neighboring cells, and subsequently converts into a TNT bridge (114, 115). For the second mechanism, cells form TNTs by retaining a thin thread of membrane upon dislodgement (115-117). However, the significance and the differences between these two types of formation and whether they result in various structures remain unclear. Recently, Amin Rustom proposed a mechanistic model of reactive oxygen species-dependent tunneling nanotube

formation (118). Based on this model, TNTs provide a potent intercellular communication and rescue mechanism to exchange information and to maintain redox and metabolic homeostasis among injured and healthy cells (118). Local stress leads to increasing reactive oxidative species (ROS) levels. Stressed cells then distribute 'call-for-help' signals (eg. S100A4 etc.) in their surroundings to determine the position of unstressed cells. Directing by concentration gradient of 'call-for-help' signal between cells, TNT forms through actin-based, filopodia-like cell protrusions in order to restore redox/metabolic homeostasis by intercellular material exchange. Further increasing ROS levels lead to microtubule containing TNT formation, through which mitochondria can be transported to rescue stressed cells. However, not all stressed cells can be rescued; cells with exaggerated ROS levels will be finally removed by apoptosis and isolated from the healthy cells (118).

A number of studies showed that TNT-like structures were present in cultures of different cell types including fibroblasts, epithelial cells, immune cells, and neurons (114, 116, 119-125). In macrophages, two types of nanotubes were described (120). The thin nanotubes were found to contain actin filament only (also named as AT-TNT), whereas thicker nanotubes, with diameters larger than 0.7 μm, contained both F-actin and microtubules (also name as MT-TNT). These two different types of TNTs appeared to have distinct functions; in comparison to AT-TNTs, which appear to mediate unidirectional transfer (114, 121, 122), MT-TNTs are able to bi-directionally transport vesicles and various organelles in a microtubule dependent mechanism. Apart from immune cells, Wang and colleagues have shown that stress induced by hydrogen peroxide (H_2O_2) treatment led to an increase in TNT formation in both astrocytes and neurons. They also observed the transfer of various organelles, such as ER, Golgi, endosomes, and mitochondria via

TNTs in astrocyte cultures. Further study showed that mitochondria transferring via MT-TNTs were able to rescue ultraviolet-induced apoptotic cells (133).

1.4.2 TNT-Mediated Transfer, from Signal to Organelles

As an important component of intercellular communication network, TNTs have showed potent capability to transport signals and organelles from cell to cell (Figure 3). Several studies have demonstrated that calcium signals could spread between remote cells through TNTs. Death signals, such as FasL and caspase3, have been transported by nanotubes in Jurkat and primary T cells to peripherally delete activated T lymphocytes (129, 130). FasL and active caspase-3 passage from Fas-activated cells in neighboring non-activated ones was detected, thus resulting in the spreading of apoptosis, which might be an efficient way to shut down cellular responses (130). Besides, TNTs have been shown to be highways for diverse organelle transfer, including endosomes (114, 120, 122, 131), lysosomes (114, 120, 125), mitochondria (121, 131-134), ER/Golgi, and numerous membrane components (114, 126, 130).

1.4.3 Viruses hijack TNT for surviving under immune surveillance and transmission

For many enveloped viruses, entry into a host cell is primarily through the binding of cellular receptors and subsequent endocytosis of the viral particle into the cells. The fusion of envelope with the endosomal membrane releases viral capsid into the cytosol of the infected cell (135). However, for some enveloped viruses, alternative pathways for cell-to-cell transmission have been described. One emerging model proposes that some viruses can use long, filamentous intercellular connections (nanotubes) as a means to transport infectious viral materials to neighboring naive cells. In a previous study, a detailed characterization of HIV-1 mediated transportation of the virus along TNTs connecting macrophages has been made (136). In the same study, the authors observed a quick increase of TNT formation in HIV-1 infected

macrophages. Viral materials including viral RNA and Env and Gag proteins have been found transporting from cell to cell through TNTs. Rab9 endosomes have been shown to act as a cargo to transport infectious viruses through the TNTs (136). Further study showed that HIV-1 promotes TNT formation per se via its protein Nef and a cellular protein M-Sec (137). Similarly, Roberts et al. recently demonstrated the transfer of viral proteins via TNTs in cells infected with influenza or parainfluenza virus. A live cell movie showed the real-time movement of GFP-tagged NS1 proteins through the TNT. Treatment with a neuraminidase inhibitor alone did not inhibit the development of IAV micro-plaques, demonstrating that infectious virus cores (RNPs) can move from one cell to another without budding and release of cell-free virions. Cytoskeleton inhibitor treatments further confirmed that TNTs have a core of F-actin, which are involved in transporting virus particles together with a myosin motor (138). Amrita Kumar and colleagues confirmed the intercellular transportation of influenza A virus and further showed that by connecting epithelial cells, influenza A virus is able to evade immune and antiviral defenses (139). TNTs are transient structures (114). But, a recent study showed that US3 of pseudorabies virus can induce formation of TNTs, which appeared to be very stable and can remain intact for as long as 24 hours. Further results showed that US3-induced TNTs were detected containing stabilized (acetylated and detyrosinated) microtubules. Interestingly, mitochondria transportation was reported through these US3-induced TNTs (140).

1.4.4 Potentials of TNT in cell therapy

As indicated above, virus infection can cause oxidative stress in local cells (118, 141-143). Stressed or injured cells can be influenced by intercellular communicative networks. In recent years, there are emerging evidences that small cellular organelles, in particular mitochondria, can be transferred from the cell to cell to rescue a stressed/injured cell (118, 144,

145). Mesenchymal stem cells interact with other cells, reprograming their function through the secretion of small molecules like growth factors, chemokines, cytokines, and molecular mediators (bioactive lipids, nucleotides, among others). Different intercellular transport pathways have been reported for cell to cell transferring of small molecules and cellular organelles. TNT has been increasingly recognized as an important pathway for intercellular transportation. The human mesenchymal stem cells (MSCs) have been shown to display the ability to connect to target cells through tunneling nanotubes and to transfer the mitochondria through these TNTs. Spees et al. (2006) have showed the passage of mitochondria from adult non-hematopoietic stem cells (from human bone marrow hMSCs) or progenitor cells to A549 ρ° epithelial cells that were defective or deleted in mtDNA rescue aerobic respiration *in vitro* (144). For *in vivo* assays, mitochondrial transfer from bone-marrow-derived stromal cells to pulmonary alveolar epithelial cells protected against acute lung injury in a mouse model (146). A recent study also showed that mitochondrial transfer by human mesenchymal stem cells (hMSCs) to airway epithelial cells was able to attenuate cigarette smoke-induced lung damage in rats (147). Up to now, these target cells expanded to cardiomyocytes, endothelial cells, pulmonary alveolar epithelial cells, renal tubular cells, and cancer cells, leading to modifications of the functional properties of these cells (148).

1.5 Purpose of this research

The overall goal of this research is to understand novel pathogenic mechanisms of PRRSV infection. Two aims will be fulfilled in this dissertation, including: (1) to study how PRRSV utilized TNTs as an alternative pathway for cell to cell transmission; (2) to explore the potential role of PRRSV dsRNA in PRRSV persistent infection stage *in vitro* and *in vivo*.

1.6 References

1. Keffaber KK. 1989. Reproductive failure of unknown etiology. Am Assoc Swine Pract Newsl:1-9.
2. Hill H. 1990. Overview and history of Mystery Swine Disease (Swine infertility/respiratory syndrome). Proc Mystery Swine Disease Committee Meeting, Livestock Conservation Institute, Denver, Colorado:29-31.
3. Reotutar R. 1989. Swine reproductive failure syndrome mystifies scientists. J Am Vet Med Assoc:425-428.
4. Wensvoort G, Terpstra C, Pol JM, ter Laak EA, Bloemraad M, de Kluyver EP, Kragten C, van Buiten L, den Besten A, Wagenaar F. 1991. Mystery swine disease in The Netherlands: the isolation of Lelystad virus. Vet Q 13:121-30.
5. Collins JE, Benfield DA, Christianson WT, Harris L, Hennings JC, Shaw DP, Goyal SM, McCullough S, Morrison RB, Joo HS. 1992. Isolation of swine infertility and respiratory syndrome virus (isolate ATCC VR-2332) in North America and experimental reproduction of the disease in gnotobiotic pigs. J Vet Diagn Invest 4:117-26.
6. Benfield DA, Nelson E, Collins JE, Harris L, Goyal SM, Robison D, Christianson WT, Morrison RB, Gorcyca D, Chladek D. 1992. Characterization of swine infertility and respiratory syndrome (SIRS) virus (isolate ATCC VR-2332). J Vet Diagn Invest 4:127-33.
7. Feng Y, Zhao T, Nguyen T, Inui K, Ma Y, Nguyen TH, Nguyen VC, Liu D, Bui QA, To LT, Wang C, Tian K, Gao GF. 2008. Porcine respiratory and reproductive syndrome virus variants, Vietnam and Chinatttrrrrrrrrrrrrrrreea. Emerg Infect Dis 14:1774-6.
8. Tian K, Yu X, Zhao T, Feng Y, Cao Z, Wang C, Hu Y, Chen X, Hu D, Tian X, Liu D, Zhang S, Deng X, Ding Y, Yang L, Zhang Y, Xiao H, Qiao M, Wang B, Hou L, Wang X, Yang X, Kang L, Sun M, Jin P, Wang S, Kitamura Y, Yan J, Gao GF. 2007. Emergence of fatal PRRSV variants: unparalleled outbreaks of atypical PRRS in China and molecular dissection of the unique hallmark. PLoS One 2:e526.
9. Karniychuk UU, Geldhof M, Vanhee M, Van Doorsselaere J, Saveleva TA, Nauwynck HJ. 2010. Pathogenesis and antigenic characterization of a new East European subtype 3

porcine reproductive and respiratory syndrome virus isolate. BMC Veterinary Research 6:30.

10. Holtkamp DJ, Kliebenstein JB, Neumann EJ, Zimmerman JJ, Rotto HF, Yoder TK, Wang C, Yeske PE, Mowrer CL, Haley CA. 2013. Assessment of the economic impact of porcine reproductive and respiratory syndrome virus on United States pork producers. Journal of Swine Health and Production 21:72-84.
11. Christianson WT, Joo H. 1994. Porcine reproductive and respiratory syndrome:A review. Swine Health and Production 2:10-28.
12. Hu SP, Zhang Z, Liu YG, Tian ZJ, Wu DL, Cai XH, He XJ. 2013. Pathogenicity and distribution of highly pathogenic porcine reproductive and respiratory syndrome virus in pigs. Transbound Emerg Dis 60:351-9.
13. Xiao S, Jia J, Mo D, Wang Q, Qin L, He Z, Zhao X, Huang Y, Li A, Yu J, Niu Y, Liu X, Chen Y. 2010. Understanding PRRSV Infection in Porcine Lung Based on Genome-Wide Transcriptome Response Identified by Deep Sequencing. PLOS ONE 5:e11377.
14. Wills RW, Zimmerman JJ, Yoon KJ, Swenson SL, McGinley MJ, Hill HT, Platt KB, Christopher-Hennings J, Nelson EA. 1997. Porcine reproductive and respiratory syndrome virus: a persistent infection. Vet Microbiol 55:231-40.
15. Allende R, Laegreid WW, Kutish GF, Galeota JA, Wills RW, Osorio FA. 2000. Porcine reproductive and respiratory syndrome virus: description of persistence in individual pigs upon experimental infection. J Virol 74:10834-7.
16. Rowland RR, Lawson S, Rossow K, Benfield DA. 2003. Lymphoid tissue tropism of porcine reproductive and respiratory syndrome virus replication during persistent infection of pigs originally exposed to virus in utero. Vet Microbiol 96:219-35.
17. Christopher-Hennings J, Nelson EA, Hines RJ, Nelson JK, Swenson SL, Zimmerman JJ, Chase CL, Yaeger MJ, Benfield DA. 1995. Persistence of porcine reproductive and respiratory syndrome virus in serum and semen of adult boars. J Vet Diagn Invest 7:456-64.
18. Fang Y, Snijder EJ. 2010. The PRRSV replicase: exploring the multifunctionality of an intriguing set of nonstructural proteins. Virus Res 154:61-76.
19. Snijder EJ, Kikkert M, Fang Y. 2013. Arterivirus molecular biology and pathogenesis. J Gen Virol 94:2141-63.

20. Snijder EJ, Meulenberg JJM. 1998. The molecular biology of arteriviruses. J Gen Virol 79.
21. Fang Y, Treffers EE, Li Y, Tas A, Sun Z, van der Meer Y, de Ru AH, van Veelen PA, Atkins JF, Snijder EJ, Firth AE. 2012. Efficient -2 frameshifting by mammalian ribosomes to synthesize an additional arterivirus protein. Proc Natl Acad Sci U S A 109:E2920-8.
22. Li Y, Treffers EE, Napthine S, Tas A, Zhu L, Sun Z, Bell S, Mark BL, van Veelen PA, van Hemert MJ, Firth AE, Brierley I, Snijder EJ, Fang Y. 2014. Transactivation of programmed ribosomal frameshifting by a viral protein. Proc Natl Acad Sci U S A 111:E2172-81.
23. Kim HS, Kwang J, Yoon IJ, Joo HS, Frey ML. 1993. Enhanced replication of porcine reproductive and respiratory syndrome (PRRS) virus in a homogeneous subpopulation of MA-104 cell line. Arch Virol 133:477-83.
24. Schneider-Schaulies J. 2000. Cellular receptors for viruses: links to tropism and pathogenesis. J Gen Virol 81:1413-29.
25. Nauwynck HJ, Duan X, Favoreel HW, Van Oostveldt P, Pensaert MB. 1999. Entry of porcine reproductive and respiratory syndrome virus into porcine alveolar macrophages via receptor-mediated endocytosis. J Gen Virol 80 (Pt 2):297-305.
26. Zhang Q, Yoo D. 2015. PRRS virus receptors and their role for pathogenesis. Vet Microbiol 177:229-41.
27. Gao J, Xiao S, Xiao Y, Wang X, Zhang C, Zhao Q, Nan Y, Huang B, Liu H, Liu N, Lv J, Du T, Sun Y, Mu Y, Wang G, Syed SF, Zhang G, Hiscox JA, Goodfellow I, Zhou EM. 2016. MYH9 is an Essential Factor for Porcine Reproductive and Respiratory Syndrome Virus Infection. Sci Rep 6:25120.
28. Guo R, Katz BB, Tomich JM, Gallagher T, Fang Y. 2016. Porcine Reproductive and Respiratory Syndrome Virus Utilizes Nanotubes for Intercellular Spread. J Virol 90:5163-75.
29. An TQ, Tian ZJ, He YX, Xiao Y, Jiang YF, Peng JM, Zhou YJ, Liu D, Tong GZ. 2010. Porcine reproductive and respiratory syndrome virus attachment is mediated by the N-terminal domain of the sialoadhesin receptor. Vet Microbiol 143:371-8.

30. Prather RS, Rowland RR, Ewen C, Trible B, Kerrigan M, Bawa B, Teson JM, Mao J, Lee K, Samuel MS, Whitworth KM, Murphy CN, Egen T, Green JA. 2013. An intact sialoadhesin (Sn/SIGLEC1/CD169) is not required for attachment/internalization of the porcine reproductive and respiratory syndrome virus. J Virol 87:9538-46.
31. Calvert JG, Slade DE, Shields SL, Jolie R, Mannan RM, Ankenbauer RG, Welch SK. 2007. CD163 expression confers susceptibility to porcine reproductive and respiratory syndrome viruses. J Virol 81:7371-9.
32. Whitworth KM, Rowland RRR, Ewen CL, Trible BR, Kerrigan MA, Cino-Ozuna AG, Samuel MS, Lightner JE, McLaren DG, Mileham AJ, Wells KD, Prather RS. 2016. Gene-edited pigs are protected from porcine reproductive and respiratory syndrome virus. Nat Biotech 34:20-22.
33. Burkard C, Lillico SG, Reid E, Jackson B, Mileham AJ, Ait-Ali T, Whitelaw CBA, Archibald AL. 2017. Precision engineering for PRRSV resistance in pigs: Macrophages from genome edited pigs lacking CD163 SRCR5 domain are fully resistant to both PRRSV genotypes while maintaining biological function. PLOS Pathogens 13:e1006206.
34. Ma H, Jiang L, Qiao S, Zhi Y, Chen X-X, Yang Y, Huang X, Huang M, Li R, Zhang G-P. 2017. The Crystal Structure of the Fifth Scavenger Receptor Cysteine-Rich Domain of Porcine CD163 Reveals an Important Residue Involved in Porcine Reproductive and Respiratory Syndrome Virus Infection. Journal of Virology 91:e01897-16.
35. Van Gorp H, Van Breedam W, Van Doorsselaere J, Delputte PL, Nauwynck HJ. 2010. Identification of the CD163 protein domains involved in infection of the porcine reproductive and respiratory syndrome virus. J Virol 84:3101-5.
36. Wells KD, Bardot R, Whitworth KM, Trible BR, Fang Y, Mileham A, Kerrigan MA, Samuel MS, Prather RS, Rowland RR. 2017. Replacement of Porcine CD163 Scavenger Receptor Cysteine-Rich Domain 5 with a CD163-Like Homolog Confers Resistance of Pigs to Genotype 1 but Not Genotype 2 Porcine Reproductive and Respiratory Syndrome Virus. J Virol 91.
37. Peng C, Haller SL, Rahman MM, McFadden G, Rothenburg S. 2016. Myxoma virus M156 is a specific inhibitor of rabbit PKR but contains a loss-of-function mutation in Australian virus isolates. Proc Natl Acad Sci U S A 113:3855-60.

38. Beura LK, Sarkar SN, Kwon B, Subramaniam S, Jones C, Pattnaik AK, Osorio FA. 2010. Porcine reproductive and respiratory syndrome virus nonstructural protein 1beta modulates host innate immune response by antagonizing IRF3 activation. J Virol 84:1574-84.
39. Chen Z, Lawson S, Sun Z, Zhou X, Guan X, Christopher-Hennings J, Nelson EA, Fang Y. 2010. Identification of two auto-cleavage products of nonstructural protein 1 (nsp1) in porcine reproductive and respiratory syndrome virus infected cells: nsp1 function as interferon antagonist. Virology 398:87-97.
40. Kim O, Sun Y, Lai FW, Song C, Yoo D. 2010. Modulation of type I interferon induction by porcine reproductive and respiratory syndrome virus and degradation of CREB-binding protein by non-structural protein 1 in MARC-145 and HeLa cells. Virology 402:315-26.
41. Huang C, Zhang Q, Guo XK, Yu ZB, Xu AT, Tang J, Feng WH. 2014. Porcine reproductive and respiratory syndrome virus nonstructural protein 4 antagonizes beta interferon expression by targeting the NF-kappaB essential modulator. J Virol 88:10934-45.
42. Sun Z, Chen Z, Lawson SR, Fang Y. 2010. The cysteine protease domain of porcine reproductive and respiratory syndrome virus nonstructural protein 2 possesses deubiquitinating and interferon antagonism functions. J Virol 84:7832-46.
43. Sun Y, Han M, Kim C, Calvert JG, Yoo D. 2012. Interplay between Interferon-Mediated Innate Immunity and Porcine Reproductive and Respiratory Syndrome Virus. Viruses 4:424-446.
44. Van Reeth K, Labarque G, Nauwynck H, Pensaert M. 1999. Differential production of proinflammatory cytokines in the pig lung during different respiratory virus infections: correlations with pathogenicity. Research in Veterinary Science 67:47-52.
45. Albina E, Carrat C, Charley B. 1998. Interferon-alpha response to swine arterivirus (PoAV), the porcine reproductive and respiratory syndrome virus. Journal of Interferon and Cytokine Research 18:485-490.
46. Murtaugh MP, Xiao ZG, Zuckermann F. 2002. Immunological responses of swine to porcine reproductive and respiratory syndrome virus infection. Viral Immunology 15:533-547.

47. Luo R, Xiao S, Jiang Y, Jin H, Wang D, Liu M, Chen H, Fang L. 2008. Porcine reproductive and respiratory syndrome virus (PRRSV) suppresses interferon-β production by interfering with the RIG-I signaling pathway. Molecular Immunology 45:2839-2846.
48. Miller LC, Laegreid WW, Bono JL, Chitko-McKown CG, Fox JM. 2004. Interferon type I response in porcine reproductive and respiratory syndrome virus-infected MARC-145 cells. Arch Virol 149:2453-63.
49. Sun Y, Ke H, Han M, Chen N, Fang W, Yoo D. 2016. Nonstructural Protein 11 of Porcine Reproductive and Respiratory Syndrome Virus Suppresses Both MAVS and RIG-I Expression as One of the Mechanisms to Antagonize Type I Interferon Production. PLoS One 11:e0168314.
50. Brown E, Lawson S, Welbon C, Gnanandarajah J, Li J, Murtaugh MP, Nelson EA, Molina RM, Zimmerman JJ, Rowland RRR, Fang Y. 2009. Antibody Response to Porcine Reproductive and Respiratory Syndrome Virus (PRRSV) Nonstructural Proteins and Implications for Diagnostic Detection and Differentiation of PRRSV Types I and II. Clinical and Vaccine Immunology : CVI 16:628-635.
51. Johnson CR, Yu W, Murtaugh MP. 2007. Cross-reactive antibody responses to nsp1 and nsp2 of Porcine reproductive and respiratory syndrome virus. J Gen Virol 88:1184-95.
52. Darwich L, D áz I, Mateu E. 2010. Certainties, doubts and hypotheses in porcine reproductive and respiratory syndrome virus immunobiology. Virus Research 154:123-132.
53. Lopez OJ, Osorio FA. 2004. Role of neutralizing antibodies in PRRSV protective immunity. Vet Immunol Immunopathol 102:155-63.
54. Ostrowski M, Galeota JA, Jar AM, Platt KB, Osorio FA, Lopez OJ. 2002. Identification of Neutralizing and Nonneutralizing Epitopes in the Porcine Reproductive and Respiratory Syndrome Virus GP5 Ectodomain. Journal of Virology 76:4241-4250.
55. Bautista EM, Molitor TW. 1997. Cell-mediated immunity to porcine reproductive and respiratory syndrome virus in swine. Viral Immunol 10:83-94.
56. Meier W, Wheeler J, Husmann R, J., Osorio F, Zuckermann F, A. 2000. Characteristics of the immune response of pigs to PRRS virus. Vet Res 31:41.

57. Meier WA, Galeota J, Osorio FA, Husmann RJ, Schnitzlein WM, Zuckermann FA. 2003. Gradual development of the interferon-γ response of swine to porcine reproductive and respiratory syndrome virus infection or vaccination. Virology 309:18-31.
58. Xiao Z, Batista L, Dee S, Halbur P, Murtaugh MP. 2004. The level of virus-specific T-cell and macrophage recruitment in porcine reproductive and respiratory syndrome virus infection in pigs is independent of virus load. J Virol 78:5923-33.
59. Costers S, Lefebvre DJ, Goddeeris B, Delputte PL, Nauwynck HJ. 2009. Functional impairment of PRRSV-specific peripheral CD3+CD8high cells. Vet Res 40.
60. Wongyanin P, Buranapraditkul S, Yoo D, Thanawongnuwech R, Roth JA, Suradhat S. 2012. Role of porcine reproductive and respiratory syndrome virus nucleocapsid protein in induction of interleukin-10 and regulatory T-lymphocytes (Treg). J Gen Virol 93:1236-46.
61. Gómez-Laguna J, Rodríguez-Gómez IM, Barranco I, Pallarés FJ, Salguero FJ, Carrasco L. 2012. Enhanced expression of TGFβ protein in lymphoid organs and lung, but not in serum, of pigs infected with a European field isolate of porcine reproductive and respiratory syndrome virus. Veterinary Microbiology 158:187-193.
62. Dwivedi V, Manickam C, Patterson R, Dodson K, Murtaugh M, Torrelles JB, Schlesinger LS, Renukaradhya GJ. 2011. Cross-protective immunity to porcine reproductive and respiratory syndrome virus by intranasal delivery of a live virus vaccine with a potent adjuvant. Vaccine 29:4058-66.
63. Renukaradhya GJ, Alekseev K, Jung K, Fang Y, Saif LJ. 2010. Porcine reproductive and respiratory syndrome virus-induced immunosuppression exacerbates the inflammatory response to porcine respiratory coronavirus in pigs. Viral Immunol 23:457-66.
64. Diaz I, Darwich L, Pappaterra G, Pujols J, Mateu E. 2005. Immune responses of pigs after experimental infection with a European strain of Porcine reproductive and respiratory syndrome virus. J Gen Virol 86:1943-51.
65. Suradhat S, Thanawongnuwech R, Poovorawan Y. 2003. Upregulation of IL-10 gene expression in porcine peripheral blood mononuclear cells by porcine reproductive and respiratory syndrome virus. J Gen Virol 84:453-9.
66. Fink SL, Cookson BT. 2005. Apoptosis, pyroptosis, and necrosis: mechanistic description of dead and dying eukaryotic cells. Infect Immun 73:1907-16.

67. Thomson BJ. 2001. Viruses and apoptosis. Int J Exp Pathol 82:65-76.
68. Costers S, Lefebvre DJ, Delputte PL, Nauwynck HJ. 2008. Porcine reproductive and respiratory syndrome virus modulates apoptosis during replication in alveolar macrophages. Arch Virol 153:1453-65.
69. Miller LC, Fox JM. 2004. Apoptosis and porcine reproductive and respiratory syndrome virus. Vet Immunol Immunopathol 102:131-42.
70. Chang HW, Jeng CR, Liu JJ, Lin TL, Chang CC, Chia MY, Tsai YC, Pang VF. 2005. Reduction of porcine reproductive and respiratory syndrome virus (PRRSV) infection in swine alveolar macrophages by porcine circovirus 2 (PCV2)-induced interferon-alpha. Vet Microbiol 108:167-77.
71. Kim TS, Benfield DA, Rowland RR. 2002. Porcine reproductive and respiratory syndrome virus-induced cell death exhibits features consistent with a nontypical form of apoptosis. Virus Res 85:133-40.
72. Labarque G, Van Gucht S, Van Reeth K, Nauwynck H, Pensaert M. 2003. Respiratory tract protection upon challenge of pigs vaccinated with attenuated porcine reproductive and respiratory syndrome virus vaccines. Veterinary Microbiology 95:187-197.
73. Lee SM, Kleiboeker SB. 2007. Porcine reproductive and respiratory syndrome virus induces apoptosis through a mitochondria-mediated pathway. Virology 365:419-34.
74. Sur JH, Doster AR, Osorio FA. 1998. Apoptosis induced in vivo during acute infection by porcine reproductive and respiratory syndrome virus. Vet Pathol 35:506-14.
75. Randall RE, Griffin DE. 2017. Within host RNA virus persistence: mechanisms and consequences. Current Opinion in Virology 23:35-42.
76. Lunney JK, Fang Y, Ladinig A, Chen N, Li Y, Rowland B, Renukaradhya GJ. 2016. Porcine Reproductive and Respiratory Syndrome Virus (PRRSV): Pathogenesis and Interaction with the Immune System. Annu Rev Anim Biosci 4:129-54.
77. Zimmerman J, T. Sanderson, K. A. Eernisse, H. T. Hill, M. L. Frey. . 1992. Transmission of SIRS virus in convalescent animals to commingled penmates under experimental conditions. . Am Assoc Swine Pract Newsl 4.
78. Bierk MD, Dee SA, Rossow KD, Otake S, Collins JE, Molitor TW. 2001. Transmission of porcine reproductive and respiratory syndrome virus from persistently infected sows to contact controls. Canadian Journal of Veterinary Research 65:261-266.

79. Wills RW, Doster AR, Galeota JA, Sur JH, Osorio FA. 2003. Duration of infection and proportion of pigs persistently infected with porcine reproductive and respiratory syndrome virus. J Clin Microbiol 41:58-62.
80. Robinson SR, Li J, Nelson EA, Murtaugh MP. 2015. Broadly neutralizing antibodies against the rapidly evolving porcine reproductive and respiratory syndrome virus. Virus Res 203:56-65.
81. Pileri E, Mateu E. 2016. Review on the transmission porcine reproductive and respiratory syndrome virus between pigs and farms and impact on vaccination. Veterinary Research 47:108.
82. Sur JH, Cooper VL, Galeota JA, Hesse RA, Doster AR, Osorio FA. 1996. In vivo detection of porcine reproductive and respiratory syndrome virus RNA by in situ hybridization at different times postinfection. J Clin Microbiol 34:2280-6.
83. Anderson GW, Rowland RR, Palmer GA, Even C, Plagemann PG. 1995. Lactate dehydrogenase-elevating virus replication persists in liver, spleen, lymph node, and testis tissues and results in accumulation of viral RNA in germinal centers, concomitant with polyclonal activation of B cells. J Virol 69:5177-85.
84. Ahmed R, Canning WM, Kauffman RS, Sharpe AH, Hallum JV, Fields BN. 1981. Role of the host cell in persistent viral infection: coevolution of L cells and reovoirus during persistent infection. Cell 25:325-32.
85. Tenser RB, Edris WA, Hay KA. 1989. Herpes simplex latent infection: quantitation of latency-associated transcript-positive neurons and reactivable neurons. Yale J Biol Med 62:197-204.
86. Nicoll MP, Proenca JT, Efstathiou S. 2012. The molecular basis of herpes simplex virus latency. FEMS Microbiol Rev 36:684-705.
87. Thanawongnuwech R, Thacker EL, Halbur PG. 1997. Effect of porcine reproductive and respiratory syndrome virus (PRRSV) (isolate ATCC VR-2385) infection on bactericidal activity of porcine pulmonary intravascular macrophages (PIMs): in vitro comparisons with pulmonary alveolar macrophages (PAMs). Vet Immunol Immunopathol 59.
88. Connick E, Mattila T, Folkvord JM, Schlichtemeier R, Meditz AL, Ray MG, McCarter MD, Mawhinney S, Hage A, White C, Skinner PJ. 2007. CTL fail to accumulate at sites of HIV-1 replication in lymphoid tissue. J Immunol 178:6975-83.

89. Connick E, Folkvord JM, Lind KT, Rakasz EG, Miles B, Wilson NA, Santiago ML, Schmitt K, Stephens EB, Kim HO, Wagstaff R, Li S, Abdelaal HM, Kemp N, Watkins DI, MaWhinney S, Skinner PJ. 2014. Compartmentalization of simian immunodeficiency virus replication within secondary lymphoid tissues of rhesus macaques is linked to disease stage and inversely related to localization of virus-specific CTL. J Immunol 193:5613-25.
90. Tjernlund A, Zhu J, Laing K, Diem K, McDonald D, Vazquez J, Cao J, Ohlen C, McElrath MJ, Picker LJ, Corey L. 2010. In situ detection of Gag-specific CD8+ cells in the GI tract of SIV infected Rhesus macaques. Retrovirology 7:12.
91. Sasikala-Appukuttan AK, Kim HO, Kinzel NJ, Hong JJ, Smith AJ, Wagstaff R, Reilly C, Piatak M, Jr., Lifson JD, Reeves RK, Johnson RP, Haase AT, Skinner PJ. 2013. Location and Dynamics of the Immunodominant CD8 T Cell Response to SIVΔnef Immunization and SIVmac251 Vaginal Challenge. PLOS ONE 8:e81623.
92. Li S, Folkvord JM, Rakasz EG, Abdelaal HM, Wagstaff RK, Kovacs KJ, Kim HO, Sawahata R, MaWhinney S, Masopust D, Connick E, Skinner PJ. 2016. Simian Immunodeficiency Virus-Producing Cells in Follicles Are Partially Suppressed by CD8+ Cells In Vivo. J Virol 90:11168-11180.
93. Tam PE, Messner RP. 1999. Molecular mechanisms of coxsackievirus persistence in chronic inflammatory myopathy: viral RNA persists through formation of a double-stranded complex without associated genomic mutations or evolution. J Virol 73:10113-21.
94. Feuer R, Ruller CM, An N, Tabor-Godwin JM, Rhoades RE, Maciejewski S, Pagarigan RR, Cornell CT, Crocker SJ, Kiosses WB, Pham-Mitchell N, Campbell IL, Whitton JL. 2009. Viral persistence and chronic immunopathology in the adult central nervous system following Coxsackievirus infection during the neonatal period. J Virol 83:9356-69.
95. Klepper A, Eng FJ, Doyle EH, El-Shamy A, Rahman AH, Fiel MI, Avino GC, Lee M, Ye F, Roayaie S, Bansal MB, MacDonald MR, Schiano TD, Branch AD. 2017. Hepatitis C virus double-stranded RNA is the predominant form in human liver and in interferon-treated cells. Hepatology (Baltimore, Md) 66:357-370.
96. Detjen BM, Lucas J, Wimmer E. 1978. Poliovirus single-stranded RNA and double-stranded RNA: differential infectivity in enucleate cells. Journal of Virology 27:582-586.

97. Graeber I, Tischer J, Heinrich J, Hachula G, Lopez-Pila JM. 1998. Persistence of heterologous nucleic acids after uptake by mammalian cells. DNA Cell Biol 17:945-9.
98. Knoops K, Barcena M, Limpens RW, Koster AJ, Mommaas AM, Snijder EJ. 2012. Ultrastructural characterization of arterivirus replication structures: reshaping the endoplasmic reticulum to accommodate viral RNA synthesis. J Virol 86:2474-87.
99. Rowland RR, Steffen M, Ackerman T, Benfield DA. 1999. The evolution of porcine reproductive and respiratory syndrome virus: quasispecies and emergence of a virus subpopulation during infection of pigs with VR-2332. Virology 259:262-6.
100. Chen N, Trible BR, Kerrigan MA, Tian K, Rowland RR. 2016. ORF5 of porcine reproductive and respiratory syndrome virus (PRRSV) is a target of diversifying selection as infection progresses from acute infection to virus rebound. Infect Genet Evol 40:167-75.
101. Chen W, Baric RS. 1996. Molecular anatomy of mouse hepatitis virus persistence: coevolution of increased host cell resistance and virus virulence. J Virol 70:3947-60.
102. Colbere-Garapin F, Christodoulou C, Crainic R, Pelletier I. 1989. Persistent poliovirus infection of human neuroblastoma cells. Proc Natl Acad Sci U S A 86:7590-4.
103. Couderc T, Hogle J, Le Blay H, Horaud F, Blondel B. 1993. Molecular characterization of mouse-virulent poliovirus type 1 Mahoney mutants: involvement of residues of polypeptides VP1 and VP2 located on the inner surface of the capsid protein shell. J Virol 67:3808-17.
104. Couderc T, Guedo N, Calvez V, Pelletier I, Hogle J, Colbere-Garapin F, Blondel B. 1994. Substitutions in the capsids of poliovirus mutants selected in human neuroblastoma cells confer on the Mahoney type 1 strain a phenotype neurovirulent in mice. J Virol 68:8386-91.
105. Chan PK, To KF, Lo AW, Cheung JL, Chu I, Au FW, Tong JH, Tam JS, Sung JJ, Ng HK. 2004. Persistent infection of SARS coronavirus in colonic cells in vitro. J Med Virol 74:1-7.
106. Mizutani T, Fukushi S, Ishii K, Sasaki Y, Kenri T, Saijo M, Kanaji Y, Shirota K, Kurane I, Morikawa S. 2006. Mechanisms of establishment of persistent SARS-CoV-infected cells. Biochem Biophys Res Commun 347:261-5.

107. Arbour N, Cote G, Lachance C, Tardieu M, Cashman NR, Talbot PJ. 1999. Acute and persistent infection of human neural cell lines by human coronavirus OC43. J Virol 73:3338-50.
108. Arbour N, Ekande S, Cote G, Lachance C, Chagnon F, Tardieu M, Cashman NR, Talbot PJ. 1999. Persistent infection of human oligodendrocytic and neuroglial cell lines by human coronavirus 229E. J Virol 73:3326-37.
109. Chen W, Baric RS. 1995. Function of a 5'-end genomic RNA mutation that evolves during persistent mouse hepatitis virus infection in vitro. J Virol 69:7529-40.
110. Hofmann MA, Sethna PB, Brian DA. 1990. Bovine coronavirus mRNA replication continues throughout persistent infection in cell culture. J Virol 64:4108-14.
111. Hofmann MA, Senanayake SD, Brian DA. 1993. A translation-attenuating intraleader open reading frame is selected on coronavirus mRNAs during persistent infection. Proc Natl Acad Sci U S A 90:11733-7.
112. Stueckemann JA, Holth M, Swart WJ, Kowalchyk K, Smith MS, Wolstenholme AJ, Cafruny WA, Plagemann PG. 1982. Replication of lactate dehydrogenase-elevating virus in macrophages. 2. Mechanism of persistent infection in mice and cell culture. J Gen Virol 59:263-72.
113. Zhang J, Timoney PJ, MacLachlan NJ, McCollum WH, Balasuriya UB. 2008. Persistent equine arteritis virus infection in HeLa cells. J Virol 82:8456-64.
114. Rustom A, Saffrich R, Markovic I, Walther P, Gerdes HH. 2004. Nanotubular highways for intercellular organelle transport. Science 303:1007-10.
115. Wang X, Gerdes HH. 2012. Long-distance electrical coupling via tunneling nanotubes. Biochim Biophys Acta 1818:2082-6.
116. Sowinski S, Jolly C, Berninghausen O, Purbhoo MA, Chauveau A, Kohler K, Oddos S, Eissmann P, Brodsky FM, Hopkins C, Onfelt B, Sattentau Q, Davis DM. 2008. Membrane nanotubes physically connect T cells over long distances presenting a novel route for HIV-1 transmission. Nat Cell Biol 10:211-9.
117. Wang X, Veruki ML, Bukoreshtliev NV, Hartveit E, Gerdes HH. 2010. Animal cells connected by nanotubes can be electrically coupled through interposed gap-junction channels. Proc Natl Acad Sci U S A 107:17194-9.

118. Rustom A. 2016. The missing link: does tunnelling nanotube-based supercellularity provide a new understanding of chronic and lifestyle diseases? Open Biol 6.
119. Gerdes HH, Carvalho RN. 2008. Intercellular transfer mediated by tunneling nanotubes. Curr Opin Cell Biol 20:470-5.
120. Onfelt B, Nedvetzki S, Benninger RK, Purbhoo MA, Sowinski S, Hume AN, Seabra MC, Neil MA, French PM, Davis DM. 2006. Structurally distinct membrane nanotubes between human macrophages support long-distance vesicular traffic or surfing of bacteria. J Immunol 177:8476-83.
121. Koyanagi M, Brandes RP, Haendeler J, Zeiher AM, Dimmeler S. 2005. Cell-to-cell connection of endothelial progenitor cells with cardiac myocytes by nanotubes: a novel mechanism for cell fate changes? Circ Res 96:1039-41.
122. Gurke S, Barroso JF, Gerdes HH. 2008. The art of cellular communication: tunneling nanotubes bridge the divide. Histochem Cell Biol 129:539-50.
123. Eugenin EA, Gaskill PJ, Berman JW. 2009. Tunneling nanotubes (TNT) are induced by HIV-infection of macrophages: a potential mechanism for intercellular HIV trafficking. Cell Immunol 254:142-8.
124. Gousset K, Zurzolo C. 2009. Tunnelling nanotubes: a highway for prion spreading? Prion 3:94-8.
125. Domhan S, Ma L, Tai A, Anaya Z, Beheshti A, Zeier M, Hlatky L, Abdollahi A. 2011. Intercellular communication by exchange of cytoplasmic material via tunneling nano-tube like structures in primary human renal epithelial cells. PLoS One 6:e21283.
126. Watkins SC, Salter RD. 2005. Functional connectivity between immune cells mediated by tunneling nanotubules. Immunity 23:309-18.
127. Hase K, Kimura S, Takatsu H, Ohmae M, Kawano S, Kitamura H, Ito M, Watarai H, Hazelett CC, Yeaman C, Ohno H. 2009. M-Sec promotes membrane nanotube formation by interacting with Ral and the exocyst complex. Nat Cell Biol 11:1427-32.
128. Smith IF, Shuai J, Parker I. 2011. Active generation and propagation of Ca2+ signals within tunneling membrane nanotubes. Biophys J 100:L37-9.
129. Green DR, Droin N, Pinkoski M. 2003. Activation-induced cell death in T cells. Immunol Rev 193:70-81.

130. Arkwright PD, Luchetti F, Tour J, Roberts C, Ayub R, Morales AP, Rodriguez JJ, Gilmore A, Canonico B, Papa S, Esposti MD. 2010. Fas stimulation of T lymphocytes promotes rapid intercellular exchange of death signals via membrane nanotubes. Cell Res 20:72-88.
131. He K, Luo W, Zhang Y, Liu F, Liu D, Xu L, Qin L, Xiong C, Lu Z, Fang X, Zhang Y. 2010. Intercellular transportation of quantum dots mediated by membrane nanotubes. ACS Nano 4:3015-22.
132. Plotnikov EY, Khryapenkova TG, Galkina SI, Sukhikh GT, Zorov DB. 2010. Cytoplasm and organelle transfer between mesenchymal multipotent stromal cells and renal tubular cells in co-culture. Exp Cell Res 316:2447-55.
133. Wang X, Gerdes HH. 2015. Transfer of mitochondria via tunneling nanotubes rescues apoptotic PC12 cells. Cell Death and Differentiation 22:1181-1191.
134. Kadiu I, Gendelman HE. 2011. Macrophage bridging conduit trafficking of HIV-1 through the endoplasmic reticulum and Golgi network. J Proteome Res 10:3225-38.
135. Yamauchi Y, Helenius A. 2013. Virus entry at a glance. Journal of Cell Science 126:1289-1295.
136. Kadiu I, Gendelman HE. 2011. Human Immunodeficiency Virus type 1 Endocytic Trafficking Through Macrophage Bridging Conduits Facilitates Spread of Infection. Journal of Neuroimmune Pharmacology 6:658-675.
137. Hashimoto M, Bhuyan F, Hiyoshi M, Noyori O, Nasser H, Miyazaki M, Saito T, Kondoh Y, Osada H, Kimura S, Hase K, Ohno H, Suzu S. 2016. Potential Role of the Formation of Tunneling Nanotubes in HIV-1 Spread in Macrophages. J Immunol 196:1832-41.
138. Roberts AJ, Kon T, Knight PJ, Sutoh K, Burgess SA. 2013. Functions and mechanics of dynein motor proteins. Nature reviews Molecular cell biology 14:713-726.
139. Kumar A, Kim JH, Ranjan P, Metcalfe MG, Cao W, Mishina M, Gangappa S, Guo Z, Boyden ES, Zaki S, York I, Garc ́a-Sastre A, Shaw M, Sambhara S. 2017. Influenza virus exploits tunneling nanotubes for cell-to-cell spread. Scientific Reports 7:40360.
140. Jansens RJJ, Van den Broeck W, De Pelsmaeker S, Lamote JAS, Van Waesberghe C, Couck L, Favoreel HW. 2017. Pseudorabies virus US3-induced tunneling nanotubes contain stabilized microtubules, interact with neighbouring cells via cadherins and allow intercellular molecular communication. J Virol doi:10.1128/jvi.00749-17.

141. Schwarz KB. 1996. Oxidative stress during viral infection: a review. Free Radic Biol Med 21:641-9.
142. Liu M, Chen F, Liu T, Chen F, Liu S, Yang J. 2017. The role of oxidative stress in influenza virus infection. Microbes and Infection 19:580-586.
143. Paracha UZ, Fatima K, Alqahtani M, Chaudhary A, Abuzenadah A, Damanhouri G, Qadri I. 2013. Oxidative stress and hepatitis C virus. Virology Journal 10:251.
144. Spees JL, Olson SD, Whitney MJ, Prockop DJ. 2006. Mitochondrial transfer between cells can rescue aerobic respiration. Proc Natl Acad Sci U S A 103:1283-8.
145. Torralba D, Baixauli F, Sanchez-Madrid F. 2016. Mitochondria Know No Boundaries: Mechanisms and Functions of Intercellular Mitochondrial Transfer. Front Cell Dev Biol 4:107.
146. Islam MN, Das SR, Emin MT, Wei M, Sun L, Westphalen K, Rowlands DJ, Quadri SK, Bhattacharya S, Bhattacharya J. 2012. Mitochondrial transfer from bone-marrow-derived stromal cells to pulmonary alveoli protects against acute lung injury. Nat Med 18:759-65.
147. Li X, Zhang Y, Yeung SC, Liang Y, Liang X, Ding Y, Ip MS, Tse HF, Mak JC, Lian Q. 2014. Mitochondrial transfer of induced pluripotent stem cell-derived mesenchymal stem cells to airway epithelial cells attenuates cigarette smoke-induced damage. Am J Respir Cell Mol Biol 51:455-65.
148. Vignais M-L, Caicedo A, Brondello J-M, Jorgensen C. 2017. Cell Connections by Tunneling Nanotubes: Effects of Mitochondrial Trafficking on Target Cell Metabolism, Homeostasis, and Response to Therapy. Stem Cells International 2017:6917941.

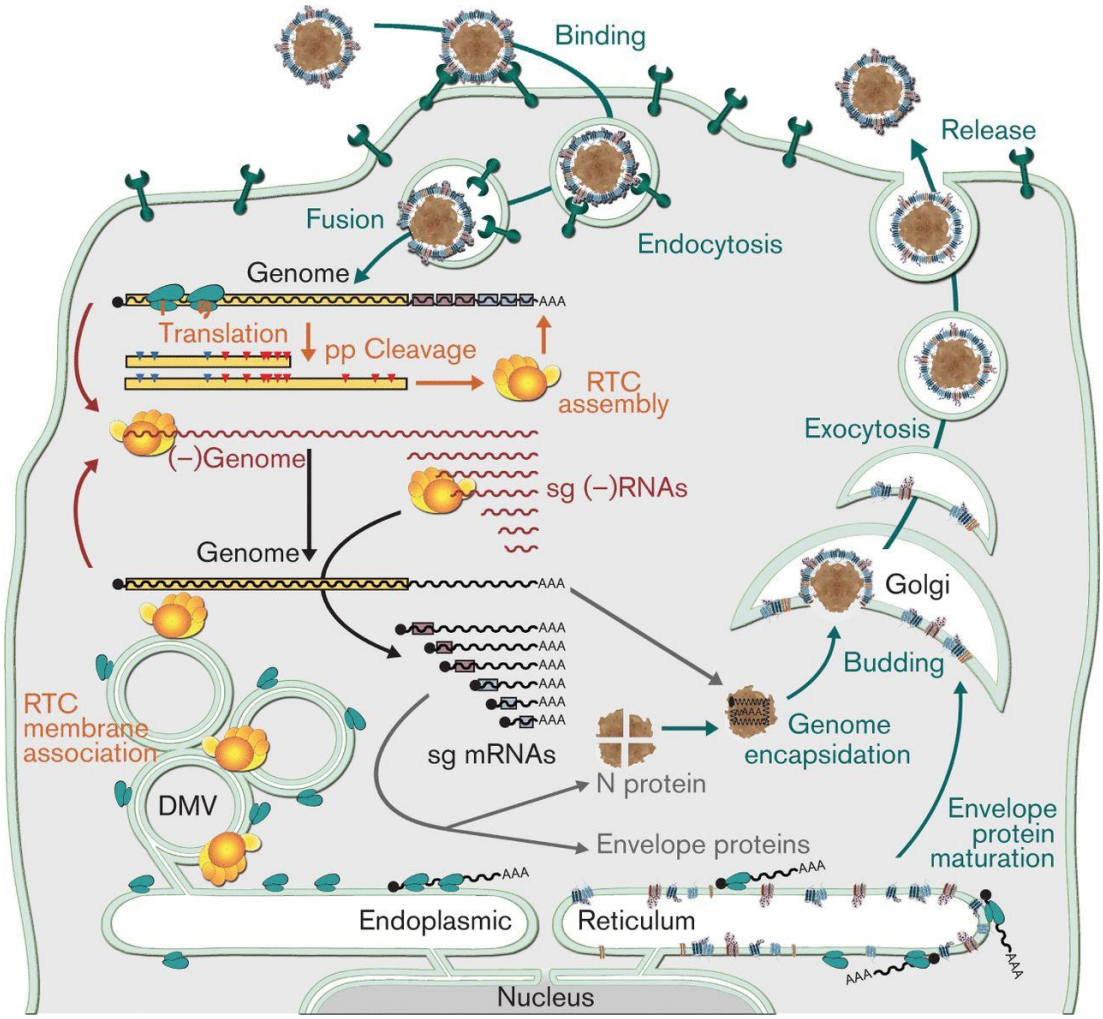

Figure 1.1 Life cycle of PRRSV replication. PRRSV enters the cells by receptor-mediated endocytosis. Genomic RNA released into cytosol and subsequent translation yields replicase polyproteins pp1a and pp1ab. These polyproteins are cleaved by internal proteinases yielding 11 nsps, which are further assembled into a replication and transcription complex (RTC). Both full-length and subgenome-length minus strands are produced with RTCs, the latter serving as templates for the synthesis of sg mRNAs required to express the structural protein genes. Newly synthesized genomes are encapsulated into nucleocapsids that become enveloped by budding from smooth intracellular membranes, after which the new virions leave the cell using the exocytic pathway. Picture adapted from Snijder et al., 2013 (19).

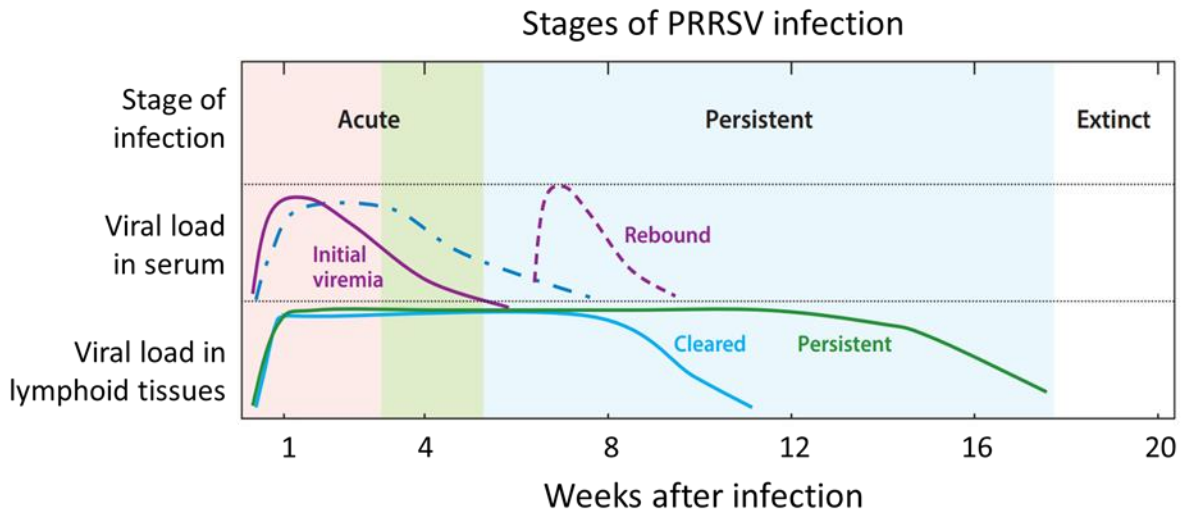

Figure 1.2 Stages of PRRSV infection. PRRSV infection can be divided into at least three distinct stages: acute infection, persistence, and extinction. The first stage is represented by acute infection, during which the macrophages and dendritic cells in lungs and the upper respiratory airway serves as a preferential site of infection. At persistent infection stage, viral replication is primarily localized in lymphoid organs, including tonsil and lymph node. Viral replication can be replication can be maintained for as long as 250 days after initial infection until eventual extinction in the host. Picture modified from Lunney et al., 2016 (76).

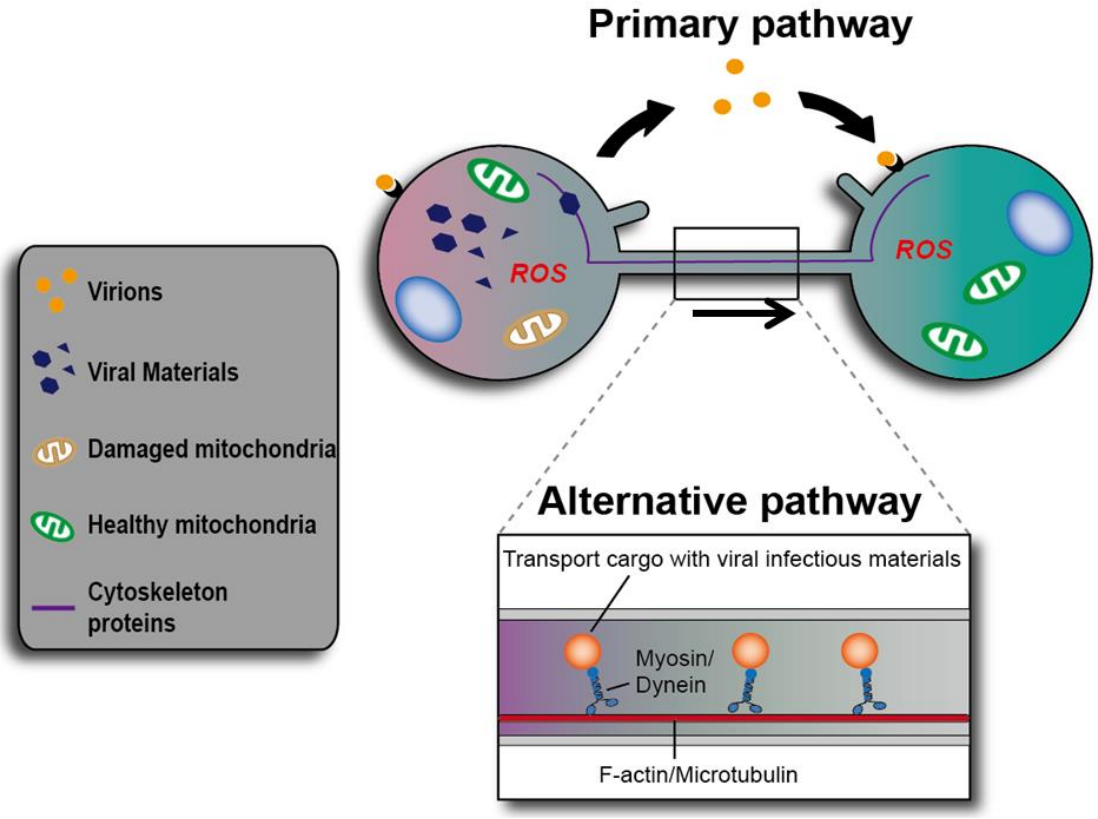

Figure 1.3 Formation of tunneling nanotubes connecting among cells. Tunneling nanotubes (TNTs) are long ultrathin structures with diameters ranging from 50 to 200 nm , which allow organelle transfer between two spatially separated cells. TNTs contain cytoskeletal elements such as actin and microtubules depending on the cell type. Numerous organelles such as mitochondria and lysosomes have been shown to be transferred intercellularly through TNTs Picture modified from Torralba et al., 2016 (145).

Chapter 2 - Porcine reproductive and respiratory syndrome virus utilizes nanotubes for intercellular spread

Rui Guo, Benjamin B. Katz, John M. Tomich, Tom Gallagher and Ying Fang

(Journal of Virology. 90(10): 5163–5175.)

Abstract: Intercellular nanotube connections have been identified as an alternative pathway for cellular spreading of certain viruses. In cells infected with porcine reproductive and respiratory syndrome virus (PRRSV), nanotubes were observed connecting two distant cells with contiguous membranes, with the core infectious viral machinery (viral RNA, certain replicases and structural proteins) present in/on the intercellular nanotubes. Live-cell movies tracked the intercellular transport of a recombinant PRRSV that expressed green fluorescent protein (GFP)-tagged nsp2. In MARC-145 cells expressing PRRSV receptors, GFP-nsp2 moved from one cell to another through nanotubes in the presence of viral neutralizing antibodies. Intercellular transport of viral proteins did not require the PRRSV receptor, as it was observed in receptor-negative HEK-293T cells after transfection with an infectious clone of GFP-PRRSV. In addition, GFP-nsp2 was detected in HEK293-T cells co-cultured with recombinant PRRSV-infected MARC-145 cells. The intercellular nanotubes contained filamentous actin (F-actin) with myosin associated motor proteins. The F-actin and myosin-IIA were identified as co-precipitates with PRRSV nsp1β, nsp2, nsp2TF, nsp4, nsp7-8, GP5 and N proteins. Drugs inhibiting actin polymerization or myosin-IIA activation prevented nanotube formations and viral clusters in virus-infected cells. These data lead us to propose that PRRSV utilizes the host cell cytoskeletal machinery inside nanotubes for efficient cell-to-cell spread. This form of virus transport represents an alternative pathway for virus spread, which is resistant to the host humoral immune response.

2.1 Introduction

For many enveloped viruses, entry into a host cell is primarily through the binding of cellular receptors and subsequent endocytosis of the viral particle into the cells. The fusion of envelope with the endosomal membrane releases viral capsid into the cytosol of infected cell (1). However, for some enveloped viruses, alternative pathways for cell-to-cell transmission have been described (2-4). One emerging model proposes that some viruses can use long, filamentous intercellular connections (nanotubes) as a means to transport infectious viral materials to neighboring naïve cells. Previously, intercellular nanotubes have been described as nanotubules, tunneling nanotubes, and bridging conduits (5-9). The fundamental feature of the intercellular nanotube is a long membrane-bound extension that connects two neighboring cells and can also link multiple cells together to form complex cellular networks (6). Nanotubes are 50 to 200 nm in diameter and can span several cell distances. These structures are primarily composed of filamentous actin (F-actin) and also contain myosin as a motor to drive the movement of organelles or other cargo into neighboring cells (6, 9). Intercellular nanotubes offer cellular communication over long distances, particularly for transporting relatively large cellular materials (10).

In this study, we investigated whether porcine reproductive and respiratory syndrome virus (PRRSV) utilizes intercellular nanotubes as an alternative pathway to spread infection. PRRSV is an enveloped, positive-sense, single-stranded RNA virus. The viral genome is about 15 kb in length. The 5' two-third of the viral genome encodes two large replicase polyproteins, pp1a and pp1ab, which are proteolytically processed into at least 14 functional nonstructural proteins (11). Recently, two novel proteins, nsp2TF and nsp2N, were found to be expressed in nsp2-coding region through a -1/-2 ribosomal frameshifting mechanism (12, 13). The 3'-end of

viral genome encodes envelope proteins (GP2a, E, GP3, GP4 and GP5, ORF5a and M); and also nucleocapsid (N) protein that encapsulates the genomic RNA (14). PRRSV has a very restricted tropism for host cells. Among many different cell lines tested, only the African green monkey kidney cell line MA-104, and derivatives such as MARC-145, are fully permissive to PRRSV infection *in vitro* (15). In previous studies, the PRRSV receptor-mediated viral entry into host cells has been studied extensively (16). It was reported that PRRSV particles gain entry into host cells through standard clathrin-mediated endocytosis. Following endosome acidification and membrane fusion, the viral genome is released into the cytosol where viral transcription and replication occur (17, 18). In this study, we found that PRRSV also uses intercellular nanotubes for transporting the infectious viral materials (viral RNA, certain replicases and structural proteins) into the cytosol of a neighboring cell. This route of viral transmission involves the interaction of certain viral proteins with cytoskeleton proteins. More importantly, intercellular transport of viral materials was still detected in the presence of viral neutralizing antibodies, which provides a new insight into mechanisms of immune evasion and viral pathogenesis.

2.2 Materials and Methods

Cells and viruses. HEK-293T and MARC-145 cells were maintained in minimum essential medium (Gibco) supplemented with 10% fetal bovine serum and antibiotics (Streptomycin, 100μg/ml). Porcine alveolar macrophages were collected by lung lavage of a 7-week-old PRRSV-naïve pig using a method described previously (19). Macrophages were cultured in RPMI 1640 medium (Gibco) supplemented with 10% fetal bovine serum and 100μg/ml Streptomycin. Cells were maintained at 37 ^{o}C with 5% $CO_{2.}$ The PRRSV isolate SD95-21 (GenBank accession KC469618) was used for subsequent experiments. The green

fluorescent protein (GFP)-tagged recombinant PRRSV (GFP-PRRSV), constructed in this study (see below), was used for tracking PRRSV infection in real-time live cells.

Antibodies and probes. Table 2. 1 lists polyclonal and monoclonal antibodies used in this study. Antibodies for detecting PRRSV proteins, including monoclonal antibody (mAb) 123-128 (α-nsp1β), mAb 140-68 (α-nsp2 N-terminus), mAb NI37 (α-GP4), mAb SDOW17 (α-N), and a rabbit antiserum (pAb; α-nsp2TF) specific to the C-terminal peptide of nsp2TF were described previously (12, 13, 19-21). The pAb (α-nsp2) specific to C-terminal epitope (NGLKIRQISKPSGG) of nsp2 was produced by GenScript. The mAb 21-79 (α-GP5) was generated by immunizing BALB/c mice with a truncated GP5 recombinant protein (contains amino acids 31-61 and 128-200 of GP5), while the mAb 69-267 (α-nsp4), mAb 108-16 (α-nsp7), mAb 101-48 (α-nsp8), and mAb 14-126 (α-N) were produced by immunizing mice with individual full-length nsp4, nsp7, nsp8 and N recombinant protein as the antigen, respectively. Detailed experimental procedures for mAb production were described previously (22, 23). Anti-beta actin (also reacts with F-actin, as indicated by the vendor) and anti-non-muscle myosin IIA mAbs were obtained from Abcam, and rabbit antiserum to myosin IIA was purchased from Sigma. The Alexa Fluor® 555 Phalloidin for staining the F-actin and 4', 6-diamidino-2-phenylindole (DAPI) for staining the nucleus were purchased from Invitrogen. Polyclonal antibody sc-20800 (α-SV40 large T antigen) and anti-mouse IgG were purchased from Santa Cruz.

Plasmids and transfections. The plasmid (pCMV-SD95-21-GFP) for expression of GFP-PRRSV was constructed by inserting GFP gene into the pSD95-21 full-length cDNA infectious clone (24), in which nsp2 hypervariable region encoding amino acids 324 to 434 was replaced with the GFP gene (GenBank accession #AAB02574) to express GFP-nsp2 fusion

protein. For obtaining recombinant GFP-PRRSV, BHK-21 cells were seeded in a 6-well plate and transfected with plasmid DNA of pSD95-21-GFP. Recombinant viruses were recovered using the method as described previously (25). For detecting the GFP-nsp2 transportation through nanotubes, HEK-293T cells were seeded in 6-well plates and transfected with plasmids DNA of pCMV-SD95-21-GFP. Transfection was performed using HD-FuGENE 6 transfection reagent followed the manufacturer's instruction (Roche Molecular Biochemicals).

Viral RNA detection. Stellaris FISH Probes were designed and generated by Biosearch Technologies. Stellaris RNA FISH Probe Designer was used to analyze the RNA coding region of PRRSV N gene. The set of probes contains 43 CAL594-labeled specific probes was generated, which covers the 100% nucleotides of the N gene of PRRSV strain SD95-21. To detect the expression of PRRSV RNA, fixed cells were hybridized with the FISH Probe set, following the manufacturer's instructions. Briefly, MARC-145 cells were infected with PRRSV at MOI of 0.1 in 35 mm glass bottom dishes (MatTek). Cells were fixed at 18 hours post infectioin (hpi) with the fixation buffer (3.7% formaldehyde solution in nuclease free PBS) and then permeabilized with 70% ethanol for 2 hours (h) at 4 ℃. After discarding the ethanol, wash buffer A (20% Stellaris RNA FISH wash buffer A and 1% deionized formamide in nuclease-free water) was added and incubated for 5 minutes (min) at room temperature. Within the humidified chamber, 100 μL of the hybridization buffer that contains RNA detecting probe and anti-N mAb SDOW17 (1:2000 dilution) was dispensed onto the cells. After 4 h incubation in the dark at 37 ℃, 1 mL of wash buffer A plus 1:500 diluted goat-anti-mouse pAb conjugated with Alexa Fluor® 488 (Jackson ImmunoResearch) was added as the secondary antibody. The petri dishes were then incubated in the dark at 37 ℃ for additional 1 h. The cell nuclei were counterstained with 1μg/mL DAPI (Invitrogen). After washing with wash buffer B, the cover slips were

removed by the bottom glass removal fluid (MatTek) and mounted on the section slides with Prolong (Invitrogen). Confocal microscopy was performed with LSM 880 (Zeiss).

Immunofluorescent assays and live-cell microscopy. MARC-145 cells or porcine alveolar macrophages were grown on glass-bottom 35 mm cell culture dishes (MatTek). MARC-145 cells were infected with 0.1 MOI of PRRSV or mock-infected with the infection medium (Dulbecco's modified Eagle's medium containing 2% horse serum, 100 ug/mL streptomycin). Alternatively, porcine alveolar macrophages were infected with 1 MOI of PRRSV or mock-infected with the infection medium. At 12 hpi, cells were fixed with 4% paraformaldehyde (PFA) for 10 min, permeabilized with 0.5% Triton X-100 for 10 min, and then blocked with 1% BSA in PBS for 30 min at room temperature. To stain PRRSV proteins, specific mAb at a concentration of 1:1000 was used as we described previously (12, 20, 22). To detect filamentous actin (F-actin) or myosin-IIA, cells were stained with Alexa Fluor 594-conjugated phalloidin (Molecular Probes) or anti-myosin IIA Rabbit pAb (Sigma). After 1 h incubation at 37 ^{o}C, cells were washed with PBS, and a secondary antibody, Alexa Fluor® 488 AffiniPure goat anti-mouse IgG (Jackson ImmunoResearch) or Alexa Fluor® 594 AffiniPure goat anti-Rabbit IgG (Jackson ImmunoResearch) was added at a concentration of 1:250 in PBS. After incubating in room temperature for 1 h, cells were washed in PBS, and then mounted onto glass slides using Prolong Gold with DAPI (Invitrogen). Slides were left to set at 4 ^{o}C in the dark. For live-cell movies, infected MARC-145 cells or transfected HEK-293T cells were set into an open cultivation system of the Zeiss confocal microscope and maintained in warm DMEM buffered with HEPES. The live-cell chamber was mounted on a heated stage to maintain the culture at 37 ℃. Immunostained and live cells were imaged with an LSM880 Zeiss confocal microscope (Zeiss). Collected images were processed using Zen 2 andAdobe Photoshop CS3.

Co-cultivation of MARC-145 and HEK-293T cells. MARC-145 cells were infected with recombinant GFP-PRRSV (MOI =1). At 12 hpi, cells were washed with PBS, trypsinized, and 2×10^4 infected MARC-145 cells were mixed with 2×10^5 HEK-293T cells. The mixed cells were seeded on the 35 mm glass-bottomed cell culture dish. As controls, the GFP-PRRSV infected MARC-145 cells and HEK-293T cells were also cultured separately. After 36 h co-cultivation, cells were fixed with 4% PFA for 10 min, permeabilized with 0.5% Triton X-100 for 10 min, and then blocked with 1% BSA in 1x PBS for 30 min at room temperature. To differentiate HEK-293T cells from MARC-145 cells, cells were stained with pAb sc-20800 (Santa Cruz) that recognizes the SV40 large T antigen in HEK-293T cells. To detect PRRSV nsp2 protein, mAb 140-68 was used at a concentration of 1:1000. After 1 h incubation at 37 ˚C, cells were washed with PBS, and secondary antibodies, Alexa Fluor® 488 AffiniPure goat anti-mouse IgG (Jackson ImmunoResearch) and Alexa Fluor® 594 AffiniPure goat anti-Rabbit IgG (Jackson ImmunoResearch) were added at a concentration of 1:250 in PBS. After incubation in room temperature for 1 hour, cells were washed in 1x PBS. Immunostained cells were imaged with an LSM880 Zeiss confocal microscope (Zeiss). Collected images were processed using Zen 2 and Adobe Photoshop CS3.

Immunoprecipitation and SDS/PAGE. Whole-cell lysates of infected or transfected cells were suspended in Pierce® IP Lysis buffer. To reduce nonspecific background, cell lysates were precleared with pre-immune rabbit sera or nonspecific mouse ascites. Protein A/G Plus Magnetic beads (Pierce) and specific mAb were added to precleared cell lysates. After incubating overnight at 4 ℃, immune complexes were washed three times with wash buffer and one time with ultrapure water. After boiling in 2 × Laemmli sample buffer for 5 min, proteins were separated on an 8-16 % SDS/PAGE gradient gel (Invitrogen).

Western Blot. Western blot was performed as we described previously (12, 22). The membrane was probed with a protein specific mAb or pAb. IRDye 680-conjugated goat anti-rabbit Ab and/or IRDye 800CW-conjugated goat anti-mouse Ab (LICOR Biosciences) were used as the secondary antibody. Imaging of the blot was performed using an Odyssey infrared imaging system (LI-COR Biosciences).

Mass Spectrometry. Immunoprecipitation was performed as we described previously (12). Myosin and actin were co-immunoprecipitated (co-IP) from PRRSV-infected MARC-145 cells using anti-GP5 mAb. Proteins from co-IP were separated on an 8-16% SDS-PAGE gradient gel and stained with Coomassie Brilliant Blue G-250 (Bio-Rad). The gel was destained, and protein bands with predicted size of myosin and actin were excised. In gel trypsin digestion and MALDI-MS analysis (Bruker Daltonics Ultraflex II) were performed at Biotechnology and Proteomics Core Facility in Kansas State University. Mass spectra were searched against a SwissProt protein database and analyzed by mMass software (http://www.mmass.org).

Neutralization assays. Immune serum from PRRSV-infected pigs was initially used in standard PRRSV neutralizing assay as described previous (26). As a control, serum sample from mock-infected pigs was included in the assay. Briefly, a 2-fold dilution of the serum sample was prepared in a 96-well plate (100ul/well). PRRSV SD95-21 (200 TCID50; 100ul/well) was added to mix with serum to incubate for 1 h at 37 ^{o}C. After incubation, the serum-virus complex was transferred onto confluent MARC-145 cells that were plated 2-3 days ahead. At 18 hpi, cells were fixed using acetone-methanol (1:1 ratio) at -20 ℃ for 30 min. Fixed cells were stained with PRRSV N protein-specific mAb and Alexa Fluor® 488 AffiniPure goat anti-mouse IgG (Jackson ImmunoResearch) was used as a secondary antibody. Fluorescent foci of infected cells were observed and counted using a phase-contrast fluorescence microscope. Virus titers were

interpreted as the number of fluorescent-focus units per mL (FFU/mL). The serum dilution that caused greater than 90% inhibition of virus infection was used in subsequent experiment to determine its effect on intercellular spreading of the virus. PRRSV SD95-21 (200 TCID50) was first added onto confluent MARC-145 cells. After 3 h incubation at 37 ^{o}C to allow the virus entry into cells, the identified serum sample with known viral neutralizing titer was added onto the PRRSV-infected cells. At 6, 12, 24 or 36 hpi, cells were fixed, stained with specific antibodies, and analyzed as described in standard neutralizing assay. Cell culture supernatant was harvested at 6, 12, 24, 36 hpi, and virus titers were determined by virus titration on MARC-145 cells.

Drugs and virus replication inhibition assay. The actin inhibitors Cytochalasin D (Sigma) and myosin II inhibitor ML7 (Sigma) were dissolved in dimethyl sulfoxide (DMSO). Cytochalasin D and ML7 were stored as a 10 mM stock at -20 ℃ in aliquots for single use. For virus replication inhibition assay, confluent MARC-145 cells in bottom-glassed 12 well tissue culture plates (MatTek) were pretreated with compounds at concentration of 0 μM or 5 μM. After 30 min incubation at 37 ℃, the cells were infected with 200 $TCID_{50}$ of PRRSV. After 1 h incubation, the infected cells were washed twice with 1x PBS and the fresh medium containing the compounds was added. The cells were fixed and stained at 24 hpi, and the supernatant was collected for virus titration. PRRSV titers were determined by fluorescent focus assay, as we described previously (27). The cell viability was determined using CellTiter-Glo® Luminescent Cell Viability Assay kit (Promega) followed the manufacturer's instruction.

2.3 Results

Intercellular nanotubes contain PRRSV proteins and RNA. In previous studies of influenza virus and retrovirus transmission, viral membrane and nucleocapsid proteins were

found to be associated with intercellular nanotubes (7, 28, 29). To investigate the spreading of viral materials through intercellular nanotubes during PRRSV infection, MARC-145 cells were first infected with PRRSV strain SD95-21. Mock-infected cells were included as a control. At 12 hpi, cells were fixed, permeabilized and immunostained using mAbs against GP5 or N proteins. Since F-actin and myosin are known to be involved in the formation of the intercellular nanotubes, cells were also double stained for F-actin or myosin IIA to visualize nanotubes. Using confocal microscopy, contiguous, long F-actin and myosin IIA-containing intercellular nanotubes were clearly visualized connecting two neighboring cells. PRRSV infection seems promoting the intercellular nanotube formation. There was about 6.5-fold increase of the number of nanotubes in infected cells at 12hpi, in comparison to that of non-infected cells (data not shown). In PRRSV-infected MARC-145 cells, GP5 was detected as punctate dot-like structures spreading through the nanotubes, while N appeared to be inside the nanotubes (**Fig. 2. 1A**-**D**). Since the porcine alveolar macrophage (PAM) is the primary host cell of PRRSV, we also examined the PRRSV-infected PAM cells. Comparing to that of MARC-145 cells, nanotubes among PAM cells appeared to be less aboundance, which could be caused by the cell morphology and density. As showing in Fig. 1E-F, PRRSV GP5 and N were also detected to be associated with nanotubes connecting two PAM cells. These results suggested that, in addition to influenza and retro viruses (7, 29, 30), PRRSV could also transport viral materials through intercellular nanotube connections. We next determined which viral proteins could be transported through the nanotubes in MARC-145 cells. A panel of available polyclonal and monoclonal antibodies (**Table 2. 1**) was used in immunofluorescent confocal microscopy. Intercellular nanotubes were detected containing PRRSV nsp1β, nsp2, nsp2TF, nsp4, nsp7, and nsp8 in infected cells (**Fig. 2.1 A-F, H-M**). In all cases, the viral proteins were in highly

localized puncta. Interestingly, few nanotubes were observed containing GP4. Under the 10 microscopic fields of view that we searched, we only found one nanotube that contains GP4, most of the nanotubes that we detected were absent of GP4, although they connect the two neighbor infected cells (**Fig. 2.1 G and N**). To further confirm this result, we repeated the experiment and cells were double stained with anti-nsp2 pAb and anti-GP4 mAb. As a comparison, another treatment of cells was double stained with anti-nsp2 pAb and anti-GP5 mAb. Nanotubes connecting two infected cells can be easily detected under each microscopic field of view, and they all contain the nsp2 and GP5 (**Fig. 2.1 O and P**), however, most of them do not contain GP4 (**Fig. 2.1 O**); again, we only found two nanotubes contain both nsp2 and GP4 within 10 microscopic fields of view (**Fig. 2.1 Q**).

Previous studies showed that arterivirus replicase proteins associated with genomic RNAs to form replication and transcription complexes (RTCs), the viral replicative machinery inside the host cell (reviewed in 11). Thus, we suspected that PRRSV may transport entire RTCs through intercellular nanotubes. We performed fluorescence in situ hybridization to determine whether PRRSV RNA might be within nanotubes. Using a set of PRRSV N gene specific FISH probes labeled with Cal-594, viral RNA was indeed found within nanotubes (**Fig. 2. 3A**). Since viral N proteins are associated with genomic RNA to form nucleocapsids, N proteins were also immunostained and imaged. N proteins were indeed found to be co-localized with the viral RNA in the nanotubes (**Fig. 2. 3B-D**), suggesting that nucleocapsid proteins transport with viral RNA through intercellular nanotubes.

Cell-free virions are not required for intercellular spread of PRRSV infection through nanotubes. To determine whether intercellular nanotube connections could serve as an alternative pathway to transfer infections between cells, we analyzed PRRSV spread in the

presence of PRRSV neutralizing antibodies. Initially, standard virus neutralizing assay was used to determine the neutralizing antibody titer of a swine immune serum. As a control, a negative serum sample from uninfected pigs was included in the analysis. The result showed that the swine immune serum at the titer of 1:4 completely blocked the virus infection (**Fig. 2. 4A**), indicating that the swine serum blocked the initial virus entry into the host cells. To determine whether the virus could use an alternative pathway to spread the infection, we first infected cells with the virus in the absence of swine serum, and then added 1:4 swine immune serum at 3 hpi. At 6, 12, 24, and 36 hpi, cells were immunostained with anti-N mAb. At 6 hpi, single fluorescent infected cells were observed at frequencies equivalent to control cultures receiving negative serum. In general, it takes about 12 h for PRRSV to complete a cycle of replication and release progeny particles. In the presence of the virus-neutralizing serum, few small foci with intercellular nanotube connections were observed at 12 hpi; and larger foci with more nanotubes were observed at 24 and 36 hpi, indicating that the viruses were continuing spread from cell to cell in the presence of neutralizing antibody (**Fig. 2. 4B**). To confirm that neutralizing antibody remained through the time course, cell cultural supernatants were inoculated onto fresh MARC-145 cells. Culture supernatants containing swine immune serum did not generate any infections, while parallel control supernatants containing pre-immune serum generated infection with virus titer reached 2.5 x10^6 FFU /ml (**Fig. 2. 4C**).

The data in Figure 4 suggested that there are two modes of PRRSV spread, in which the virus could use both extracellular pathway and nanotubes to spread the infection. Specifically, our results (**Fig. 2. 4**) showed that presence of neutralizing antibody in the cell culture supernatant could neutralize the cell-free viruses, which made the viruses only (mainly) use the intercellular nanotube connections to spread the infection from cell to cell. To confirm this, live-

cell movies were taken to visualize the real-time movement of viral proteins. To track protein movement, we used a recombinant PRRSV (GFP-PRRSV) that expresses GFP-tagged nsp2. The experiment conducted to obtain Figure 4 data was repeated using GFP-PRRSV, in which infected cells were maintained in the cultural medium containing virus neutralizing antibody. At 24 hpi, infected cells were analyzed using a living cell imaging system. The movie was taken with 30-sec frames over a 70 min time course. GFP-nsp2 was clearly observed moving through an intercellular nanotube into another neighboring cell (Movie S1, supplementary data). Selected frames from the live cell movie are presented in **Fig. 2. 5A**, in which the yellow arrow and inset squares indicate the position of GFP-nsp2 as it moves from the lower cell into the upper cell. As a comparison, GFP-PRRSV infected cells maintained without PRRSV neutralizing antibody were also included in the analyses (Movie S2, supplementary data, and **Fig. 2. 5B**). Similar results were obtained in both cell cultural conditions.

PRRSV cell receptors are not required for intercellular spread of infection through nanotubes. Cell-free virus infections require host cell receptors (reviewed in 16). To determine whether nanotube-mediated transfer of PRSSV requires receptors, we transfected the full-length cDNA infectious clone of GFP-PRRSV, pSD95-21-GFP, into HEK-293T cells, and then monitored virus spread. HEK-293T cells do not express the PRRSV receptor, and cannot be infected by PRRSV virions, but can support PRRSV replication once the viral genome is transfected into the cells. At 24 h post transfection, cell culture supernatant was harvested and the virus titer was determined by fluorescent focus assay. The result confirmed that infectious viral progenies were produced in transfected cells, with virus titer reached 2×10^4 FFU/mL. Transfected cells were analyzed by the living-cell imaging system. GFP-nsp2 was clearly observed moving through an intercellular nanotube into another neighboring HEK-293T cell

(**Fig. 2. 5C, movie S3**). Of note, GFP-nsp2 appeared to be moving slower in HEK-293T cells, in comparison to that of MARC-145 cells (compare movies S1, S2 and S3). In the nanotubes that we observed, it took about 16 minutes for the GFP-nsp2 particle to move from one MARC-145 cell to another, while 67 minutes were required for the GFP-nsp2 particle to move from one HEK-293T cell to another.

To further confirm our result, we determined whether viral components could transfer from infected MARC-145 to uninfected, PRRSV receptor-negative HEK293T cells. MARC-145 and HEK293T cells co-cultivation experiment was performed. MARC-145 cells were first infected with GFP-PRRSV (**Fig. 2. 6A**), then mixed at 12 hpi with naïve HEK-293T cells. After 36 h of cell co-cultivation, cells were fixed and visualized by confocal microscopy. Since GFP fluorescence becomes dim after cell fixation, we used anti-nsp2 mAb to detect the expression of GFP-nsp2 in the infected cells (**Fig. 2. 6**, first column). To differentiate the HEK-293T cells from MARC-145 cells, we used rabbit antiserum that specifically recognizes SV40 large T-antigen of HEK-293T cells (Fig. 6; second column). Notably, nanotubes were observed connecting infected MARC-145 cells with HEK293T cells, and GFP-nsp2 was detected in the nanotube connection and in the target HEK293T cell (**Fig. 2. 6**, row C). In this particular image, the infection transfer from the MARC-145 cell was to a fairly distant HEK293T cell.

Cytoskeleton proteins are involved in intercellular transportation of viral proteins. Given that cytoskeleton proteins F-actin and myosin are present in intercellular nanotube structures, we determined whether nanotube-associated viral proteins interact with the cytoskeleton proteins. The membrane proteins of several other viruses were previously reported to interact with myosin (8, 30). Interaction of PRRSV GP5 and myosin was initially analyzed by immunoprecipitation. Lysates of PRRSV-infected MARC-145 cells were harvested at 36 hpi,

and viral proteins were immunoprecipitated using anti-GP5 mAb and then separated by SDS-PAGE. Protein bands were detected by Coomassie Brilliant Blue staining. Excluding the two bands of 50 and 25 kDa of the mAb heavy and light chains, the other two prominent bands with apparent masses close to 250 kDa and 50 kDa were subjected for MALDI/MS analysis. The band close to 250 kDa was identified as non-muscle myosin heavy chain IIA (myosin IIA; predicted molecular weight of 215 kDa), while the band close to 50 kDa was identified as F-actin (predicted molecular weight of 42 kDa; **Fig. 2. 7A**). Subsequently, we determined whether those PRRSV proteins present in the nanotubes (**Fig. 2. 1-2. 2**) also interacted with myosin and F-actin. A panel of specific antibodies recognizing PRRSV nsp1β, nsp2, nsp2TF, nsp4, nsp7, nsp8, GP4, GP5 and N protein were used in IP and Western blot analysis. Immunoprecipitated proteins from PRRSV-infected cells were separated by SDS-PAGE, transferred to nitrocellulose membranes, and probed with antibodies against myosin IIA and F-actin. Western blots confirmed that myosin IIA and F-actin co-precipitated with GP5, but they were not detected in the co-precipitate of GP4 (**Fig. 2. 7B**). The specificity of the experimental condition was further confirmed using anti-mouse IgG as a control. Subsequently, myosin IIA and F-actin were also detected as co-precipitates with N, nsp1β, nsp2, nsp2TF, nsp4, nsp7, and nsp8 (**Fig. 2. 7B-C**). This result is consistent with those shown in Figure 1-2, in which GP5, N, nsp1β, nsp2, nsp2TF, nsp4, nsp7, and nsp8 were associated with nanotubes.

To verify the specific interaction of PRRSV proteins with myosin IIA and F-actin, co-IP was performed in PRRSV-infected cells using antibodies against myosin IIA or F-actin. Western blot analysis using PRRSV protein specific antibodies detected GP5, N, nsp1β, nsp2, and nsp4 co-precipitated with myosin-IIA (**Fig. 2. 7D-E, G-H, and J**). Again, GP4 was not detected (**Fig. 2. 7F**). In addition, nsp2TF, nsp7 and nsp8 were also not specifically detected, although they

were detected in the nanotubes and their specific mAbs were able to pull down the myosin in co-IP experiment (**Fig. 2.7B**). When analyzing the IP products with the anti-F actin mAb, none of the PRRSV proteins were found to co-precipitate with F-actin, suggesting that the specific anti-F-actin mAb might be defect for use in IP.

Since F-actin and myosin are within nanotube structures, and myosin IIA was identified to interact with certain viral proteins, we further determined whether disrupting the structure of F-actin and myosin II-A could block the intercellular nanotube pathway for cell-cell spreading of the viruses. PRRSV infected cells were treated with ML7, cytochalasin D, or solvent control dimethyl sulfoxide (DMSO; 0 uM). ML7 is a specific inhibitor of myosin light chain kinase, regulating myosin IIA function. Cytochalasin D depolymerizes actin by binding to F-actin, which causes breakage of the actin filaments. Using confocal microscopy, PRRSV-infected cells that treated with ML7 or cytochalasin D showed significantly fewer (80% less) intercellular nanotube connections in comparison to that treated with DMSO and few viral clusters were observed at 24 dpi (**Fig. 2. 8A**). In the presence of either inhibitor, cell viabilities were not affected at the tested concentrations (5 μM for ML7 and cytochalasin D; **Fig. 2. 8B**), but viral titers were reduced by several logs (2.56 log reduction for ML7; 1.93 log reduction for cytochalasin D), in comparison to that of DMSO control (**Fig. 2. 8C**).

2.4 Discussion

The primary pathway for cell-to-cell spread of the PRRSV virus, an enveloped RNA virus, involves assembly, maturation, and release from virus-producing cells and attachment, entry, and disassembly in virus target cells. These processes require abundant cellular resources and also demand that the virus particles evade extracellular host defensive components. In this study, we found that PRRSV can use intercellular nanotube connections as an alternative

pathway for cell-to-cell spread. Utilizing this pathway to directly access the cytoplasm of a naive cell presents an efficient spreading route that bypasses many of the otherwise critical assembly, budding, and cell entry steps.

Inside the host cell cytoplasm, the genomic RNA and replicase-associated RTC constitute the infectious core components that elicit a productive infection. Thus, intercellular transport of viral genomic RNA and replicase proteins is sufficient for rapid spreading of the infection. In PRRSV infected cells, confocal images showed that PRRSV replicase proteins nsp1β, nsp2, nsp4, nsp7 and nsp8 were associated with intercellular nanotubes. The presence of PRRSV nsp2 in an intercellular connection was reported previously, but the mechanism by which this protein arrived in the connection, and its relevance to virus spread, was unknown at that time (31). In our study, the movement of viral proteins from cell-to-cell was documented with live cell movies, in which GFP-tagged nsp2 transported from one cell to another in GFP-PRRSV-infected cells. This process was further demonstrated to take place between unrelated MARC-145 and HEK-293T cells. Since nsp1β, nsp2, nsp4, nsp7 and nsp8 are components of viral RTC, the data indicate that PRRSV transports RTC components through intercellular nanotubes. The PRRSV nsp9-12 proteins are also assumed to be part of the RTC. The nsp9 is generated by -1 PRF at ORF1a/1b junction, resulted the nsp9 product that contains nsp8 in its N-terminus. This means the anti-nsp8 mAb could also recognize the nsp9; however, future study using the nsp9 C-terminus specific antibody is needed to confirm the presence of nsp9 in the nanotube connections. Due to lack of specific antibodies to nsp1α, nsp5-6, and nsp10-12, whether these replicase-associated proteins are transported through the nanotube connections needs to be determined in the future. Furthermore, double-membrane vesicles (DMVs) were previously reported to be associated with RTC of arterivirus (32); it is possible that DMVs transport with the viral materials. In mouse

CAD cells, vesicles of lysosomal origin carrying prion proteins are actively transferred through intercellular nanotubes (33). In HIV type 1 infections, viral material-containing endosome cargoes were transported through nanotubes to neighboring uninfected macrophages (8). The involvement of cellular vesicles in nanotube transport of viral materials is currently under active investigation in our laboratories. Notably, the novel PRRSV -2 PRF product, nsp2TF, was also observed to associate with intercellular nanotubes, but was not co-localized with the other nanotube-associated nsps (data not shown). This is consistent with our previous findings, in which nsp2TF and nsp2 are not co-localized in infected cells (12). Therefore, there may be multiple independent mechanisms for nsp association with nanotubular components.

Theoretically, viral membrane proteins typically needed for virus-cell egress and entry might be dispensable for virus transport through intercellular nanotubes. Recent studies suggested that PRRSV minor GPs (GP2a, GP3 and GP4) are the primary determinants of host cell binding and may also involve in membrane fusion and entry (34, 35). Using the PRRSV GP4-specific mAb, few nanotubes were detected containing GP4, which support the notion that these membrane proteins may not be required for spreading the infection using the intercellular nanotube pathway. In contrast, significant amounts of GP5 proteins were detected to be associated with intercellular nanotubes. It was reported that GP5/M heterodimer of arterivirus play an important role in viral envelope formation (36-38). Gp5 and M have been proposed to be the driving force for virus budding, which may involve in the formation of the highly curved edges of the membrane (39). Our confocal microscopic images showed that GP5 proteins appeared as cell surface membrane-bound structures around the infected cells as well as on the intercellular nanotubes. The result made us suspect that GP5 could be integrated into the extended cell surface membrane during the formation of intercellular tunnels (nanotubes), in

which GP5 becomes a component of the nanotube for transporting the other viral infectious core materials. It is unknown whether GP5 is directly involved in the transporting process of viral materials or is a more passive component of nanotubes. The unavailability of the anti-M protein antibody and also antibodies to GP2a, E, and GP3 prevented us from analyzing the association of these proteins with nanotubes. Future studies are needed to determine whether M and other membrane proteins play a role in the intercellular spreading of the virus through nanotube connections. In addition, it will be interesting to know whether one or more viral membrane proteins promote nanotubular extension from a cell and fusion with a neighboring cell. Our data showed that PRRSV receptors are not required for nanotubular virus transport, which suggest that viral fusion proteins may not be needed to establish the nanotubular connections. Future in-depth analyses are needed to determine whether PRRSV infection and certain viral protein(s) promote nanotube formation.

Using the FISH method, viral RNA and N protein were observed to be largely co-localized within the nanotubes. This result is expected, since viral genomic RNA is required to generate the next cycle of viral replication. As discussed above, viral genomic RNA is packaged with N proteins to form the nucleocapsid. Transporting the N protein-bonded RNA from cell-to-cell could be a mechanism for protecting the integrity of viral RNA during the transportation process. It still needs to be elucidated whether the assembled nucleocapsid was transported or only unassembled proteins were transported.

Intercellular nanotubes are composed of F-actin, and myosin is known as a motor protein binding to the F-actin (40, 41). Myosin is encoded by a multigene family and expressed as multiple isoforms (42). Previously, myosin Va was reported to facilitate the movement of organelles along intercellular nanotubes (9). Recently, myosin X was reported to play an

important role in the formation of functional intercellular nanotubes within neuronal CAD cells (43). The findings of our study suggest that myosin IIA could be driving the transportation of PRRSV core infectious materials through the intercellular nanotube connections. In live cell movies, we noticed that the movement of GFP-nsp2 within nanotubes proceeded by leaping rather than by gradual transitions, a pattern which is consistent with motor-protein assisted cargo transport. Our co-IP results showed that myosin IIA can be co-precipitated with PRRSV nsp1β, nsp2, nsp4, GP5 and N, suggesting these viral proteins may directly or indirectly bind to myosin IIA during transport. Confocal microscopy also detected PRRSV nsp2TF, nsp7 and nsp8 in the intercellular nanotubes, and using nsp2TF, nsp7 and nsp8 specific antibodies, myosin IIA could be co-precipitated from infected cells. However, using myosin IIA-specific antibody, these viral proteins were not co-precipitated. This could be caused by lower protein expression levels, the insensitivity of our assay, or other unrevealed mechanism(s). Future studies are needed to determine the mechanisms of interaction between GP5 and other viral proteins with cytoskeleton proteins; and the detailed intercellular nanotube transporting process needs to be elucidated, including the process of how the viral materials are initially loaded, transported through the nanotubes, and unloaded in the target cells.

The use of intercellular nanotube connections as alternative pathways for viral cell-to-cell transmission could contribute to the pathogenesis of viral infection. Notably, PRRSV-neutralizing antibodies could block initial virus entry into the host cells, but could not interfere significantly with cell-to-cell transmission through intercellular nanotube connections. Previous studies also reported that viral spread through intercellular connections allows many viruses to evade neutralizing antibodies, including Influenza A virus and HIV (7, 44). Neutralizing antibodies that effectively inhibit cell-free HIV from infection are less effective or fail entirely to

inhibit cell-to-cell transmission of the virus (44). In a previous study (45), passive transfer of PRRSV-neutralizing antibodies to young weaned pigs could block viremia in blood, but could not prevent virus replication in peripheral tissues, and viral loads could reach the level similar to that of control pigs. Those pigs could still excrete infectious viruses to sentinels similar to that of control pigs. We speculate that cell-to-cell transmission of PRRSV through intercellular nanotubes could take place in peripheral tissues, a process that is resistant to neutralizing antibodies. This may contribute to viral persistence in peripheral tissues. Future studies are needed to elucidate the extent by which nanotubular intercellular transmission contributes to PRRSV spread *in vivo*, and whether this process is involved in viral pathogenesis. If this mechanism is truly central to the pathogenesis of PRRSV infection and persistence, the development of inhibitors that directly block this process would be critical to prevent the spread of viral infections.

2.5 References

1. Marsh M, Helenius A. 1989. Virus Entry into Animal-Cells. Advances in Virus Research 36:107-151.
2. Zhong P, Agosto LM, Munro JB, Mothes W. 2013. Cell-to-cell transmission of viruses. Current Opinion in Virology 3:44-50.
3. Mothes W, Sherer NM, Jin J, Zhong P. 2010. Virus Cell-to-Cell Transmission. Journal of Virology 84:8360-8368.
4. Sattentau Q. 2008. Avoiding the void: cell-to-cell spread of human viruses. Nature Reviews Microbiology 6:815-826.
5. Xu WF, Santini PA, Sullivan JS, He B, Shan MM, Ball SC, Dyer WB, Ketas TJ, Chadburn A, Cohen-Gould L, Knowles DM, Chiu A, Sanders RW, Chen K, Cerutti A. 2009. HIV-1 evades virus-specific IgG2 and IgA responses by targeting systemic and

intestinal B cells via long-range intercellular conduits. Nature Immunology 10:1008-U106.

6. Gerdes HH, Bukoreshtliev NV, Barroso JFV. 2007. Tunneling nanotubes: A new route for the exchange of components between animal cells (vol 581, pg 2194, 2007). Febs Letters 581:3332-3332.
7. Roberts KL, Manicassamy B, Lamb RA. 2015. Influenza A Virus Uses Intercellular Connections To Spread to Neighboring Cells. Journal of Virology 89:1537-1549.
8. Kadiu I, Gendelman HE. 2011. Human Immunodeficiency Virus type 1 Endocytic Trafficking Through Macrophage Bridging Conduits Facilitates Spread of Infection. Journal of Neuroimmune Pharmacology 6:658-675.
9. Rustom A, Saffrich R, Markovic I, Walther P, Gerdes HH. 2004. Nanotubular highways for intercellular organelle transport. Science 303:1007-10.
10. Ahmed KA, Xiang J. 2011. Mechanisms of cellular communication through intercellular protein transfer. Journal of Cellular and Molecular Medicine 15:1458-1473.
11. Fang Y, Snijder EJ. 2010. The PRRSV replicase: Exploring the multifunctionality of an intriguing set of nonstructural proteins. Virus Research 154:61-76.
12. Fang Y, Treffers EE, Li YH, Tas A, Sun Z, van der Meer Y, de Ru AH, van Veelen PA, Atkins JF, Snijder EJ, Firth AE. 2012. Efficient-2 frameshifting by mammalian ribosomes to synthesize an additional arterivirus protein. Proceedings of the National Academy of Sciences of the United States of America 109:E2920-E2928.
13. Li YH, Treffers EE, Napthine S, Tas A, Zhu LC, Sun Z, Bell S, Mark BL, van Veelen PA, van Hemert MJ, Firth AE, Brierley I, Snijder EJ, Fang Y. 2014. Transactivation of programmed ribosomal frameshifting by a viral protein. Proceedings of the National Academy of Sciences of the United States of America 111:E2172-E2181.
14. Snijder EJ, Kikkert M, Fang Y. 2013. Arterivirus molecular biology and pathogenesis. Journal of General Virology 94:2141-2163.
15. Kim HS, Kwang J, Yoon IJ, Joo HS, Frey ML. 1993. Enhanced Replication of Porcine Reproductive and Respiratory Syndrome (Prrs) Virus in a Homogeneous Subpopulation of Ma-104 Cell-Line. Archives of Virology 133:477-483.
16. Welch SKW, Calvert JG. 2010. A brief review of CD163 and its role in PRRSV infection. Virus Research 154:98-103.

17. Nauwynck HJ, Duan X, Favoreel HW, Van Oostveldt P, Pensaert MB. 1999. Entry of porcine reproductive and respiratory syndrome virus into porcine alveolar macrophages via receptor-mediated endocytosis. Journal of General Virology 80:297-305.
18. Kreutz LC, Ackermann MR. 1996. Porcine reproductive and respiratory syndrome virus enters cells through a low pH-dependent endocytic pathway. Virus Research 42:137-147.
19. Nelson EA, Christopherhennings J, Drew T, Wensvoort G, Collins JE, Benfield DA. 1993. Differentiation of United-States and European Isolates of Porcine Reproductive and Respiratory Syndrome Virus by Monoclonal-Antibodies. Journal of Clinical Microbiology 31:3184-3189.
20. Ropp SL, Wees CEM, Fang Y, Nelson EA, Rossow KD, Bien M, Arndt B, Preszler S, Steen P, Christopher-Hennings J, Collins JE, Benfield DA, Faaberg KS. 2004. Characterization of emerging European-like porcine reproductive and respiratory syndrome virus isolates in the United States. Journal of Virology 78:3684-3703.
21. Chen Z, Lawson S, Sun Z, Zhou X, Guan X, Christopher-Hennings J, Nelson EA, Fang Y. 2010. Identification of two auto-cleavage products of nonstructural protein 1 (nsp1) in porcine reproductive and respiratory syndrome virus infected cells: nsp1 function as interferon antagonist. Virology 398:87-97.
22. Li YH, Tas A, Snijder EJ, Fang Y. 2012. Identification of porcine reproductive and respiratory syndrome virus ORF1a-encoded non-structural proteins in virus-infected cells. Journal of General Virology 93:829-839.
23. Rowland RRR, Chauhan V, Fang Y, Pekosz A, Kerrigan M, Burton MD. 2005. Intracellular localization of the severe acute respiratory syndrome coronavirus nucleocapsid protein: Absence of nucleolar accumulation during infection and after expression as a recombinant protein in Vero cells. Journal of Virology 79:11507-11512.
24. Li YH, Zhu LC, Lawson SR, Fang Y. 2013. Targeted mutations in a highly conserved motif of the nsp1 beta protein impair the interferon antagonizing activity of porcine reproductive and respiratory syndrome virus. Journal of General Virology 94:1972-1983.
25. Fang Y, Rowland RRR, Roof M, Lunney JK, Christopher-Hennings J, Nelson EA. 2006. A full-length cDNA infectious clone of North American type 1 porcine reproductive and respiratory syndrome virus: Expression of green fluorescent protein in the Nsp2 region. Journal of Virology 80:11447-11455.

26. Yoon IJ, Joo HS, Goyal SM, Molitor TW. 1994. A Modified Serum Neutralization Test for the Detection of Antibody to Porcine Reproductive and Respiratory Syndrome Virus in Swine Sera. Journal of Veterinary Diagnostic Investigation 6:289-292.
27. Sun Z, Li Y, Ransburgh R, Snijder EJ, Fang Y. 2012. Nonstructural protein 2 of porcine reproductive and respiratory syndrome virus inhibits the antiviral function of interferon-stimulated gene 15. J Virol 86:3839-50.
28. Sowinski S, Jolly C, Berninghausen O, Purbhoo MA, Chauveau A, Kohler K, Oddos S, Eissmann P, Brodsky FM, Hopkins C, Onfelt B, Sattentau Q, Davis DM. 2008. Membrane nanotubes physically connect T cells over long distances presenting a novel route for HIV-1 transmission. Nature Cell Biology 10:211-219.
29. Jing Jin NMS, Gisela Heidecker, David Derse, Walther Mothes. 2009. Assembly of the Murine Leukemia Virus Is Directed towards Sites of Cell- Cell Contact. PLoS Biol 7(7): e1000163. doi:10.1371/journal.pbio.1000163.
30. Sun YY, Qi YH, Liu CX, Gao WQ, Chen P, Fu LR, Peng B, Wang HM, Jing ZY, Zhong GC, Li WH. 2014. Nonmuscle Myosin Heavy Chain IIA Is a Critical Factor Contributing to the Efficiency of Early Infection of Severe Fever with Thrombocytopenia Syndrome Virus. Journal of Virology 88:237-248.
31. Kappes MA, Miller CL, Faaberg KS. 2013. Highly Divergent Strains of Porcine Reproductive and Respiratory Syndrome Virus Incorporate Multiple Isoforms of Nonstructural Protein 2 into Virions. Journal of Virology 87:13456-13465.
32. Oostra M, Hagemeijer MC, van Gent M, Bekker CPJ, Lintelo EGT, Rottier PJM, de Haan CAM. 2008. Topology and Membrane Anchoring of the Coronavirus Replication Complex: Not All Hydrophobic Domains of nsp3 and nsp6 Are Membrane Spanning. Journal of Virology 82:12392-12405.
33. Gousset K, Schiff E, Langevin C, Marijanovic Z, Caputo A, Browman DT, Chenouard N, de Chaumont F, Martino A, Enninga J, Olivo-Marin JC, Mannel D, Zurzolo C. 2009. Prions hijack tunnelling nanotubes for intercellular spread. Nature Cell Biology 11:328-U232.
34. Tian DB, Wei ZZ, Zevenhoven-Dobbe JC, Liu RX, Tong GZ, Snijder EJ, Yuan SS. 2012. Arterivirus Minor Envelope Proteins Are a Major Determinant of Viral Tropism in Cell Culture. Journal of Virology 86:3701-3712.

35. Das PB, Dinh PX, Ansari IH, de Lima M, Osorio FA, Pattnaik AK. 2010. The Minor Envelope Glycoproteins GP2a and GP4 of Porcine Reproductive and Respiratory Syndrome Virus Interact with the Receptor CD163. Journal of Virology 84:1731-1740.
36. Wieringa R, de Vries AAF, van der Meulen J, Godeke GJ, Onderwater JJM, van Tol H, Koerten HK, Mommaas AM, Snijder EJ, Rottier PJM. 2004. Structural protein requirements in equine arteritis virus assembly. Journal of Virology 78:13019-13027.
37. Wissink EHJ, Kroese MV, van Wijk HAR, Rijsewijk FAM, Meulenberg JJM, Rottier PJM. 2005. Envelope protein requirements for the assembly of infectious virions of porcine reproductive and respiratory syndrome virus. Journal of Virology 79:12495-12506.
38. Nam HM, Chae KS, Song YJ, Lee NH, Lee JB, Park SY, Song CS, Seo KH, Kang SM, Kim MC, Choi IS. 2013. Immune responses in mice vaccinated with virus-like particles composed of the GP5 and M proteins of porcine reproductive and respiratory syndrome virus. Archives of Virology 158:1275-1285.
39. Veit M, Matczuk AK, Sinhadri BC, Krause E, Thaa B. 2014. Membrane proteins of arterivirus particles: Structure, topology, processing and function. Virus Research 194:16-36.
40. Lorenz M, Holmes KC. 2010. The actin-myosin interface. Proceedings of the National Academy of Sciences of the United States of America 107:12529-12534.
41. Taylor MP, Koyuncu OO, Enquist LW. 2011. Subversion of the actin cytoskeleton during viral infection. Nature Reviews Microbiology 9:427-439.
42. Weiss A, Leinwand LA. 1996. The mammalian myosin heavy chain gene family. Annual Review of Cell and Developmental Biology 12:417-439.
43. Gousset K, Marzo L, Commere PH, Zurzolo C. 2013. Myo10 is a key regulator of TNT formation in neuronal cells. Journal of Cell Science 126:4424-4435.
44. Schiffner T, Sattentau QJ, Duncan CJA. 2013. Cell-to-cell spread of HIV-1 and evasion of neutralizing antibodies. Vaccine 31:5789-5797.
45. Lopez OJ, Oliveira MF, Garcia EA, Kwon BJ, Doster A, Osorio FA. 2007. Protection against porcine reproductive and respiratory syndrome virus (PRRSV) infection through passive transfer of PRRSV-neutralizing antibodies is dose dependent. Clinical and Vaccine Immunology 14:269-275.

Table 2.1 List of antibodies used in this study.

Virus or cellular proteins	Antibody name*	Protein target	Predicted molecular mass (kDa)	References
PRRSV (SD95-21)	mAb 123-128	nsp1β	23.0	(21)
	pAb nsp2TF	nsp2TF (epitope CFLKVGVKSAGDLV)	110.1	(12, 13)
	pAb nsp2	nsp2 (C-terminus) (epitope NGLKIRQISKPSGG)	129.4	This study
	mAb 140-68	nsp2 (PLP2)	129.4	(13)
	mAb 69-267	nsp4	21.0	This study
	mAb 108-16	nsp7	28.6	This study
	mAb 101-48	nsp8	4.9	This study
	mAb NI37	GP4	19.5	(20)
	mAb 21-79	GP5	22.4	This study
	mAb SDOW17	N	13.6	(19)
	mAb 14-126	N	13.6	This study
Cellular Proteins	mAb ab8226	F-actin (beta actin)	42	Abcam
	mAb ab55456	non-muscle myosin IIA	215 (heavy chain)	Abcam
	pAb HPA001644	non-muscle myosin IIA	215 (heavy chain)	Sigma
	pAb sc-20800	SV40 large T-antigen of HEK-293T cell	94	Santa Cruz

* mAbs produced in mouse; pAbs produced in rabbit.

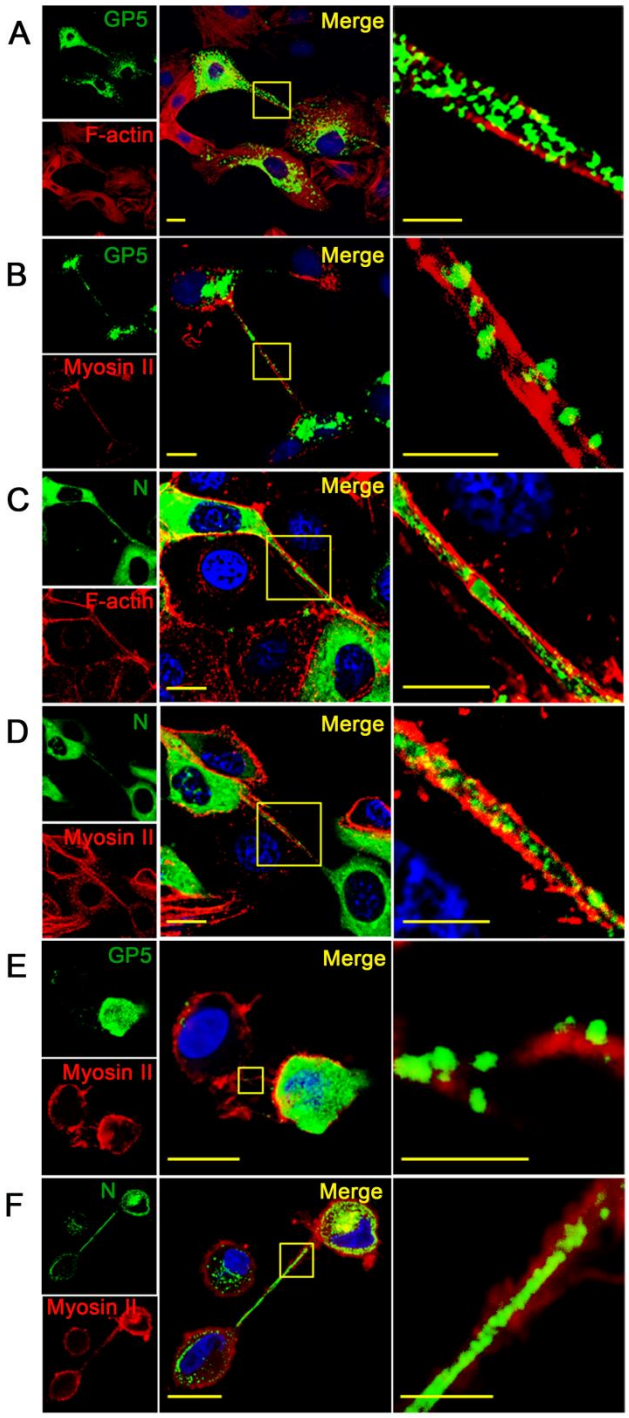
A
GP5
F-actin
Merge
B
GP5
Myosin II
Merge
C
N
F-actin
Merge
D
N
Myosin II
Merge
E
GP5
Myosin II
Merge
F
N
Myosin II
Merge

Figure 2.1 Detection of intercellular nanotubes containing PRRSV GP5 and N protein. Panels A-D: MARC-145 cells were infected by PRRSV strain SD95-21 at 0.1 moi and fixed at 12 hpi. Panel E-F: Porcine alveolar macrophages were infected with 1 MOI of PRRSV and fixed at 12 hpi. The fixed cells were immunostained for GP5 (green; A, B and E) or N protein (green; C, D and F) together with cytoskeleton protein of F-actin (red; A and C) or myosin-IIA (red; B, D, E and F). Images were taken by a confocal microscope (LSM 880, Zeiss). Scale bar for the merge pictures (middle column), 10 μm. Scale bar for the zoomed pictures (right column), 5 μm.

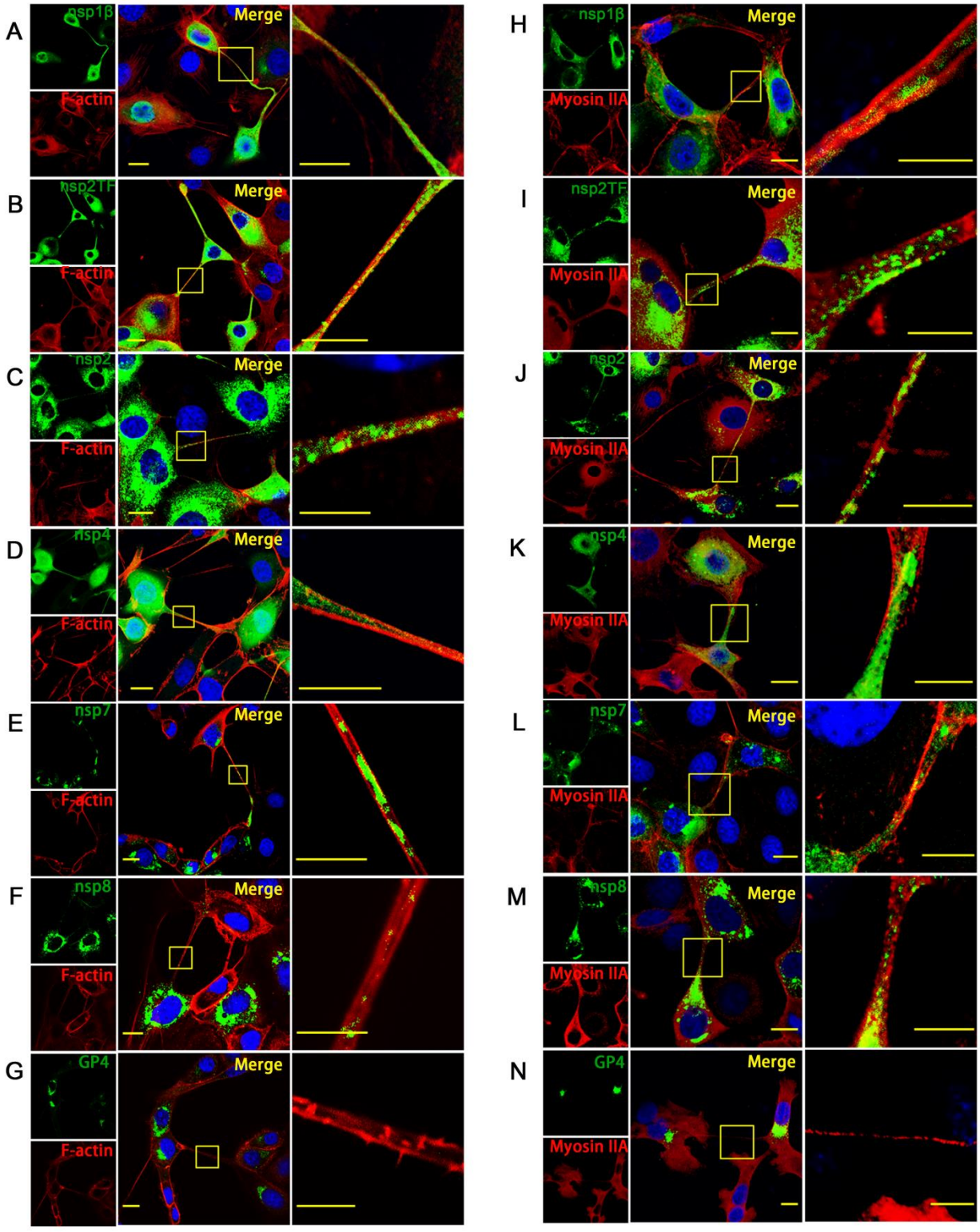
A
nsp1β
F-actin
Merge
B
nsp2TF
F-actin
Merge
C
nsp2
F-actin
Merge
D
nsp4
F-actin
Merge
E
nsp7
F-actin
Merge
F
nsp8
F-actin
Merge
G
GP4
F-actin
Merge
H
nsp1β
Myosin IIA
Merge
I
nsp2TF
Myosin IIA
Merge
J
nsp2
Myosin IIA
Merge
K
nsp4
Myosin IIA
Merge
L
nsp7
Myosin IIA
Merge
M
nsp8
Myosin IIA
Merge
N
GP4
Myosin IIA
Merge

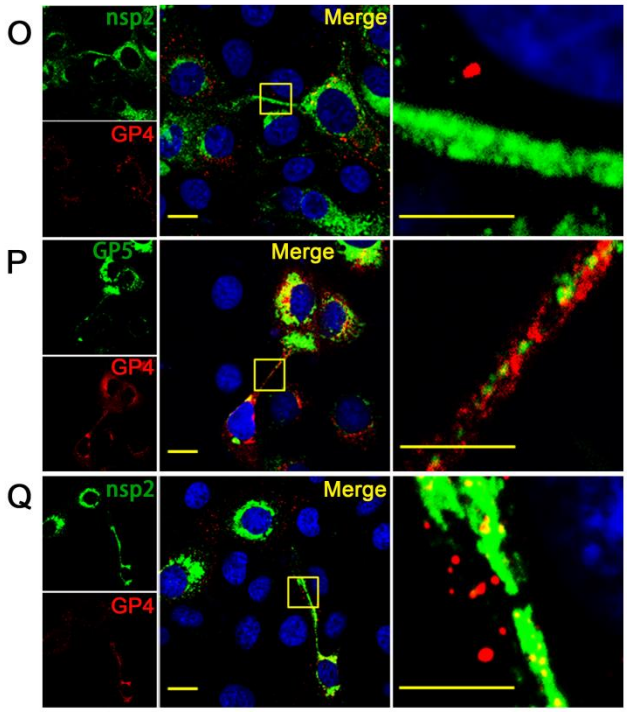

Figure 2.2 Intercellular nanotubes contain viral proteins in PRRSV-infected cells. MARC-145 cells were infected by PRRSV strain SD95-21 at 0.1 moi and fixed at 12 hpi. Panels A-N: The fixed cells were immunostained for nsp1β (A, H), nsp2TF (B, I), nsp2 (C, J), nsp4 (D, K), nsp7 (E, L), nsp8 (F, M) or GP4 (G, N) together with F-actin (A-G) or Myosin-IIA (H-N). Viral proteins were labeled with green fluorescence and cytoskeleton proteins were labeled with red fluorescence. Panels O-Q: Double staining of nsp2 with G4 (O and Q) or GP5 (P). The PRRSV nsp2 was labeled with green fluorescence; and GP4 or GP5 was labeled with red fluorescence. Pictures were taken by a confocal microscope (LSM 880, Zeiss). Scale bar for the merge pictures (middle column), 10 μm. Scale bar for the zoomed pictures (right column of each panel), 5 μm.

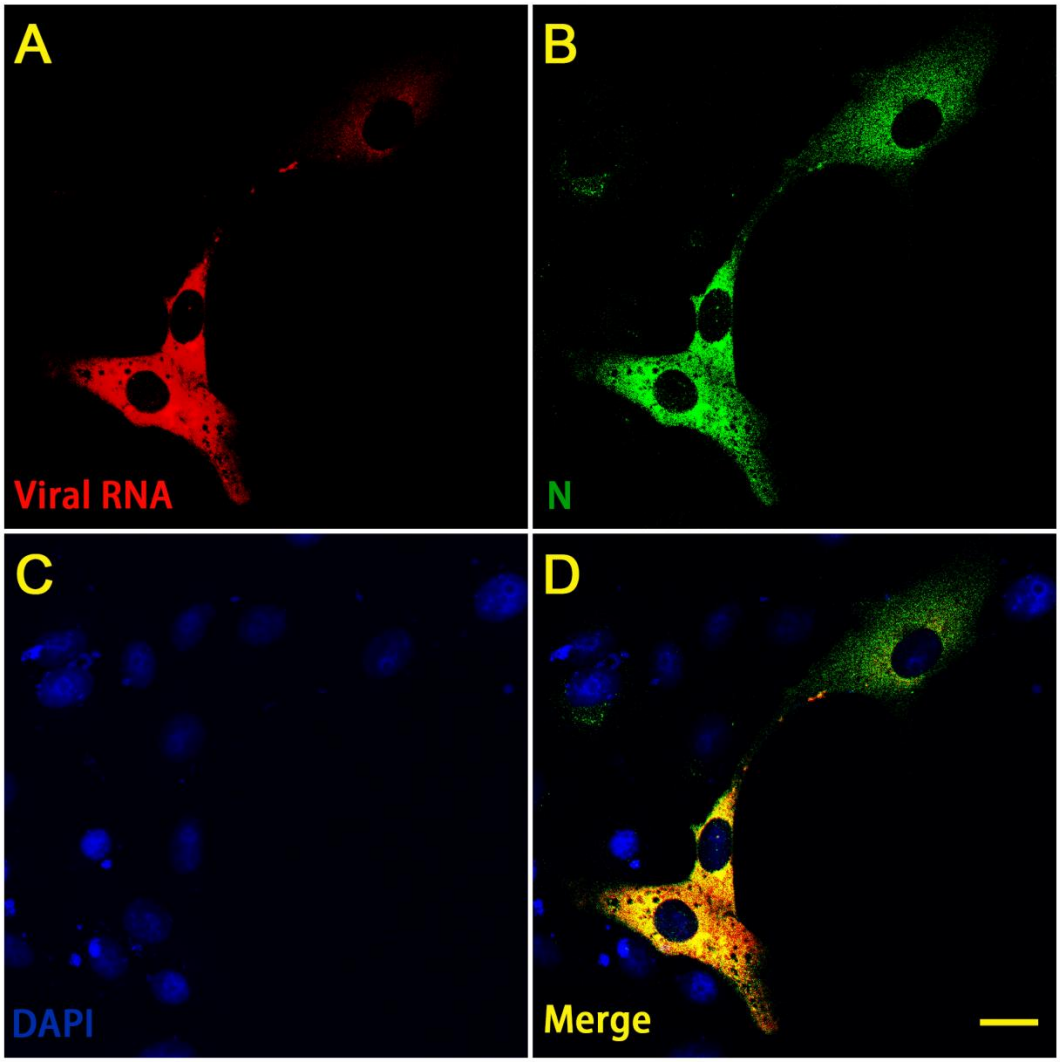

Figure 2.3 Detection of PRRSV RNA in the intercellular nanotube connections. MARC-145 cells were infected by PRRSV SD95-21 strain at 0.1 moi and fixed at 12 hpi. Viral RNA was detected by fluorescence in-situ hybridization of RNA using CAL594-labeled PRRSV N gene RNA FISH probe (A, red). PRRSV N protein was immunostained using anti-N mAb SDOW17 (B, Green). Cell nucleus is stained with DAPI (C, blue). The co-localized foci are readily visible in the nanotubes (D, yellow). Images were taken by a confocal microscope (LSM 880, Zeiss). Scale bar 20 μm.

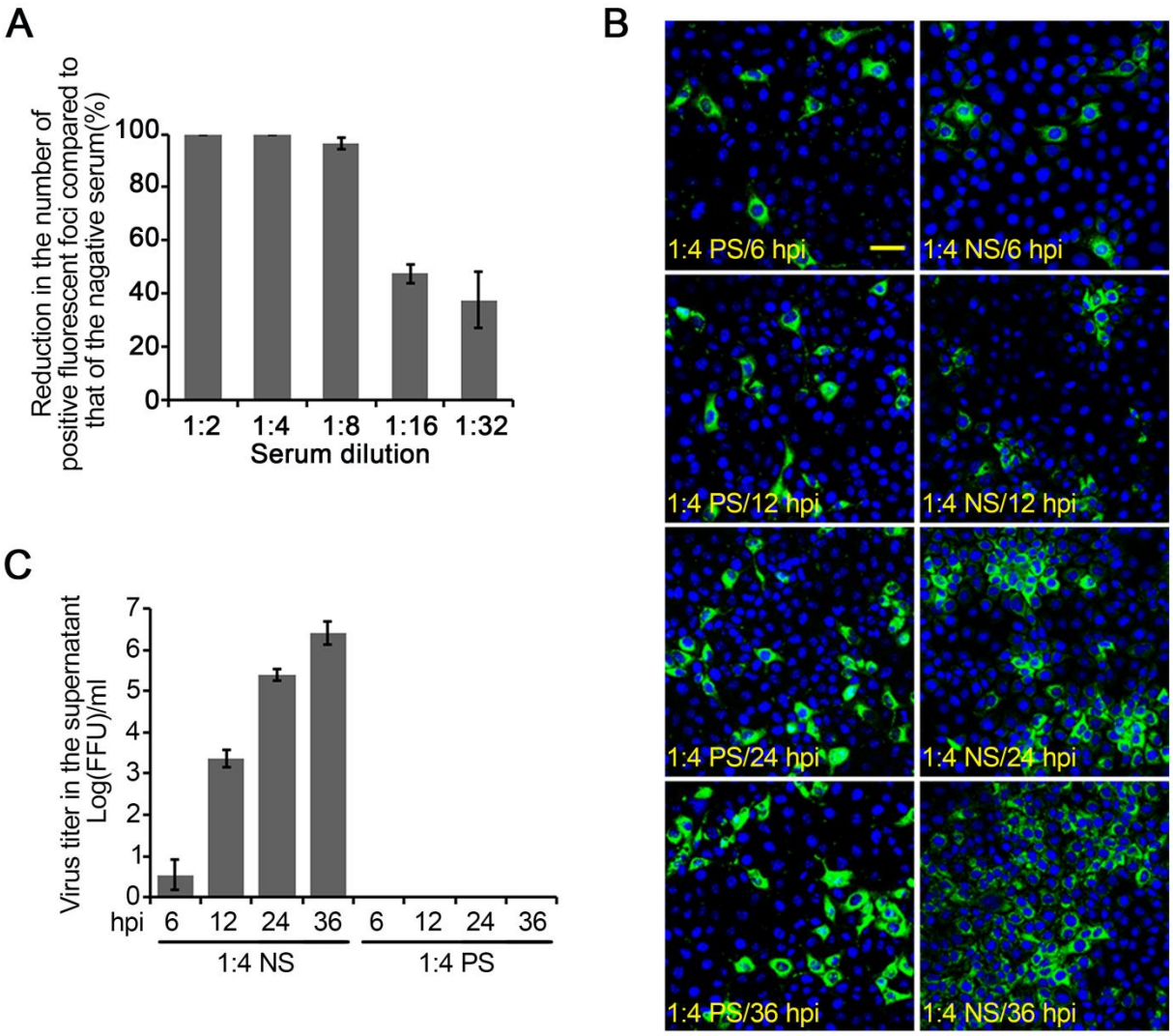
A
Reduction in the number of positive fluorescent foci compared to that of the nagative serum(%)
100
80
60
40
20
0
1:2
1:4
1:8
1:16
1:32
Serum dilution
B
1:4 PS/6 hpi
1:4 NS/6 hpi
1:4 PS/12 hpi
1:4 NS/12 hpi
1:4 PS/24 hpi
1:4 NS/24 hpi
1:4 PS/36 hpi
1:4 NS/36 hpi
C
Virus titer in the supernatant Log(FFU)/ml
7
6
5
4
3
2
1
0
hpi
6
12
24
36
6
12
24
36
1:4 NS
1:4 PS

Figure 2.4 Intercellular spreading of PRRSV infection in cells with the presence of virus-neutralizing antibody. (A) Standard viral neutralizing assay. Immune serum from PRRSV-infected pigs was serial diluted and incubated with the virus for 1 h; and the virus-antibody complex was then added on the MARC-145 cells. At 12 hpi, cells were stained with anti-N mAb and virus foci were counted under the fluorescence microscope. The percentage of viral growth reduction was calculated in comparison to the result from cells treated with negative control serum. (B) Cell-to-cell spreading of the viruses under the existence of viral neutralizing antibody. MARC-145 cells were infected with PRRSV SD95-21. At 3 hpi, the 1:4 diluted immune serum or negative control serum was added onto the infected cells. At 6, 12, 24 or 36 hpi, cell culture supernatant was harvested and cells were fixed and stained with anti-N mAb. Images were taken by a confocal microscope (LSM 880, Zeiss). Scale bar, 50 μm. (C) Virus titers in the harvested cell culture supernatant from experiment described in panel B. Virus titer was determined by counting the virus foci under the fluorescence microscope, and the result was interpreted as fluorescent-focus units (FFU) per ml. NS: negative control serum from a none-infected pig; PS: immune serum from a PRRSV-infected pig.

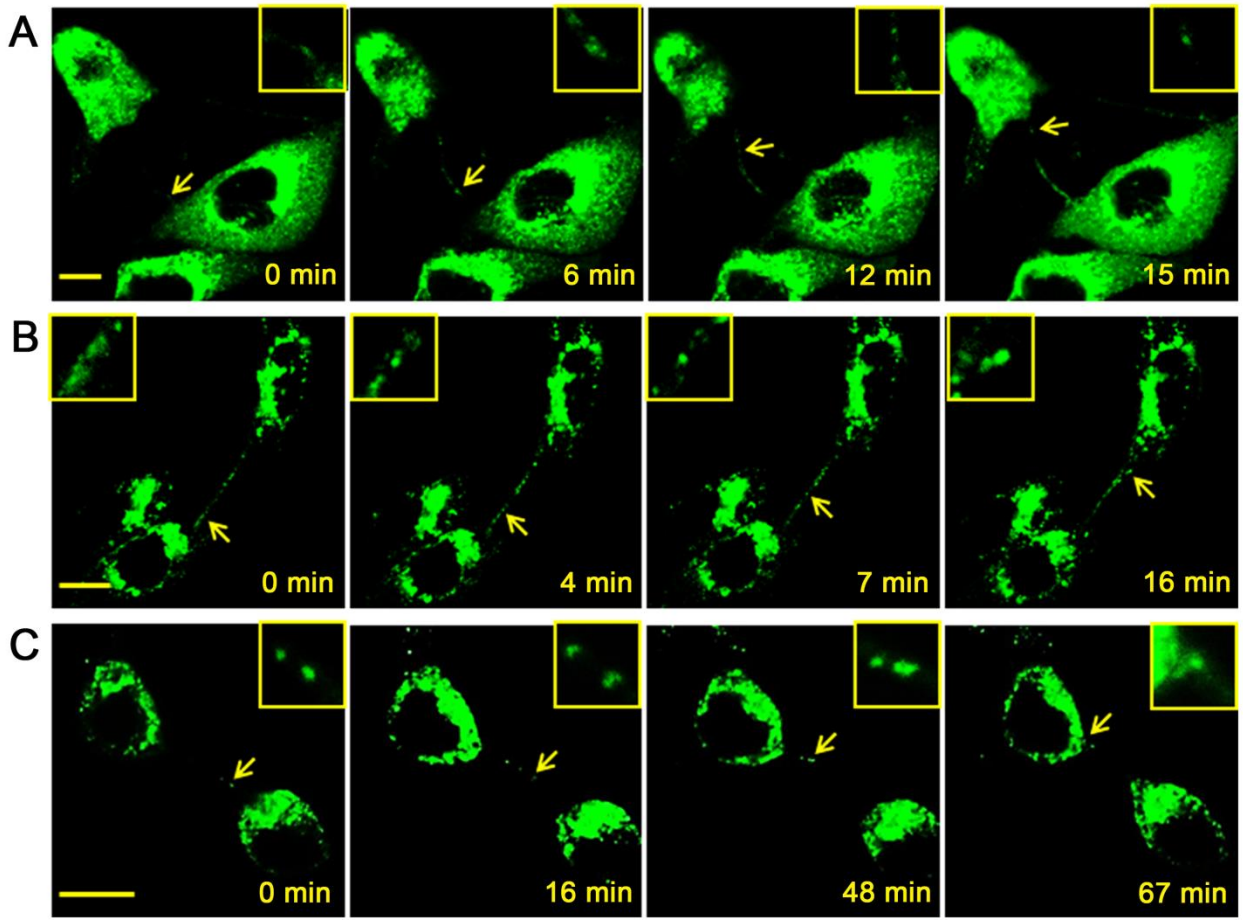
A
0 min
6 min
12 min
15 min
B
0 min
4 min
7 min
16 min
C
0 min
16 min
48 min
67 min

Figure 2.5 Live cell images demonstrating intercellular transport of PRRSV GFP-tagged nsp2 through nanotubes. (A) GFP-PRRSV infected cells maintained in cultural medium containing PRRSV neutralizing antibody. (B) GFP-PRRSV infected cells maintained in regular cultural medium (no PRRSV neutralizing antibody). (C) HEK-293T cells were transfected with PRRSV full-length cDNA infectious clone, pCMV-SD95-21-GFP. At 24 h post infection (A and B) or transfection (C), cells were analyzed using live cell image system of a confocal microscope (LSM 880, Zeiss). In both infected MARC-145 cells and transfected HEK-293T cells, the dot-like GFP-nsp2 proteins were visualized to move through an intercellular nanotube connection into the cytoplasm of a neighboring cell. Insets showed a zoomed interesting area that contains the GFP-nsp2 proteins. Specific nanotube shown between MARC-145 cells is about 20 μm in length, while specific nanotube shown between HEK-293T cells is about 12 μm in length. Scale bar, 10 μm.

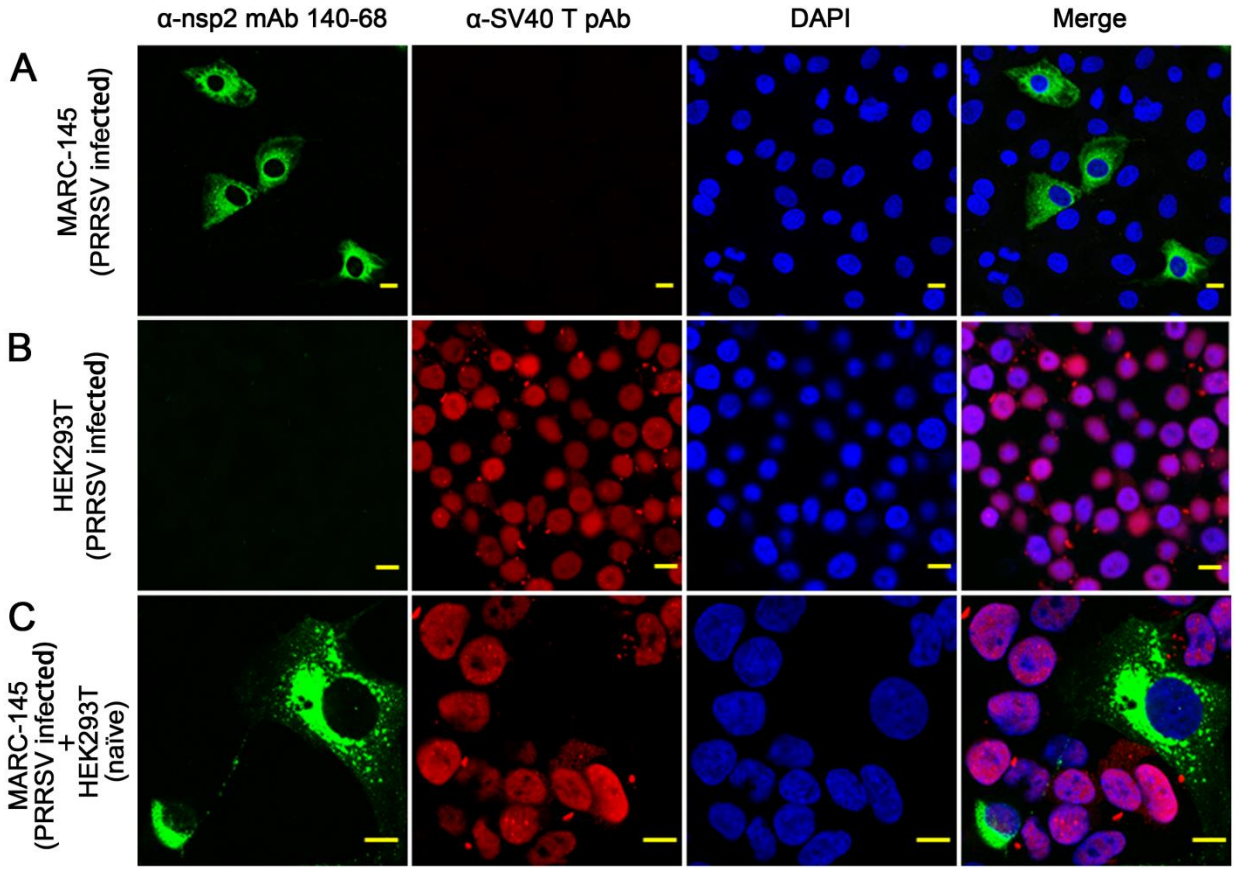

Figure 2.6 Intercellular transport of the GFP-nsp2 protein in co-cultured MARC-145 and HEK-293T cells. (A) GFP-PRRSV infected MARC145 cells were fixed and stained with anti-nsp2 mAb 140-68 and anti-SV40-T pAb sc-20800. (B) GFP-PRRSV infected HEK-293T cells were fixed and stained with anti-nsp2 mAb 140-68 and anti-SV40-T pAb sc-20800. (C) GFP-PRRSV infected MARC-145 cells were trypsinized at 12 hpi and mixed with na ïve HEK-293T cells. After 36 h post cultivation, cells were fixed and stained with anti-nsp2 mAb 140-68 and anti-SV40-T pAb sc-20800. The nsp2 was labeled with green fluorescence and SV40 large T was labeled with red fluorescence. Pictures were taken by a confocal microscope (LSM 880, Zeiss). Scale bar, 10 μm.

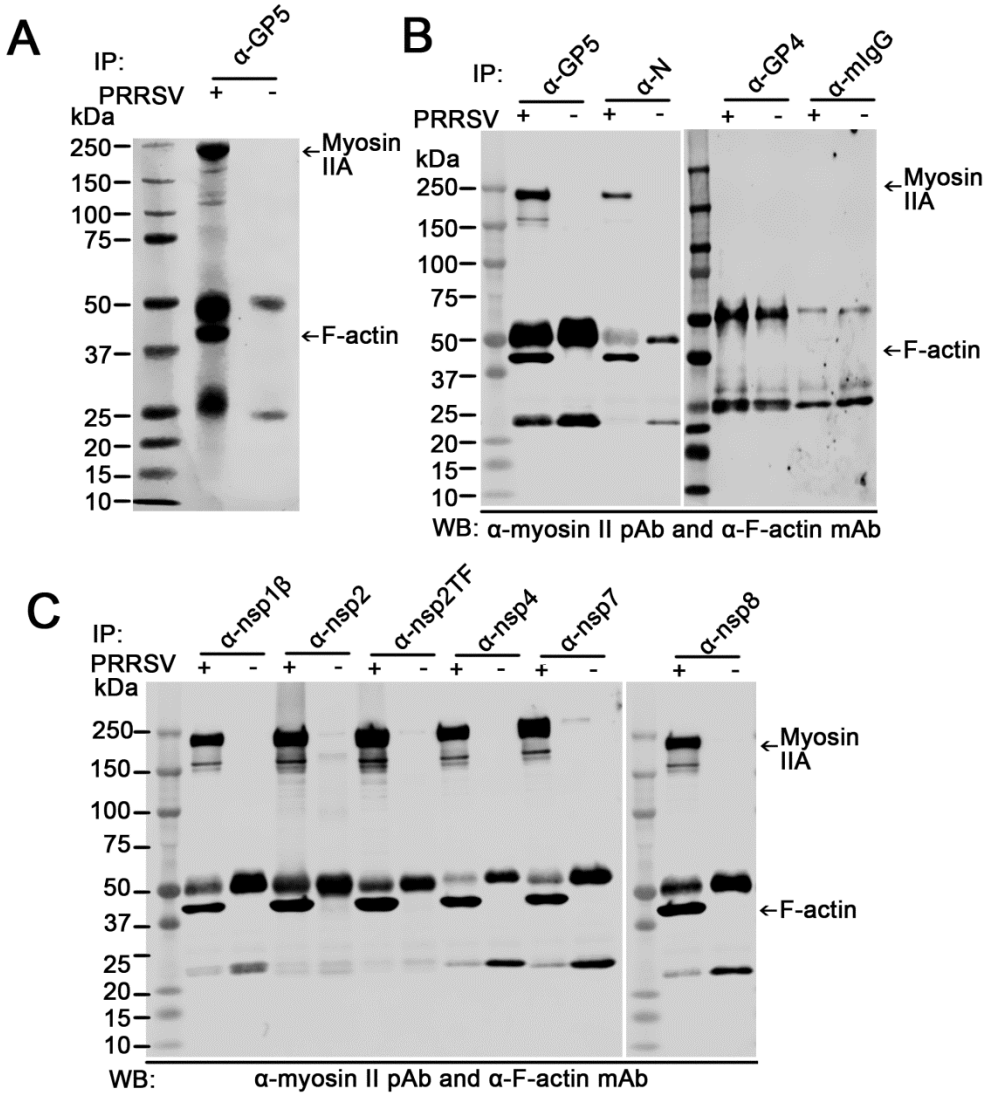
A
IP:
α-GP5
PRRSV
+
-
kDa
250
150
100
75
50
37
25
20
15
10
←Myosin IIA
←F-actin
B
IP:
α-GP5
α-N
α-GP4
α-mIgG
PRRSV
kDa
←Myosin IIA
←F-actin
WB: α-myosin II pAb and α-F-actin mAb
C
IP:
α-nsp1β
α-nsp2
α-nsp2TF
α-nsp4
α-nsp7
α-nsp8
PRRSV
kDa
←Myosin IIA
←F-actin
WB:
α-myosin II pAb and α-F-actin mAb

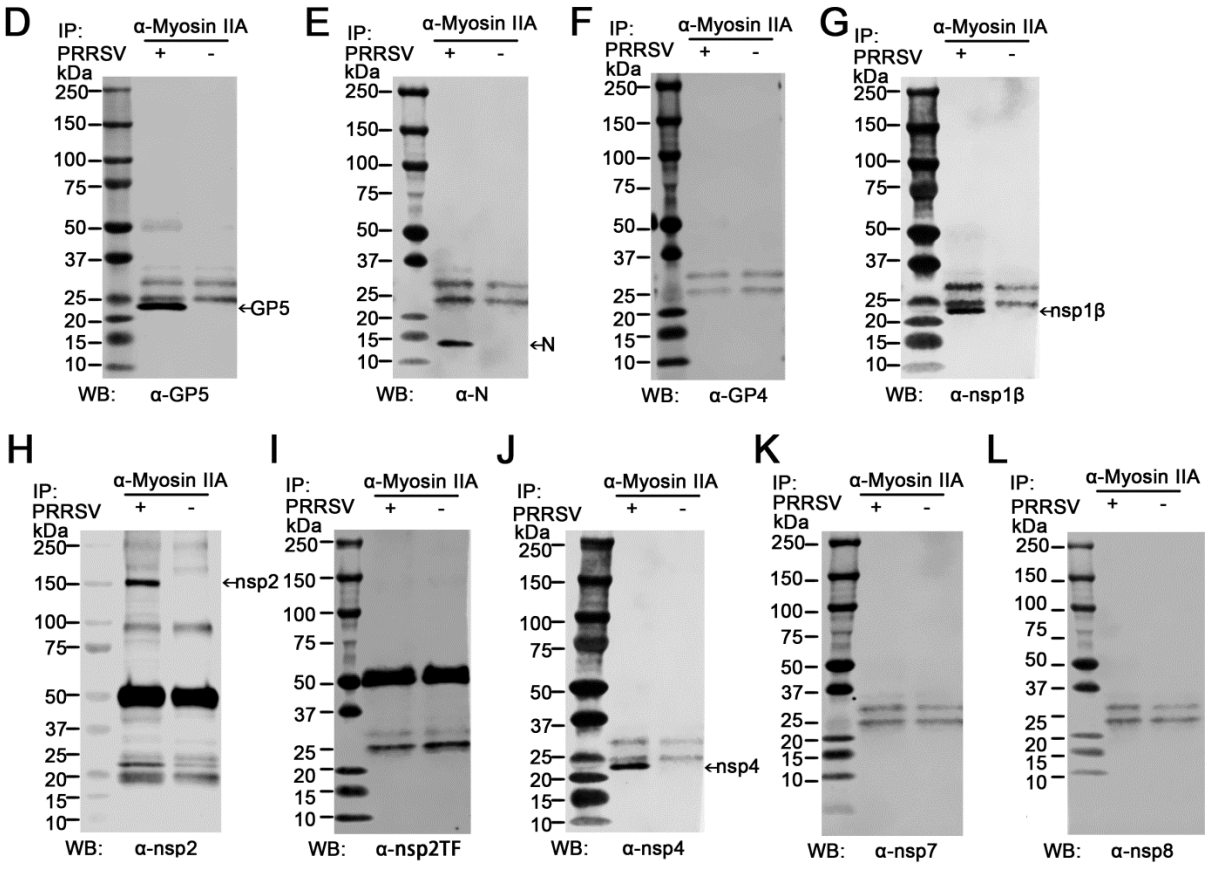
D
IP:
α-Myosin IIA
PRRSV
+
-
kDa
250
150
100
75
50
37
25
20
15
10
←GP5
WB:
α-GP5
E
IP:
α-Myosin IIA
PRRSV
+
-
kDa
250
150
100
75
50
37
25
20
15
10
←N
WB:
α-N
F
IP:
α-Myosin IIA
PRRSV
+
-
kDa
250
150
100
75
50
37
25
20
15
10
WB:
α-GP4
G
IP:
α-Myosin IIA
PRRSV
+
-
kDa
250
150
100
75
50
37
25
20
15
10
←nsp1β
WB:
α-nsp1β
H
IP:
α-Myosin IIA
PRRSV
+
-
kDa
250
150
100
75
50
37
25
20
15
10
←nsp2
WB:
α-nsp2
I
IP:
α-Myosin IIA
PRRSV
+
-
kDa
250
150
100
75
50
37
25
20
15
10
WB:
α-nsp2TF
J
IP:
α-Myosin IIA
PRRSV
+
-
kDa
250
150
100
75
50
37
25
20
15
10
←nsp4
WB:
α-nsp4
K
IP:
α-Myosin IIA
PRRSV
+
-
kDa
250
150
100
75
50
37
25
20
15
10
WB:
α-nsp7
L
IP:
α-Myosin IIA
PRRSV
+
-
kDa
250
150
100
75
50
37
25
20
15
10
WB:
α-nsp8

Figure 2.7 Co-precipitation of PRRSV proteins with cytoskeleton F-actin and myosin IIA. (A-C) PRRSV-infected (+) MARC-145 cell lysates or mock-infected (-) cell lysates were used for immunoprecipitation using PRRSV protein specific mAbs as indicated on the top of each panel. Anti-mouse IgG (α-mIgG) was used as a control. The immunoprecipitated proteins were separated by 8-16% Tris-Glycine gradient gel (A) and immunoblotted by anti-myosin-IIA pAb and anti-F-actin mAb (B-C). (D-L) PRRSV-infected MARC-145 cell lysates (+) or mock infected (-) cell lysates were used for immunoprecipitation using anti-myosin-IIA pAb. The immunoprecipitated proteins were separated by 8-16% Tris-Glycine gradient gel and immunoblotted by PRRSV protein specific mAbs as indicated on the bottom of each panel. IP: immunoprecipitation. WB: Western blotting. Arrows in panels A-C pointed F-actin (42 kDa), non-muscle myosin heavy chain IIA (215 kDa). Arrows in Panels D-E, G-H and J pointed the target protein as indicated at the bottom of each panel.

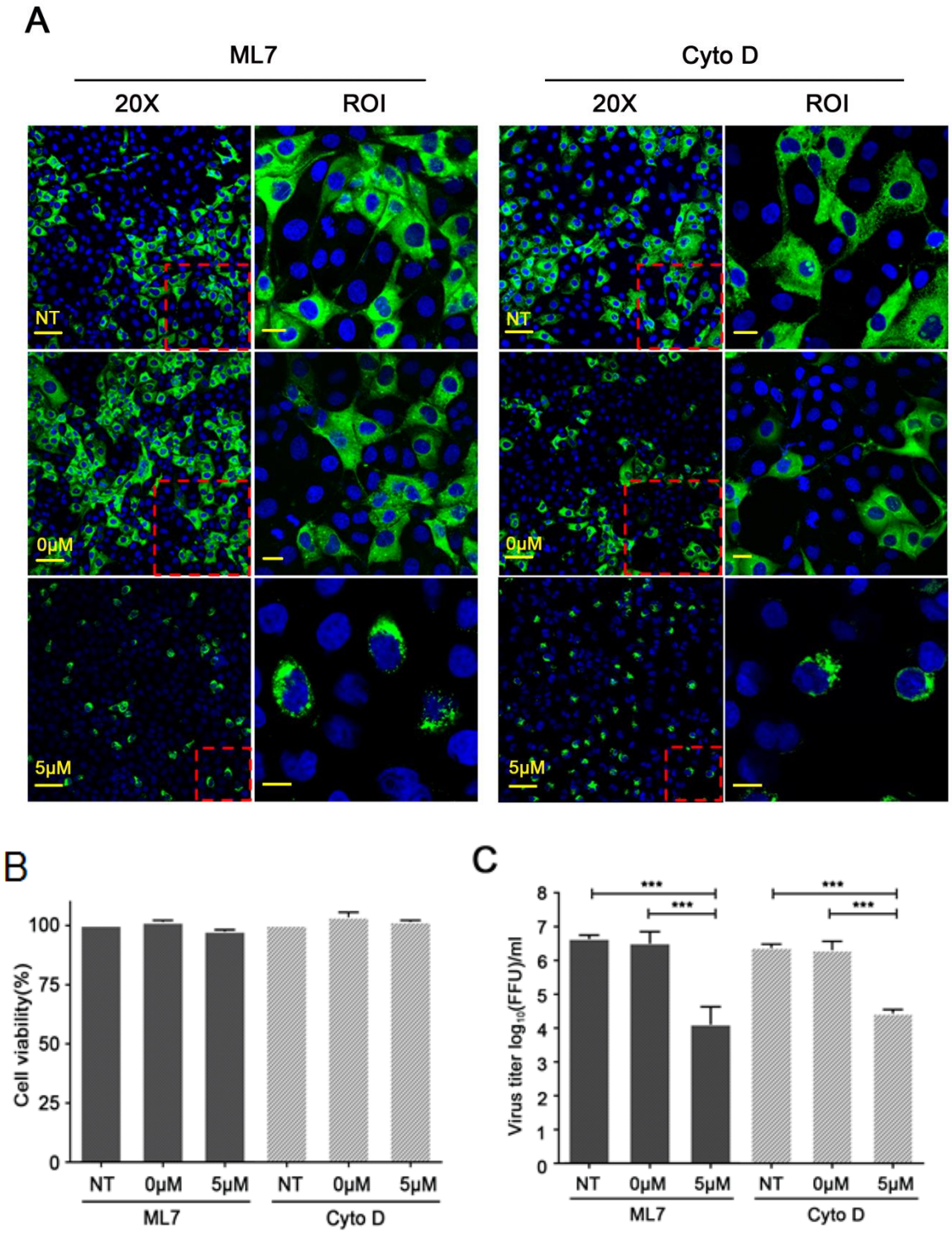
A
ML7
Cyto D
20X
ROI
20X
ROI
NT
0μM
5μM
NT
0μM
5μM
B
Cell viability(%)
100
75
50
25
0
NT
0μM
5μM
NT
0μM
5μM
ML7
Cyto D
C
Virus titer log10(FFU)/ml
8
7
6
5
4
3
2
1
0
***
***
***
***
NT
0μM
5μM
NT
0μM
5μM
ML7
Cyto D

Figure 2.8 Inhibitors of F-actin and myosin IIA affect the intercellular spread of PRRSV. (A) Confluent MARC-145 cells monolayers were pretreated with ML7 or cytochalasin D (Cyto D) compounds at concentration of 5 μM or 0 μM. Non-treated cells (NT) were used as a control. After 30 min incubation at 37 ^{0}C, the cells were infected with 0.1 moi of PRRSV. After 1 h incubation, the infected cells were washed with PBS and the fresh medium containing Cyto D or ML7 compounds was added. At 48 hpi, cells were fixed and immune-stained with PRRSV N protein specific mAb. Images in column 1 and 3 were taken under 20x objective lens (20X) with scale bar of 50 μm. Inset at the right bottom corner of each image showed a zoomed region of interest, in which the picture obtained under 40X objective lens is shown in column 2 and 4 (region of interest; ROI). Scale bar of ROI, 10 um. (B) Effect of Cyto D or ML7 on the viability of the MARC-145 cells compared to the viability of DMSO-treated (0 μM) or non-treated control cells (NT). Graphs show the results (mean and SD) of a representative experiment (n = 3). (C) Viral growth inhibition efficiency of myosin-IIA inhibitor ML7 or F-actin inhibitor Cyto D. Virus titration was conducted using cell culture supernatant collected from the experiment in (A). Virus titer was determined by counting the virus foci under the fluorescence microscope, and the result was interpreted as fluorescent-focus units (FFU) per mL. Statistical significance between the groups was determined by one-way analysis of variance (ANOVA) test using GraphPad InStat Prism (software version 5.0), and $p < 0.01$ (***) was considered statistically significant.

Chapter 3 - Intercellular transfer of mitochondria rescues virus-induced cell death but facilitates cell-to-cell spreading of porcine reproductive and respiratory syndrome virus

Rui Guo, Duane Davis, and Ying Fang

(Virology, 517:122-134.)

Abstract : Our recent study showed that intercellular nanotube connections can serve as an alternative pathway for cell-to-cell spreading of the infectious materials of porcine reproductive and respiratory syndrome virus (PRRSV) [Guo et al., 2016, J. Virology, 90(10):5163-75]. In this study, we found that PRRSV infection could induce the formation of intercellular nanotube connections between infected and uninfected MARC-145 cells in the early stage of infection. Co-culturing PRRSV-infected cells with uninfected cells, including porcine umbilical cord (PUC) mesenchymal stem cells, rescued PRRSV-induced cell apoptosis/necrosis. Mitochondria are important regulators of cell survival and cell death. We observed mitochondria transferring from uninfected cells to PRRSV-infected cells. Importantly, impaired formation of nanotubes or defective mitochondrion was unable to rescue infected cells from apoptosis/necrosis in the co-culture system. PRRSV nsp1α, nsp1β, nsp4, and nucleocapsid proteins were detected to associate with mitochondria and transported from infected to uninfected cells through the nanotubes. Our results suggest that transferring of functional mitochondria through nanotubes rescued the PRRSV-infected cell from apoptosis/necrosis in the early stage of infection. On the other hand, PRRSV takes advantage of this intercellular transport pathway, in which mitochondria could be utilized as a cargo to transport viral infectious materials for cell-to-cell spreading of the infection.

3.1 Introduction

Porcine reproductive and respiratory syndrome has caused tremendous economic losses to swine industry worldwide. The etiologic agent, porcine reproductive and respiratory syndrome virus (PRRSV) belongs to the family of the Arteriviridae, order Nidovirales (1, 2). PRRSV is an enveloped positive-stranded RNA virus. The viral genome is packed by nucleocapsid (N) proteins, and surface glycoproteins and membrane proteins are inserted into the lipid-bilayered envelope, which surrounds the nucleocapsid to form virion particles. The PRRSV genomic RNA molecule is about 15kb in length and contains eleven known open reading frames. The replicase gene consists of the large ORFs 1a and 1b, which are situated in the 5'-proximal three quarters of the polycistronic genome. They encode two long nonstructural polyproteins, pp1a and pp1ab, with expression of the latter depending on a -1 ribosomal frame shift signal in the ORF1a/ORF1b overlap region. Following their synthesis from the genomic mRNA template, the pp1a and pp1ab replicase polyproteins are processed into at least 14 nonstructural proteins (nsps), including nsp1α/β, nsp2-nsp12 (2). In our recent study (3), a novel ORF (TF) was identified, which is translated via an efficient -2 ribosomal frameshift mechanism, resulting in the expression of a transframe protein, nsp2TF. At the same frameshifting site, -1 ribosomal frame shift also occurs, yielding a truncated nsp2 protein (nsp2N). The 3' end of the genome encodes four membrane-associated glycoproteins (GP2a, GP3, GP4 and GP5), three unglycosylated membrane proteins (E, ORF5a and M) and a nucleocapsid protein (N) (4).

In infected pigs, PRRSV mainly infects subsets of swine macrophages that are present in lungs and lymphoid organs (5, 6). In cultured cells, PRRSV grows in primary porcine alveolar macrophages, monocyte-derived macrophages or monocyte-derived dendritic cells (7-11). In

addition to primary cell cultures, PRRSV replicates in a certain African green monkey kidney cell line (MA-104) and its derivatives, such as MARC-145 cells (12). Previous studies investigated the significance of apoptosis/necrosis in the pathogenesis of PRRSV infection (13-17). Necrosis and apoptosis are two major types of cell death, which differ both morphologically and biochemically. Necrosis is a passive cell death due to depletion of cellular resources. Cells undergoing necrosis are characterized by increased ion permeability of the plasma membrane, cellular swelling and osmotic lysis, which leads to extensive tissue damage and an intense inflammatory response (18, 19). In contrast, apoptosis is a highly regulated mechanism of cell death with highly characteristic morphological changes, including cell shrinkage, plasma membrane blebbing, chromatin condensation and DNA fragmentation (19). These fragments or apoptotic bodies are taken up by other cells and degraded within phagosomes (19). Apoptosis has been shown to be an important innate defense mechanism that interrupts replication of intercellular pathogens (20, 21). It was reported that PRRSV, stimulates anti-apoptotic pathways in macrophages and MARC-145 cells during the early stage of infection, and PRRSV infection caused cell death by apoptosis later in the infection (13, 14). Besides apoptosis, necrosis and necrosis-like apoptosis were also observed in PRRSV-infected cells (13, 14).

Mitochondria are master regulators of cell survival and cell death (22-24). Mitochondria react to stress conditions, such as viral infection, through release of 'call-for-help' signals. These signals include reactive oxygen species (ROS) and nucleus-encoded proteins, such as the S100 protein family. When the homeostasis of a cell loses balance, excess mitochondrial danger signals contribute to the activation of cell death pathways (24). Mitochondrial damage has been reported for a wide variety of viruses (17, 25-28). Previous studies have shown that PRRSV infection causes mitochondria dysfunction, results in the disruption of mitochondrial

transmembrane potential and increases the level of ROS production (17). It was reported that PRRSV infection could cause mitochondrial fission and mitophagy formation to attenuate apoptosis in order to facilitate virus replication (29). Mitochondria are also involved in the antiviral signaling pathway that is mediated by RIG-I like receptors and mitochondrial antiviral signaling protein (MAVS)(24). Viruses have developed various strategies to evade this immune surveillance (29-31). The PRRSV nsp4 protein was reported to be able to cleave MAVS off the mitochondria in order to evade innate immune responses (30, 31).

As indicated above, virus infection can cause oxidative stress in local cells (32-34). Stressed or injured cells can be influenced by intercellular communicative networks. There is emerging evidence that small cellular organelles, in particular mitochondria, can be transferred from the cell to cell to rescue a stressed/injured cell (35). It was reported that co-culturing human bone marrow nonhematopoietic stem/progenitor cells with mitochondria-damaged A549 cells rescued the cells with functional mitochondria (36); and mitochondrial transfer from bone-marrow-derived stromal cells to pulmonary alveolar epithelial cells protected against acute lung injury in a mouse model (37). Different intercellular transport pathways have been reported for cell to cell transfer of small molecules and cellular organelles (35). Intercellular tunneling nanotubes (TNT) have been increasingly recognized as an important pathway for intercellular transportation (38). TNTs appear to be long membrane-derived tubes of 50 to 200 nm in diameter connecting spatially separated cells. Filamentous actin (F-actin) and myosin are the primary components of nanotubes. TNTs can form a network for cellular communication over long distances. Various cellular components have been reported to be transferred through TNTs, including organelles such as mitochondria (39). TNTs have also been reported to be an

alternative pathway for intercellular spreading of viral infection (40, 41). Recently, we demonstrated that PRRSV utilized TNTs to spread infection from host cell to cell (42).
In the present study, we observed a novel mechanism of anti-apoptosis/necrosis in PRRSV infected cells. We demonstrated that PRRSV infection induces increased formation of intercellular nanotube connections, and TNTs were determined to be involved in mitochondria transfer between infected and non-infected cells. More importantly, transferring of functional mitochondria through nanotubes rescued the host cell from apoptosis/necrosis in the early stage of infection. On the other hand, mitochondria were observed as a potential transporter of viral infectious materials for cell-to-cell spreading of the infection.

3.2 Materials and Methods

Cells and Viruses. MARC-145 cells were maintained in minimum essential medium (MEM, Gibco) supplemented with 10% fetal bovine serum and antibiotics (100 μg/ml penicillin and streptomycin). Porcine alveolar macrophages (PAMs) were collected by lung lavage from a 9-week-old PRRSV-naive pig using a method described previously (43). (The pig experiment was performed according to protocols approved by the Institutional Animal Care and Use Committee of Kansas State University.) Macrophages were cultured in RPMI-1640 medium (Gibco) supplemented with 10% fetal bovine serum and 100 ug/ml penicillin and streptomycin. Porcine umbilical cord mesenchymal stem cells (PUCs) were obtained from umbilical cords collected at birth using the explant method previously described (44). DMEM (high glucose, Gibco) was used for explants and maintaining the cells in culture. It was supplemented with 20% FBS, 110 nmol/ml β-mecaptoethanol (Sigma-Aldrich), 25 μg/ml gentamycin (Sigma-Aldrich) and Antibiotic Antimycotic Solution (Sigma-Aldrich). The PUCs were passaged twice (when

80% confluent) in cell culture and then used for the experiments. Mitochondria-defective MARC-145 cells or PUCs were maintained in their specific cell culture medium containing 0.1 μg/ml ethidium bromide and 50 μg/ml uridine for at least one month, as described previously (45, 46). Cells were maintained at 37 ℃ with 5% CO2 in air of incubator. The PRRSV isolate SD95-21 (GenBank accession number KC469618) was used. A green fluorescent protein (GFP)-tagged recombinant PRRSV (GFP-PRRSV) of SD95-21 was constructed in our previous studies (42, 47) and was used for live cell image and flow cytometry analysis.

Plasmids and antibodies. Antibodies for detecting PRRSV proteins, including monoclonal antibody (MAb) 123-128 (anti-nsp1β), MAb 69-267 (anti-nsp4), MAb 108-16 (anti-nsp7), MAb NI37(anti-GP4), MAb 21-79 (anti-GP5), and MAb14-126 (anti-N), MAb SDOW17 (anti-N), and rabbit polyclonal antibody (PAb) specific to the C-terminal peptide of nsp2 (anti-nsp2C) or the C-terminal peptide of nsp2TF (anti-nsp2TF) were described previously (42, 47-52). The MAb 73-14 (anti-nsp1α) was generated by immunizing BALB/c mice with a truncated nsp1α recombinant protein (contains amino acids 1-16 and 42-180 of nsp1α), while the MAb 120-29 (α-GP3) was produced by immunizing mice with full-length GP3 recombinant protein as the antigen. Experimental procedures for MAb production were described previously (53). The rabbit polyclonal antibody specific to the C-terminal peptide (LKSLVLGGRKAVK) of M protein was generated by Genscript. Anti-α-tubulin MAb (sc-5286) and anti-TOM20 PAb (sc-11415) were purchased from Santa Cruz. Anti-MAVS/Cardif PAb recognizing the C-Terminal region of MAVS was purchased from Millipore.

Quantitative PCR. To analyze the expression level of mitochondrial DNA, total cellular DNA was extracted from the cells using Quick DNA Miniprep kit (Zymo) and subsequently quantified by quantitative PCR (qPCR). Primers used for amplifying the mtDNA cytochrome c

oxidase subunit I (COI) were synthesized as: 5'- CTAACAGACCGCAACCTCAAC-3' (forward), 5'-TCCGAAGCCTGGTAGGATAAG-3' (reverse). The 18s rDNA was used as an internal control that was amplified using the primer pair of 5'- TGTGATGCCCTTAGATGTCC -3' (forward), 5'- TGGGGTTCAGCGGGTTAC -3' (reverse). PCR was performed under the following conditions: 95 ℃ for 3 min, followed by 40 cycles of 95 ℃ for 10s, 60 ℃ for 20s. SYBR Premix ExTaqTM kit (Bio-Rad) was used according to the manufacturer's instruction. The real-time PCR results were analyzed using Comparative CT Method (54) and interpreted as relative cycle threshold (CT) value.

Virus infection and cell co-cultivation system. The cell co-culture system was established using the modified method as described previously (16), with different cell types used in the present study. For the MARC-145 cell co-culture system, cells were initially infected with recombinant GFP-PRRSV at MOI of 1. At 24 hours post-infection (hpi), cells were washed with PBS, trypsinized, and mixed with an equal number (5×10^4/ml) of infected or uninfected MARC-145 cells; Hoechst 33342 was used to label uninfected cells in order to differentiate the uninfected cells from the initially infected cells. Before mixing uninfected cells with the infected cells, the uninfected cells were trypsinized, cultured in 0.5 ml MEM and then stained with 50ng/ml of Hoechst for 1 hour at 37˚C. After incubation, cells were washed thoroughly with 50 ml of pre-warmed MEM three times, and then mixed with the PRRSV-infected cells. For Cytochalasin D (Cyto D) treatment, 5μM of CytoD was suspended in Dimethyl sulfoxide (DMSO, 0.1%) and added into the cell culture medium at 1 hour post co-culture. For the solvent control, DMSO was added to a different well of co-cultured cells. After an additional 24 hours of incubation, co-cultured cells were subjected to immunofluorescence assay, live cell imaging or cell death analysis. For PAMs/PAMs coculture system, PAMs (5×10^5 cells/ml) were initially

seeded on a 6-well tissue culture plate. Cells were then infected with GFP-PRRSV (1 MOI). After 1 hour incubation, the cells were collected from the plate using a soft-blade cell scraper (Thermofisher) and mixed with an equal number (5×10^5/ml) of uninfected PAMs. In order to differentiate the uninfected PAMs from the initially infected PAMs, the uninfected cell nucleus was labeled by Hoechst as described above, while the mitochondria were labelled with Tetramethylrhodamine, methyl ester (TMRM) following the manufacturer's instruction (Thermofisher). After coculturing, cells were incubated for additional 6 hours, and then subjected to live cell imaging under confocal microcsopy. For PAMs/PUCs co-culture, PAMs were seeded and infected using the same method as in PAMs/PAMs co-culture. PUCs (5×10^5 cells/ml) were co-cultured with an equal number of infected-PAMs at 1 hpi. After additional 23 hours incubation, the co-cultured cells were subjected to live cell image and flow cytometry.

Analysis of cell death. PAMs or MARC-145 cells were infected with recombinant GFP-PRRSV (MOI of 1). The infected MARC-145 cells were collected at 6, 12, 24, 36, 48, 72 hpi. Alternatively, infected PAMs were collected at 6, 12, 14, 16, 18, 20, 22, and 24 hpi. Cell necrosis was determined by staining the collected samples with 7-Aminoactinomycin D (7-AAD, enzo), while apoptosis was determined using a CellEvent™ Caspase-3/7 Red Flow Cytometry Assay Kit (ThermoFisher) to detect active caspase 3 expression. Data were acquired by flow cytometry (BD LSR Fortessa X-20, BD Biosciences) and analyzed using flowjo 10.2.

Detection of ROS expression. MARC-145 cells were grown in 96-Well Clear Bottom White Polystyrene Microplates (Corning). Cells were then infected with PRRSV SD95-21 at a MOI of 1 or mock-infected with infection medium (1×MEM containing 2% horse serum and 100 μg/ml streptomycin). Cells were incubated for 6, 12, 24, 36, 48 and 72 hpi. Expression of intracellular ROS was detected by using a 2', 7' – dichlorofluorescin diacetate (DCFDA)

Cellular Reactive Oxygen Species Detection Assay Kit (abcam). The fluorescence signals were recorded by a FLUOstar Omega microplate reader (BMG Lab Tech).

Quantitative RT-PCR for measuring S100A4 expression level. MARC-145 cells were infected with PRRSV SD95-21 at a MOI of 1. At 6, 12, 24, 36, 48 hpi, cells were subjected to total RNA extraction by using SV total RNA isolation kit (Promega). One microgram of total RNA was used to synthesize first-strand cDNA using SuperScript® VILO™ cDNA Synthesis Kit (ThermoFisher). Subsequently, real-time PCR was performed to quantify the mRNA expression levels of S100A4 and GAPDH using predesigned primer/probe sets (ThermoFisher), following the manufacturer's instruction. The amount of S100A4 was normalized to the endogenous GAPDH mRNA.

Quantification of nanotubes. MARC-145 cells (1×10^5/ml) were infected with GFP-PRRSV at a MOI of 1 or mock-infected with infection medium. The cells were harvested at 0, 6, 12, 18 and 24 hpi and then stained with wheat germ agglutinin-Alexa Fluo 350 (WGA-AF350; ThermoFisher) for 15 min to visualize cell membranes. The cells were then fixed with 4% paraformaldehyde (PFA). Confocal microscopy was conducted using a LSM 880 equipped with 40× oil immersion objective lens (Zeiss). The number of nanotubes was counted from 20 random fields of view and expressed as the number of nanotubes per 500 cells.

Immunofluorescence assays. MARC-145 cells or PAMs were grown on glass-bottom 35-mm cell culture dishes (MatTek). MARC-145 cells or PAMs were infected with PRRSV at an MOI of 1 or mock-infected with infection medium. At 12 hpi, cells were fixed with 4% PFA for 10 min, permeabilized with 0.5% Triton X-100 for 10 min, and then blocked with 1% bovine serum albumin (BSA) in PBS for 30 min at room temperature. To detect PRRSV proteins, a specific mAb was used as described previously (42, 55). To detect mitochondria, cells were

stained by anti-Tom20 rabbit pAb (Santa Cruz). After 1 h incubation at 37 ℃, cells were washed with PBS, and a secondary antibody, Alexa Fluor 488 AffiniPure goat anti-mouse IgG (Jackson ImmunoResearch) or Alexa Fluor 594 AffiniPure goat anti-rabbit IgG (Jackson ImmunoResearch) was added at a concentration of 1:250 in PBS. After cells were incubated at room temperature for 1 h, they were washed in PBS and then stained with DAPI (Invitrogen). For detection of F-actin and microtubulin in nanotubes, GFP-PRRSV infected or mock infected MARC-145 cells were fixed, and then stained with Alexa Fluor 594-conjugated phalloidin (Molecular Probes) or anti-α-tubulin rabbit PAb as described previously (42).

Live-cell movies. The co-cultured cells seeded on a glass bottom dish were set into an open cultivation system of the Zeiss confocal microscope and maintained in warm DMEM buffered with HEPES. The live-cell chamber was mounted on a heated stage to maintain the culture at 37 ℃. Live cells were imaged with an LSM 880 Zeiss confocal microscope (Zeiss). Collected images were processed using Zen 2. The movement of GFP-nsp2 or mitochondria was tracked by using the MTrackJ plugin in Image J software. The GFP-nsp2 protein movement was tracked with green circle, while the mitochondrion movement was tracked with red circle.

Mitochondrial isolation and Western Blot. The mitochondrial isolation was conducted by using Mitochondria Isolation Kit for Cultured Cells (ThermoFisher) following the manufacturer's instruction. Proteins localized on mitochondria were detected by Western blot using the method described previously (26). The membrane was probed with a protein-specific mAb or pAb. IRDye 680-conjugated goat anti-rabbit Ab and/or IRDye 800CW-conjugated goat anti-mouse Ab (Li-Cor Biosciences) were used as the secondary antibody. Imaging of the blot was performed using an Odyssey Infrared Imaging System (Li-Cor Biosciences)

Statistical analysis. All the data were shown as mean values with standard deviation, and

evaluated by one-way analysis of variance (ANOVA) followed by Tukey's post hoc test using programs in GraphPad Prism version 5.0 (La Jolla, CA). Significance differences were indicated by P-values of <0.05 (*), <0.01 (**), <0.001 (***), and <0.0001 (****).

3.3 Results

PRRSV-infected cells release 'call-for-help' signals and increase formation of nanotubes. It has been well documented that stressed cells release 'call-for-help' signals to unstressed cells in their surroundings (56). ROS and S100A4 are two major signals that were reported to play important roles in the cell survival pathway (57). To determine whether PRRSV-infected cells also release 'call-for-help' signals, we initially measured ROS and S100A4 expression levels in PRRSV-infected cells. MARC-145 cells that were infected with GFP-PRRSV were harvested at different time points and then subjected to measures of ROS and S100A4 mRNA expression. As shown in **Fig. 3. 1A**, in comparison to mock- infected cells, significantly higher level of ROS can be detected as early as 6 hours post infection (hpi) in PRRSV-infected cells. The ROS expression reached peak level at 24 hpi. Consistently, quantitative RT-PCR showed increased S100A4 mRNA expression levels in PRRSV-infected cells. In comparison to the mock-infected cells, PRRSV-infected MARC-145 cells had a 2.71-fold higher level of S100A4 mRNA at 12 hpi and 4.62-fold higher level of S100A4 mRNA at 36 hpi (**Fig. 3. 1B**).

The ROS-S100 dependent pathway has been reported to be involved in the induction of intercellular nanotube formation (58, 59). In our previous study, we observed about 6.5-fold increase in the total number of nanotubes in PRRSV-infected MARC-145 cells, compared to that in uninfected cells (42). In the present study, we further counted the number of nanotubes

connecting PRRSV-infected cells with non-infected cells. MARC-145 cells were initially infected with GFP-PRRSV. At 12 hpi, the cells were co-cultured with uninfected cells. To visualize nanotubes, the cell membrane was stained with WGA-350 and demonstrated a blue fluorescent signal. The number of nanotubes was counted under confocal microscopy at 12 hours post co-culture. In comparison to uninfected cells (4.4 ±2.6 nanotubes/500 cells), the total number of nanotubes was significantly increased in infected cells (45.6 ±12.8 nanotubes/500 cells). In comparison to non-infected cells, there was a 5.27-fold increase in the number of nanotubes connecting PRRSV-infected cells with non-infected cells, but only a 2.45-fold and 2.63-fold increase of nanotubes connecting between uninfected cells and between infected cells, respectively (**Fig.3. 1C and 1D**). These data suggest that PRRSV-infected cells may release the 'call-for-help' signals and use the TNTs to reach out to healthy cells for transferring cellular resources for recovery/control of infection.

Mitochondria were observed transferring through TNTs from uninfected cells to PRRSV infected cells. The mitochondrion is a key regulator of cell survival and cell death, and its intercellular transfer is associated with the recovery of injured cells as reported previously (24, 45). We examined whether mitochondria were localized in the TNTs connecting between PRRSV-infected cells and uninfected cells. Initially, MARC-145 cells were infected with GFP-PRRSV and then co-cultured with uninfected MARC-145 cells containing red fluorescent (TMRM)-labeled mitochondria and blue fluorencent (Hoechst 33342) labeled nuclei. Thus, the GFP-PRRSV+/Hoechst 33342- cells can be identified as the initially infected cells. Live cell images were taken under confocal microscopy at 12 hours post co-culture. In the real-time images, mitochondria were clearly observed transferring from the uninfected cell to infected cell (**Fig. 3. 2A, Movie S1**). To confirm this result, the experiment was repeated using porcine

alveolar macrophages (PAMs) in the co-cultures. Consistent with the result shown in Figure 2A, mitochondria were observed transferring from an uninfected macrophage to an infected macrophage (**Fig. 3. 2B, Movie S2**). Interestingly, GFP-nsp2 proteins were observed transporting in the opposite direction from infected to uninfected cells (**Fig. 3. 2A-B, Movie S1-S2**).

To confirm the presence to mitochondria in TNTs, localization of mitochondria with nanotube marker proteins were detected. In previous studies, cytoskeleton protein F-actin has been determined to be associated with the nanotubes (60). However, other studies showed that microtubulin is an important component that facilitates mitochondria transportation (45, 61). Thus, localization of mitochondria with F-actin and microtubulin in TNTs was determined. MARC-145 cells were infected with GFP-PRRSV, and then immunostained by the mAb against TOM20 (translocase of the mitochondrial outer membrane) for visualizing mitochondria. Cells were also double-stained for F-actin or microtubulin. Results showed that as early as 12 hpi, microtubulin can be observed present in some of the nanotubes (**Fig. 3. 3A**). Mitochondria can only be observed present in those microtubulin containing nanotubes (MT-TNT), which is consistent with the results from previous studies (62, 63). In comparison to microtubulin, F-actin was found in every nanotube that was observed (**Fig. 3. 3B**). These data suggest that mitochondria could be transported through specific TNTs from uninfected cells to PRRSV infected cells.

Mitochondria transfer rescued necrosis/apoptosis in PRRSV infected cells. To determine whether intercellular transfer of mitochondria from uninfected/healthy cells altered the fate of PRRSV-infected cells, we first quantified the percentage of the cell population undergoing apoptosis and necrosis followed the time course of PRRSV infection. Flow

cytometry was used to quantify the percentage of cell population using Cellevent caspase 3/7 red flow assay for apoptosis and 7-AAD assay for necrosis. In GFP-PRRSV-positive MARC-145 cells, both apoptosis and necrosis were observed starting from 24-36 hpi (**Fig. 3. 4A-B**), and reached peak numbers (20.8% apoptosis, 13.32% necrosis) at 72 hpi. In GFP-PRRSV positive macrophages, apoptotic or necrotic cells were observed starting from 12-14 hpi, and reached peak numbers (54.4% apoptosis, 37.1% necrosis) at 22 hpi (**Fig. 3. 4C-D**). These data made us suspect that certain viral/cellular mechanisms were involved in rescuing the cell death during the early stage of infection.

Since the mitochondrion is the master regulator of apoptosis/necrosis, mitochondria transferring through TNTs could be one of the mechanisms to rescue the PRRSV-infected cells. To prove this hypothesis, a cell co-cultural experiment was performed. MARC-145 cells were initially infected with GFP-PRRSV and then co-cultured with uninfected cells (**Fig. 3. 4**; Infected/Mock). To differentiate the uninfected cells from infected cells, the uninfected cells were labeled with Hoechst (blue fluorescent dye). As a comparison, a monoculture system was established, in which cells initially infected with GFP-PRRSV were co-cultured with Hoechst-labeled GFP-PRRSV infected cells (**Fig. 3. 4**; Infected/Infected). In both co-culture and monoculture systems, GFP-PRRSV of 1 MOI was used for initial infection in order to obtain over a 95% infection rate at 24 hpi. In addition, a negative control was included, in which uninfected cells were co-cultured with Hoechst-labeled uninfected cells (**Fig. 3. 4**; Mock/Mock). Cells were stained for active caspase 3/7 for determination of apoptosis by flow cytometry. The initial infected cell population was selected by gating GFP+/Hoechst- subsets (**Fig. 3. 5A-C**). Flow cytometry analysis showed that there were lower percentage of apoptotic cells in the initial GFP-PRRSV positive population in infected/mock co-culture condition (8.41% $\pm$0.52%) than in

the infected/infected monoculture condition (13.59% ±1.84%) (**Fig. 3. 5A-D**). To confirm the involvement of TNTs, cells were treated with Cyto D, an inhibitor of nanotube formation. The result showed that in co-cultures, the percentage of apoptotic cells in the initial GFP-PRRSV positive population was higher in the presence of Cyto D (11.83% ±1.86%) than that in the absence of Cyto D (8.41% ±0.52%), suggesting that the nanotubes are required for the cell rescuing process (**Fig. 3. 5D**). We further determined whether intercellular mitochondrial transfer can rescue PRRSV-induced necrosis. Cells were stained with 7-AAD for determination of necrosis (**Fig. 3. 5E**). The data consistently showed that there was lower percentage of necrotic cells in GFP-PRRSV positive population (7.94% ±0.56%) in co-cultured infected/mock condition than in the infected/infected monoculture condition (11.75% ±1.39%) (**Fig. 3. 5E**). Moreover, in the co-culture, the percentage of necrotic cells in the GFP-PRRSV positive population was higher in the presence of Cyto D (9.95% ±1.06%) than that in the absence of Cyto D (7.94% ±0.56%)(Fig. 5E). To confirm that intercellular mitochondrial transfer from uninfected cells provided a cell death rescue effect on PRRSV-infected cells, we generated MARC-145 cells lacking mitochondrial DNA (mtDNA) and thus carrying defective mitochondria (**compare Fig. 3. 6A with 3. 6B**). The relative mtDNA content in normal MARC-145 cells or mitochondria defective MARC-145 cells were further compared by qPCR. The results showed that only trace amounts of mtDNA was detected in mitochondria defective cells (about 0.002% of mtDNA in normal cells, **Fig. 3. 6C**). More apoptotic cells were observed when the GFP-PRRSV infected MARC-145 cells were co-cultured with mitochondria defective cells (10.89% ±1.52%), in comparison to those co-cultured with cells containing functional mitochondria (8.41% ±0.52%) (**Fig. 3. 6C and 3. 6D**). IFA results further confirmed that mitochondria can be transferred from mitochondria-defect cells to PRRSV infected cells (**Fig. 3.**

6E). To rule out the possibility that depleting mtDNA in MARC-145 cells may inhibit nanotube formation, we compared the number of nanotubes in normal cells and mitochondria defective cells under PRRSV infection or uninfected conditions. As shown in **Fig. 3. 6F**, there was no significant difference of numbers of nanotubes in normal cells and mitochondria defective cells.

Next, we repeated the co-cultural experiment using PAMs, the primary host cells for PRRSV infection in pigs. Since the primary porcine macrophages could not be cultured for more than a week, we could not to generate mitochondria defective PAM cells (takes at least 30 days, see Materials &Methods section). We used porcine umbilical cord mesenchymal stem cells (PUCs) as the mitochondria donor cells. Mesenchymal stem cells have previously been used as a potential therapeutic to rescue injured cells from cell death (36, 64). In cell culture, PUC cells are easily differentiated from that of PAMs. PUC cells showed as bipolar or multi-polar shape with average diameter of 50um while PAMs are round shape with an average diameter of 10um. Furthermore, PUC cells do not support PRRSV replication, since no infectious virus was recovered after PRRSV infection or directly transfecting the PRRSV cDNA infectious clone into the PUC cells (**Fig. 3. 7A**). In this study, PAMs were initially infected with GFP-PRRSV. After 1 hpi, infected PAMs were co-cultured with PUCs. At 24 hpi, the cells were subjected to flow cytometry analysis. The results consistently showed that few GFP-PRRSV positive PAMs could be detected in the infected PAMs/infected PAMs co-culture condition (2.29% ± 1.32%), while about 25.6% ± 1.76% of GFP-PRRSV positive PAMs can be detected in the infected PAMs/PUCs co-culture condition at 24 hpi. In contrast, in PAMs/mitochondria defective PUCs co-culture fewer GFP-PRRSV+ cells were detected (12.6% ± 3.25%) compared to the cells in PAMs/healthy PUCs cocultures, indicating that mitochondria play a role in rescuing the infected PAMs. However, in comparison to the cells in the infected PAMs/infected PAMs co-cultures

(2.29% ± 1.32%), higher numbers of GFP-PRRSV+ PAMs were still detected in cells in PAMs/mitochondria defective PUCs (12.6% ± 3.25%) at 24 hpi, indicating that there might be other mechanism(s) underlying the cell rescue effect of PUCs. We observed a typical viral growth curve in infected PAMs/infected PAMs co-cultured cells, in which the virus titer reached a peak value at 24 hpi and then rapidly decreased due to the cell death. In contrast, an atypical growth curve was observed in infected PAMs/PUCs co-cultured cells, in which the virus titer was maintained at a lower level, but prolonged virus production was detected (**Fig. 3. 7D**). Nanotubes connecting the PUCs and GFP-PRRSV positive PAMs could also be observed, in which mitochondria and the GFP-tagged PRRSV protein were observed present in the nanotube (**Fig. 3. 7B**). The results further confirmed that functional mitochondria transferring from healthy cells could be involved in rescuing PRRSV-infected cells, although other mechanism(s) may also contribute to this rescuing effect.

PRRSV proteins associate with mitochondria and their intercellular transportation. In our previous study (42), we demonstrated that PRRSV utilized nanotubes for intercellular spread of infection. PRRSV RNA and certain viral proteins were observed presenting in/on the nanotubes, in which we suspected that some of these viral materials could be associated with mitochondria transport. To determine whether mitochondria could be utilized as a cargo to transport viral infectious materials for cell to cell spreading, we analyzed co-localization of mitochondria with viral proteins. MARC-145 cells were initially infected with PRRSV. At 12 hpi, cells were immunostained using a mAb against PRRSV nsp1α, nsp1β, nsp2, nsp4, nsp7, N, GP3, GP4 and GP5 protein. Mitochondria were visualized by staining for pAb TOM20. For PRRSV nsp2TF and M protein, PRRSV infected cells were initially stained by MitoTracker Red CMXRos, and the cells were then fixed, permeablized and stained using a pAb against PRRSV nsp2TF or M.

Confocal microscopy analysis showed that nsp1α, nsp1β, nsp4, N protein, but not other PRRSV proteins were detected to be co-localized with mitochondria in the nanotubes (**Fig. 3. 6A-E**). To confirm this data, mitochondria were isolated from PRRSV-infected cells and subjected to Western blot analysis. The result consistently showed that nsp1α, nsp1β, nsp4, and N, but not GP3 were detected in both cytosol and mitochondria fractions (**Fig. 3. 6F**), suggesting these viral proteins could be associated with mitochondria for intercellular transportation.

3.4 Discussion

In previous studies, cellular apoptosis and necrosis were observed during the later stage of PRRSV infection (13, 14, 17). In those studies, it was presumed that PRRSV itself evolved strategies to attenuate apoptosis during the early stage of infection in order to complete sufficient viral replication in host cells (14). In our present study, we demonstrated a novel mechanism of rescuing host cell death in PRRSV-infected cells. Our data showed that active transfer of mitochondria from healthy cells to PRRSV-infected cells through intercellular TNT connections could rescue the infected cells from apoptosis/necrosis. The mitochondria rescue effect was further confirm by the inability of mitochondria-damaged cells to rescue PRRSV-infected cells, indicating that functional mitochondria are necessary. In addition, cells treated with TNT inhibitors blocked the mitochondria transfer and inhibited the rescue effect during the early stage of viral infection, which demonstrates that nanotubes are required for the cell rescuing process. Intercellular nanotubes used for transferring cellular organelles and infectious viral materials have been reported previously (40-42, 61, 65). However, the type of TNTs (MT-TNT, AT-TNT or other unknown types) has not been specifically analyzed during viral infection. In our present study, both microtubulin containing nanotubes and F-actin containing nanotubes can be observed

in PRRSV-infected cells, and viral materials were observed to be present in both types of nanotubes. However, mitochondria were only detected in microtubulin containing nanotubes. These data suggest that the type of nanotube formation and viral/cellular material transportation are highly regulated processes. It was reported that the AT-TNTs and MT-TNTs are highly regulated structures compared to cellular protrusion passively pulled by neighboring cells (38, 45). MT-TNT was determined to have larger diameter tube than AT-TNT (45), which may facilitate more efficient transfer of cellular materials. MT-TNT was reported only formed in stressed cells at a very early apoptotic stages, before the activation of caspase-3; Cells at the execution phase of apoptosis/necrosis may not form MT-TNT and were not be rescued by healthy cells (45). Wang and Gerdes (2015) showed that ultraviolet light treated pheochromocytoma (PC) 12 cells form the MT-TNTs at the very early apoptotic stage, and the active movement of EB3 (microtubule binding protein) and the accumulation of detyrosinated tubulin were observed in these MT-TNTs (45). Our time course study consistently showed that there was a rapid (about 10 fold) increase of the nanotubes in PRRSV-infected MARC-145 cells at 12 hpi. In TNTs connecting between PRRSV-infected and uninfected cells, continuous microtubules were detected localizing inside the nanotubes as early as 12 hpi. This time period also correlates with the (none) low percentage of apoptotic and necrotic cells.

TNT formation was reported to be associated with ROS expression levels (38). Rustom (2016) proposed a ROS-dependent TNT formation model to explain this process. According to Rustom's model, local stress, such as viral infection, triggers the increasing level of ROS and distribution 'call-for-help' signals (S100) to unstressed cells in their surroundings. Corresponding receptors on the target cells function as 'signal receivers', which stimulates the local cytoplasmic ROS production that initiates TNT formation. TNTs provides an intercellular

connection for material/resource exchange in order to restore redox/metabolic homeostasis in stressed cells. Further increased levels of ROS and 'call-for-help' signals production resulted in MT-TNT formation, which allows more efficient intercellular material exchange to rescue stressed cells, including motor protein-mediated intercellular transfer of mitochondria along microtubules. Finally, exaggerated levels of ROS production induce apoptosis in stressed cells. The dynamic process of ROS production and TNT formation appears to share a common feature in PRRSV infected cells. Our results showed that significantly higher level of ROS can be detected as early as 6 hpi in PRRSV-infected cells. The ROS expression reached peak level at 24 hpi. Consistently, significantly increased level of danger signal S100A4 mRNA expression was detected from 12-36 hpi.

Intercellular exchange of mitochondria through TNTs has been shown as a general mechanism to rescue stressed cells (37, 45). However, those studies were dealing with physically injured cells (non-infected cells). Under the viral infection condition, specifically during the PRRSV infection, the TNT-mitochondria transport pathway appears to be used as a double-edged sword. On one hand, mitochondria transfer from uninfected to infected cells rescued the virus-stressed cells and delayed cell death. On the other hand, PRRSV takes advantage of delayed the cell death with additional time for virus replication and further utilizes the nanotube/ mitochondria pathway to transfer infectious materials and spread the infection to TNT-connected healthy cells. In our previous study, PRRSV RNA and certain proteins were observed to be transported through the TNT to neighbor cells (42). In the present study, PRRSV proteins nsp1α, nsp1β, nsp4, and N were detected to be co-localized with mitochondria in the TNTs; and Western blot results also confirmed the interaction between these viral proteins and mitochondria. These data suggest that mitochondria could function as a vehicle to transport

certain PRRSV materials through TNTs to neighboring cells. We did not find the colocalization of other viral proteins with mitochondria, suggesting other transporting mechanisms may also exist in TNTs.

In previous studies, mitochondrial transfer has been demonstrated in injured cells as a therapeutic strategy. In a mouse model, transferring mitochondria from bone marrow-derived stromal cells to alveolar epithelium cells protected the mouse against acute lung injury (37). A recent study also showed that mitochondrial transfer by human mesenchymal stem cells (hMSCs) to airway epithelial cells was able to attenuate cigarette smoke-induced damage in rats (64). Similarly we demonstrated that porcine umbilical cord mesenchymal stem cells could protect PAMs from cell death by transferring mitochondria to PRRSV-infected macrophages. Mitochondria-defect PUCs showed reduced ability to rescue infected PAMs, indicating the involvement of mitochondria in the cell rescuing effect. However, in comparison to the treatment group co-cultured with infected PAMs (**Fig. 3. 7C**, Infected/Infected), the group co-cultured with mitochondria-defect PUCs (**Fig. 3.7C**, Infected/defect PUCs) still showed higher percentage of GFP-PRRSV+ PAMs, suggesting that other mechanism(s) may also contribute to the cell rescue effect of PUCs. Indeed, a previous study demonstrated that the growth factors Ang1 and/or KGF secreted by hMSCs were partially involved in reducing high pathogenic influenza A H5N1-associated acute lung injury (66). Further studies are needed to elucidate the role of other cellular factors of PUCs in the cell rescuing effect. PUCs appear to not support PRRSV replication, since no infectious viruses were recovered after PRRSV infection or after directly transfecting the PRRSV cDNA infectious clone into PUC cells. The reason why PUCs were resistant to PRRSV infection is not known. Our data showed that PUCs are CD163 negative (data not shown). However, other cellular factors may also involve in the anti-PRRSV property of PUCs, since no

infectious viruses were recovered after directly transfecting the PRRSV cDNA infectious clone into PUC cells. As demonstrated by a previous study, canine DH82 cells support PRRSV internalization and viral protein expression, but progeny virus cannot be generated from this cell line, indicating an inhibition in late stages of viral replication (67). For our study, a reduced but prolonged viral production was detected in the PAMs/PUCs co-culture condition. At 24hpi, virus titers were significantly lower, but higher numbers of GFP-PRRSV+ PAMs was detected in PAMs/PUCs condition, indicating that certain cellular factors of co-cultured PUCs may inhibit later stage of viral replication for generating viral particles, but may not interfere viral protein expression (**Fig. 3. 7C and D**). The PUCs-rescued PAMs live longer, which account for the prolonged viral production. The detailed mechanism(s) of the anti-PRRSV property of PUCs needs to be further studied. To our knowledge, this study is the first to demonstrate mitochondrial rescue in virus-infected cells. Mitochondrial transferring from stem cells to virus-stressed cells is intriguing and could potentially be exploited as a therapeutic strategy.

3.5 References

1. Snijder EJ, Meulenberg JJM. 1998. The molecular biology of arteriviruses. Journal of General Virology 79:961-979.
2. Fang Y, Snijder EJ. 2010. The PRRSV replicase: Exploring the multifunctionality of an intriguing set of nonstructural proteins. Virus Research 154:61-76.
3. Li YH, Treffers EE, Napthine S, Tas A, Zhu LC, Sun Z, Bell S, Mark BL, van Veelen PA, van Hemert MJ, Firth AE, Brierley I, Snijder EJ, Fang Y. 2014. Transactivation of programmed ribosomal frameshifting by a viral protein. Proceedings of the National Academy of Sciences of the United States of America 111:E2172-E2181.
4. Snijder EJ, Kikkert M, Fang Y. 2013. Arterivirus molecular biology and pathogenesis. Journal of General Virology 94:2141-2163.

5. Duan X, Nauwynck HJ, Pensaert MB. 1997. Virus quantification and identification of cellular targets in the lungs and lymphoid tissues of pigs at different time intervals after inoculation with porcine reproductive and respiratory syndrome virus (PRRSV). Veterinary Microbiology 56:9-19.
6. Labarque GG, Nauwynck HJ, Van Reeth K, Pensaert MB. 2000. Effect of cellular changes and onset of humoral immunity on the replication of porcine reproductive and respiratory syndrome virus in the lungs of pigs. Journal of General Virology 81:1327-1334.
7. Oleksiewicz MB, Nielsen J. 1999. Effect of porcine reproductive and respiratory syndrome virus (PRRSV) on alveolar lung macrophage survival and function. Veterinary Microbiology 66:15-27.
8. Chitko-McKown CG, Chapes SK, Miller LC, Riggs PK, Ortega MT, Green BT, McKown RD. 2013. Development and characterization of two porcine monocyte-derived macrophage cell lines. Results Immunol 3:26-32.
9. Singleton H, Graham SP, Bodman-Smith KB, Frossard JP, Steinbach F. 2016. Establishing Porcine Monocyte-Derived Macrophage and Dendritic Cell Systems for Studying the Interaction with PRRSV-1. Frontiers in Microbiology 7.
10. Duan XB, Nauwynck HJ, Favoreel HW, Pensaert MB. 1998. Identification of a putative receptor for porcine reproductive and respiratory syndrome virus on porcine alveolar macrophages. Journal of Virology 72:4520-4523.
11. Loving CL, Brockmeier SL, Sacco RE. 2007. Differential type I interferon activation and susceptibility of dendritic cell populations to porcine arterivirus. Immunology 120:217-229.
12. Kim HS, Kwang J, Yoon IJ, Joo HS, Frey ML. 1993. Enhanced replication of porcine reproductive and respiratory syndrome (PRRS) virus in a homogeneous subpopulation of MA-104 cell line. Arch Virol 133:477-83.
13. Miller LC, Fox JM. 2004. Apoptosis and porcine reproductive and respiratory syndrome virus. Veterinary Immunology and Immunopathology 102:131-142.
14. Costers S, Lefebvre DJ, Delputte PL, Nauwynck HJ. 2008. Porcine reproductive and respiratory syndrome virus modulates apoptosis during replication in alveolar macrophages. Archives of Virology 153:1453-1465.

15. Kim TS, Benfield DA, Rowland RR. 2002. Porcine reproductive and respiratory syndrome virus-induced cell death exhibits features consistent with a nontypical form of apoptosis. Virus Res 85:133-40.
16. Wang X, Eaton M, Mayer M, Li H, He D, Nelson E, Christopher-Hennings J. 2007. Porcine reproductive and respiratory syndrome virus productively infects monocyte-derived dendritic cells and compromises their antigen-presenting ability. Arch Virol 152:289-303.
17. Lee SM, Kleiboeker SB. 2007. Porcine reproductive and respiratory syndrome virus induces apoptosis through a mitochondria-mediated pathway. Virology 365:419-34.
18. Schwartz LM, Osborne BA. 1993. Programmed Cell-Death, Apoptosis and Killer Genes. Immunology Today 14:582-590.
19. Fink SL, Cookson BT. 2005. Apoptosis, pyroptosis, and necrosis: Mechanistic description of dead and dying eukaryotic cells. Infection and Immunity 73:1907-1916.
20. Thomson BJ. 2001. Viruses and apoptosis. International Journal of Experimental Pathology 82:65-76.
21. Gao LY, Kwaik YA. 2000. The modulation of host cell apoptosis by intracellular bacterial pathogens. Trends in Microbiology 8:306-313.
22. Liesa M, Palacin M, Zorzano A. 2009. Mitochondrial Dynamics in Mammalian Health and Disease. Physiological Reviews 89:799-845.
23. Youle RJ, van der Bliek AM. 2012. Mitochondrial Fission, Fusion, and Stress. Science 337:1062-1065.
24. Galluzzi L, Kepp O, Kroemer G. 2012. Mitochondria: master regulators of danger signalling. Nature Reviews Molecular Cell Biology 13:780-788.
25. Kramer T, Enquist LW. 2012. Alphaherpesvirus Infection Disrupts Mitochondrial Transport in Neurons. Cell Host & Microbe 11:504-514.
26. Li YC, Boehning DF, Qian T, Popov VL, Weinman SA. 2007. Hepatitis C virus core protein increases mitochondrial ROS production by stimulation of Ca2+ uniporter activity. Faseb Journal 21:2474-2485.
27. Carrere-Kremer S, Montpellier-Pala C, Cocquerel L, Wychowski C, Penin F, Dubuisson J. 2002. Subcellular localization and topology of the p7 polypeptide of hepatitis C virus. Journal of Virology 76:3720-3730.

28. de Mendoza C, Martin-Carbonero L, Barreiro P, de Baar M, Zahonero N, Rodriguez-Novoa S, Renito JM, Gonzalez-Lahoz J, Soriano V. 2007. Mitochondrial DNA depletion in HIV-infected patients with chronic hepatitis C and effect of pegylated interferon plus ribavirin therapy. Aids 21:583-588.
29. Li S, Wang J, Zhou A, Khan FA, Hu L, Zhang S. 2016. Porcine reproductive and respiratory syndrome virus triggers mitochondrial fission and mitophagy to attenuate apoptosis. Oncotarget doi:10.18632/oncotarget.10817.
30. Li XD, Sun L, Seth RB, Pineda G, Chen ZJ. 2005. Hepatitis C virus protease NS3/4A cleaves mitochondrial antiviral signaling protein off the mitochondria to evade innate immunity. Proc Natl Acad Sci U S A 102:17717-22.
31. Dong J, Xu S, Wang J, Luo R, Wang D, Xiao S, Fang L, Chen H, Jiang Y. 2015. Porcine reproductive and respiratory syndrome virus 3C protease cleaves the mitochondrial antiviral signalling complex to antagonize IFN-beta expression. J Gen Virol 96:3049-58.
32. Schwarz KB. 1996. Oxidative stress during viral infection: a review. Free Radic Biol Med 21:641-9.
33. Lin X, Wang RF, Zou W, Sun X, Liu XK, Zhao LZ, Wang SY, Jin ML. 2016. The Influenza Virus H5N1 Infection Can Induce ROS Production for Viral Replication and Host Cell Death in A549 Cells Modulated by Human Cu/Zn Superoxide Dismutase (SOD1) Overexpression. Viruses-Basel 8.
34. Bottero V, Chakraborty S, Chandran B. 2013. Reactive Oxygen Species Are Induced by Kaposi's Sarcoma-Associated Herpesvirus Early during Primary Infection of Endothelial Cells To Promote Virus Entry. Journal of Virology 87:1733-1749.
35. Torralba D, Baixauli F, Sanchez-Madrid F. 2016. Mitochondria Know No Boundaries: Mechanisms and Functions of Intercellular Mitochondrial Transfer. Front Cell Dev Biol 4:107.
36. Spees JL, Lee RH, Gregory CA. 2016. Mechanisms of mesenchymal stem/stromal cell function. Stem Cell Res Ther 7:125.
37. Islam MN, Das SR, Emin MT, Wei M, Sun L, Westphalen K, Rowlands DJ, Quadri SK, Bhattacharya S, Bhattacharya J. 2012. Mitochondrial transfer from bone-marrow-derived stromal cells to pulmonary alveoli protects against acute lung injury. Nature Medicine 18:759-U153.

38. Rustom A. 2016. The missing link: does tunnelling nanotube-based supercellularity provide a new understanding of chronic and lifestyle diseases? Open Biol 6.
39. Marzo L, Gousset K, Zurzolo C. 2012. Multifaceted roles of tunneling nanotubes in intercellular communication. Frontiers in Physiology 3.
40. Hashimoto M, Bhuyan F, Hiyoshi M, Noyori O, Nasser H, Miyazaki M, Saito T, Kondoh Y, Osada H, Kimura S, Hase K, Ohno H, Suzu S. 2016. Potential Role of the Formation of Tunneling Nanotubes in HIV-1 Spread in Macrophages. Journal of Immunology 196:1832-1841.
41. Roberts KL, Manicassamy B, Lamb RA. 2015. Influenza A Virus Uses Intercellular Connections To Spread to Neighboring Cells. Journal of Virology 89:1537-1549.
42. Guo R, Katz BB, Tomich JM, Gallagher T, Fang Y. 2016. Porcine Reproductive and Respiratory Syndrome Virus Utilizes Nanotubes for Intercellular Spread. Journal of Virology 90:5163-5175.
43. Zeman D, Neiger R, Yaeger M, Nelson E, Benfield D, Leslie-Steen P, Thomson J, Miskimins D, Daly R, Minehart M. 1993. Laboratory investigation of PRRS virus infection in three swine herds. J Vet Diagn Invest 5:522-8.
44. Carlin R, Davis D, Weiss M, Schultz B, Troyer D. 2006. Expression of early transcription factors Oct-4, Sox-2 and Nanog by porcine umbilical cord (PUC) matrix cells. Reproductive Biology and Endocrinology 4.
45. Wang X, Gerdes HH. 2015. Transfer of mitochondria via tunneling nanotubes rescues apoptotic PC12 cells. Cell Death and Differentiation 22:1181-1191.
46. King MP, Attardi G. 1996. Isolation of human cell lines lacking mitochondrial DNA. Methods Enzymol 264:304-13.
47. Li Y, Treffers EE, Napthine S, Tas A, Zhu L, Sun Z, Bell S, Mark BL, van Veelen PA, van Hemert MJ, Firth AE, Brierley I, Snijder EJ, Fang Y. 2014. Transactivation of programmed ribosomal frameshifting by a viral protein. Proc Natl Acad Sci U S A 111:E2172-81.
48. Kappes MA, Miller CL, Faaberg KS. 2013. Highly Divergent Strains of Porcine Reproductive and Respiratory Syndrome Virus Incorporate Multiple Isoforms of Nonstructural Protein 2 into Virions. Journal of Virology 87:13456-13465.

49. Chen Z, Lawson S, Sun Z, Zhou X, Guan X, Christopher-Hennings J, Nelson EA, Fang Y. 2010. Identification of two auto-cleavage products of nonstructural protein 1 (nsp1) in porcine reproductive and respiratory syndrome virus infected cells: nsp1 function as interferon antagonist. Virology 398:87-97.
50. Nelson EA, Christopher-Hennings J, Drew T, Wensvoort G, Collins JE, Benfield DA. 1993. Differentiation of U.S. and European isolates of porcine reproductive and respiratory syndrome virus by monoclonal antibodies. J Clin Microbiol 31:3184-9.
51. Ropp SL, Wees CE, Fang Y, Nelson EA, Rossow KD, Bien M, Arndt B, Preszler S, Steen P, Christopher-Hennings J, Collins JE, Benfield DA, Faaberg KS. 2004. Characterization of emerging European-like porcine reproductive and respiratory syndrome virus isolates in the United States. J Virol 78:3684-703.
52. Fang Y, Treffers EE, Li Y, Tas A, Sun Z, van der Meer Y, de Ru AH, van Veelen PA, Atkins JF, Snijder EJ, Firth AE. 2012. Efficient -2 frameshifting by mammalian ribosomes to synthesize an additional arterivirus protein. Proc Natl Acad Sci U S A 109:E2920-8.
53. Li YH, Tas A, Snijder EJ, Fang Y. 2012. Identification of porcine reproductive and respiratory syndrome virus ORF1a-encoded non-structural proteins in virus-infected cells. Journal of General Virology 93:829-839.
54. Livak KJ, Schmittgen TD. 2001. Analysis of relative gene expression data using real-time quantitative PCR and the 2(-Delta Delta C(T)) Method. Methods 25:402-8.
55. Li Y, Tas A, Sun Z, Snijder EJ, Fang Y. 2015. Proteolytic processing of the porcine reproductive and respiratory syndrome virus replicase. Virus Res 202:48-59.
56. Srikrishna G, Freeze HH. 2009. Endogenous Damage-Associated Molecular Pattern Molecules at the Crossroads of Inflammation and Cancer. Neoplasia 11:615-628.
57. Leclerc E, Fritz G, Weibel M, Heizmann CW, Galichet A. 2007. S100B and S100A6 differentially modulate cell survival by interacting with distinct RAGE (receptor for advanced glycation end products) immunoglobulin domains. Journal of Biological Chemistry 282:31317-31331.
58. Zhang L, Zhang Y. 2015. Tunneling nanotubes between rat primary astrocytes and C6 glioma cells alter proliferation potential of glioma cells. Neuroscience Bulletin 31:371-378.

59. Zhu DH, Tan KS, Zhang XL, Sun AY, Sun GY, Lee JCM. 2005. Hydrogen peroxide alters membrane and cytoskeleton properties and increases intercellular connections in astrocytes. Journal of Cell Science 118:3695-3703.
60. Gerdes H-H, Bukoreshtliev NV, Barroso JFV. 2007. Tunneling nanotubes: A new route for the exchange of components between animal cells. FEBS Letters 581:2194-2201.
61. Frederick RL, Shaw JM. 2007. Moving mitochondria: Establishing distribution of an essential organelle. Traffic 8:1668-1675.
62. Morris RL, Hollenbeck PJ. 1995. Axonal transport of mitochondria along microtubules and F-actin in living vertebrate neurons. J Cell Biol 131:1315-26.
63. Ligon LA, Steward O. 2000. Role of microtubules and actin filaments in the movement of mitochondria in the axons and dendrites of cultured hippocampal neurons. J Comp Neurol 427:351-61.
64. Li X, Zhang Y, Yeung SC, Liang Y, Liang X, Ding Y, Ip MS, Tse HF, Mak JC, Lian Q. 2014. Mitochondrial transfer of induced pluripotent stem cell-derived mesenchymal stem cells to airway epithelial cells attenuates cigarette smoke-induced damage. Am J Respir Cell Mol Biol 51:455-65.
65. Rustom A, Saffrich R, Markovic I, Walther P, Gerdes HH. 2004. Nanotubular highways for intercellular organelle transport. Science 303:1007-10.
66. Chan MC, Kuok DI, Leung CY, Hui KP, Valkenburg SA, Lau EH, Nicholls JM, Fang X, Guan Y, Lee JW, Chan RW, Webster RG, Matthay MA, Peiris JS. 2016. Human mesenchymal stromal cells reduce influenza A H5N1-associated acute lung injury in vitro and in vivo. Proc Natl Acad Sci U S A 113:3621-6.
67. Calvert JG, Slade DE, Shields SL, Jolie R, Mannan RM, Ankenbauer RG, Welch SK. 2007. CD163 expression confers susceptibility to porcine reproductive and respiratory syndrome viruses. J Virol 81:7371-9.

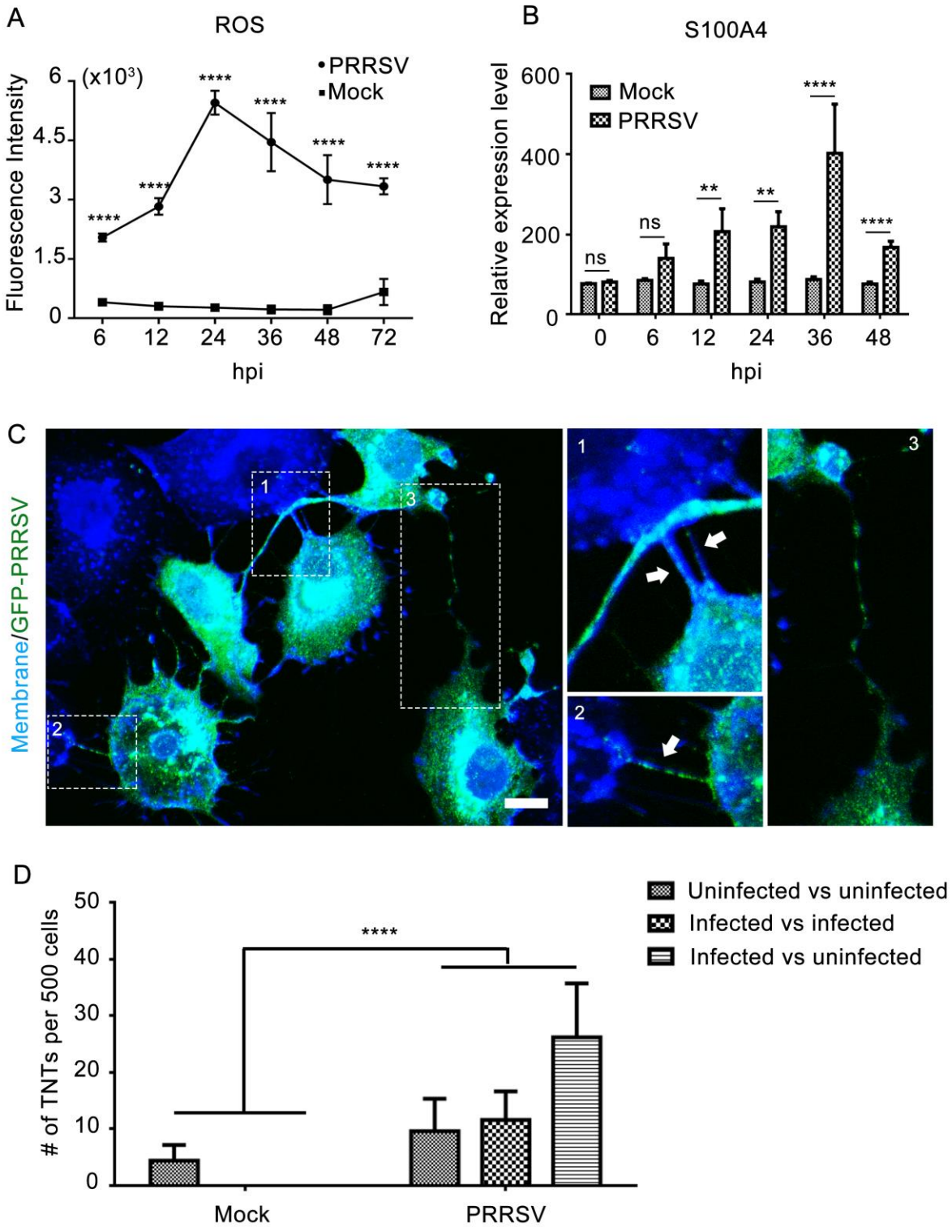
A
ROS
Fluorescence Intensity
(x10³)
PRRSV
Mock
hpi
B
S100A4
Relative expression level
Mock
PRRSV
hpi
C
Membrane/GFP-PRRSV
D
# of TNTs per 500 cells
Uninfected vs uninfected
Infected vs infected
Infected vs uninfected
Mock
PRRSV

Figure 3.1 PRRSV-infected cells release 'call-for-help' signals (ROS, S100A4) and increased formation of nanotubes. (A) Intracellular ROS levels detected in PRRSV-infected or uninfected MARC-145 cells. MARC-145 cells were infected with PRRSV strain SD95-21 or mock-infected with cell culture medium. Cells collected from indicated time points were subject to cellular assay for detecting ROS expression. The fluorescence signals were recorded by FLUOstar Omega microplate reader (BMG Lab Tech) at 485 nm for excitation and 535 nm for emission. (B) Relative expression level of S100A4 in PRRSV-infected or uninfected MARC-145 cells. MARC-145 cells were infected with PRRSV or mock infected with cell culture medium. Cells collected from indicated time points were subjected to cellular total RNA isolation and qRT-PCR analysis. The amount of S100A4 was normalized to the expression level of endogenous GAPDH mRNA. (C-E) Formation of intercellular nanotube connections between infected and uninfected cells during early stage of PRRSV infection. MARC-145 cells were infected with GFP-PRRSV or mock-infected with cell culture medium. At indicated time points, cell membrane was stained by red fluorescent dye, WGA-AF350 (Invitrogen), and fixed with 4% paraformaldehyde. Nanotube formation was visualized by confocal microscopy with 40× oil immersion objective lens. Arrows indicate nanotubes between GFP-PRRSV-infected and uninfected cells (C). Nanotubes connecting between uninfected and uninfected cells; infected and uninfected cells; and infected and infected cells were counted at 12 hours post infection. Images were taken by a confocal microscope (LSM 880, Zeiss). Scale bar, 10 μm.

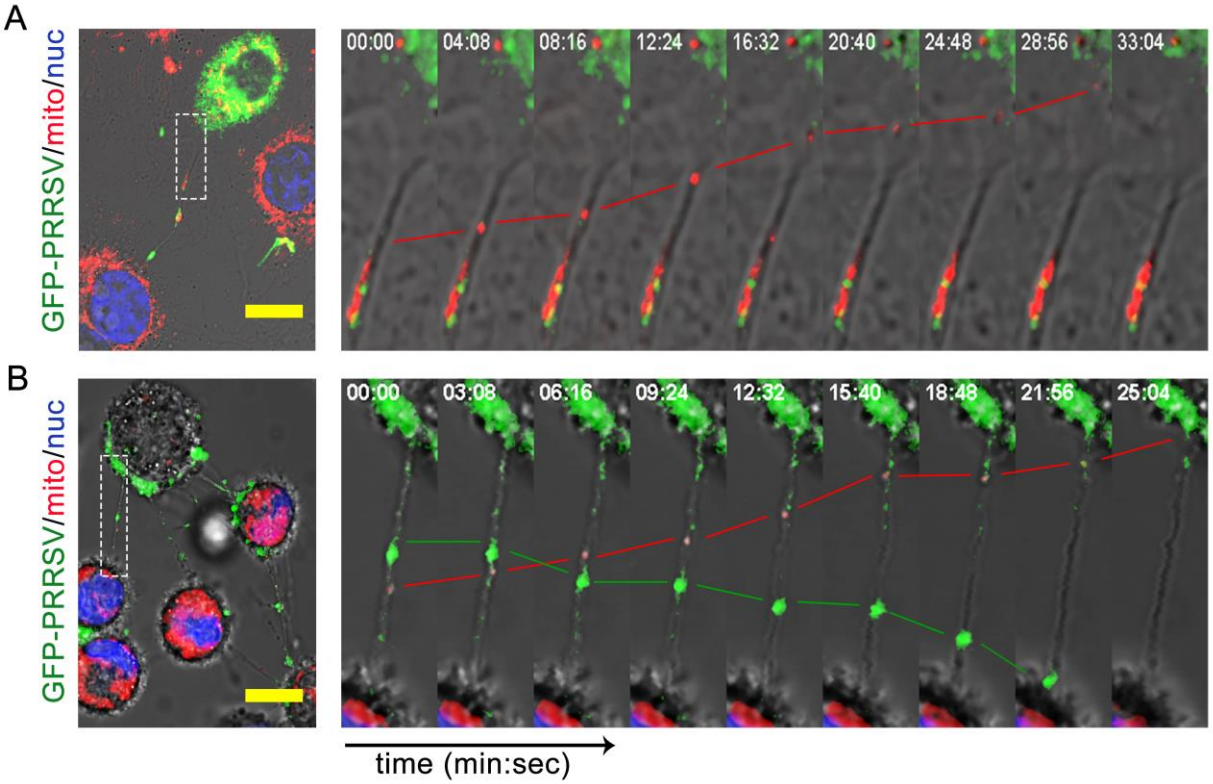
A
GFP-PRRSV/mito/nuc
00:00
04:08
08:16
12:24
16:32
20:40
24:48
28:56
33:04
B
GFP-PRRSV/mito/nuc
00:00
03:08
06:16
09:24
12:32
15:40
18:48
21:56
25:04
time (min:sec)

Figure 3.2 Confocal cell image demonstrating intercellular mitochondria transportation from uninfected to infected cells through tunneling nanotubes. (A) MARC-145 cells were initially infected with GFP-PRRSV; and at 12 hpi, cells were co-cultured with uninfected MARC-145 cells containing TMRM-labeled mitochondria and Hoechst 33342 labeled nucleus. After additional 12 hours incubation, cells were subjected to live cell image under confocal microscopy. (B) PAMs were initially infected with GFP-PRRSV; and at 6 hpi, cells were co-cultured with uninfected PAMs containing TMRM-labeled mitochondria and Hoechst 33342 labeled nucleus. After additional 6 hours incubation, macrophages were analyzed by live cell image system of a confocal microscope (LSM 880, Zeiss). GFP-PRRSV infected cells were showed in green. Mitochondria were showed in red. Nucleus was shown in blue. Boxed area showing a specific nanotube that contains mitochondria moving from a bottom uninfected cell to a top infected cell. The direction of mitochondria movement was demonstrated with red bars. The direction of GFP-nsp2 movement was demonstrated with green bars. Pictures were taken under a confocal microscope (LSM 880, Zeiss). Scale bar, 10 μm.

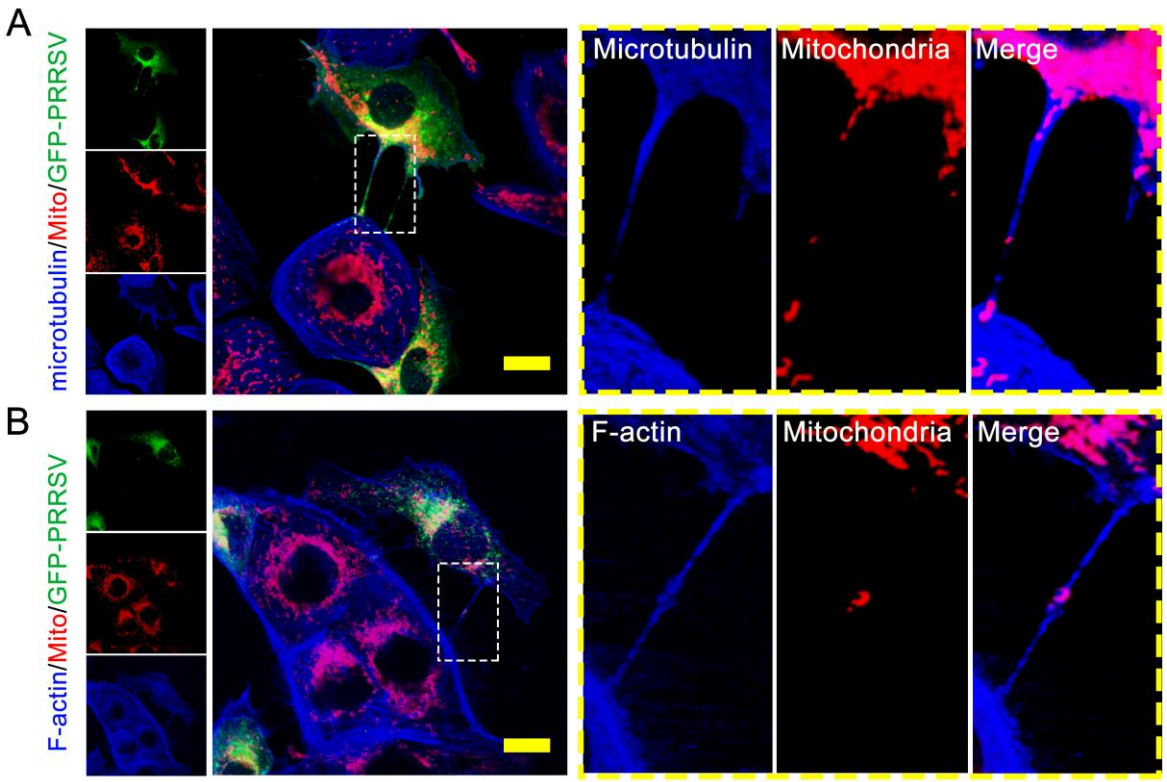

Figure 3.3 Microtubulins were associated with nanotubes containing mitochondria. **(A)** Detection of microtubulins in nanotubes during PRRSV infection. MARC-145 cells were infected with GFP-PRRSV. At 12 hpi, cells were immunostained with a mAb against microtubulin and a pAb against mitochondria marker protein, TOM20. **(B)** Detection of F-actin in nanotubes during PRRSV infection. F-actin was stained with Alexa Fluor 594-conjugated phalloidin. Pictures were taken under a confocal microscope (LSM 880, Zeiss). Scale bar, 10 μm.

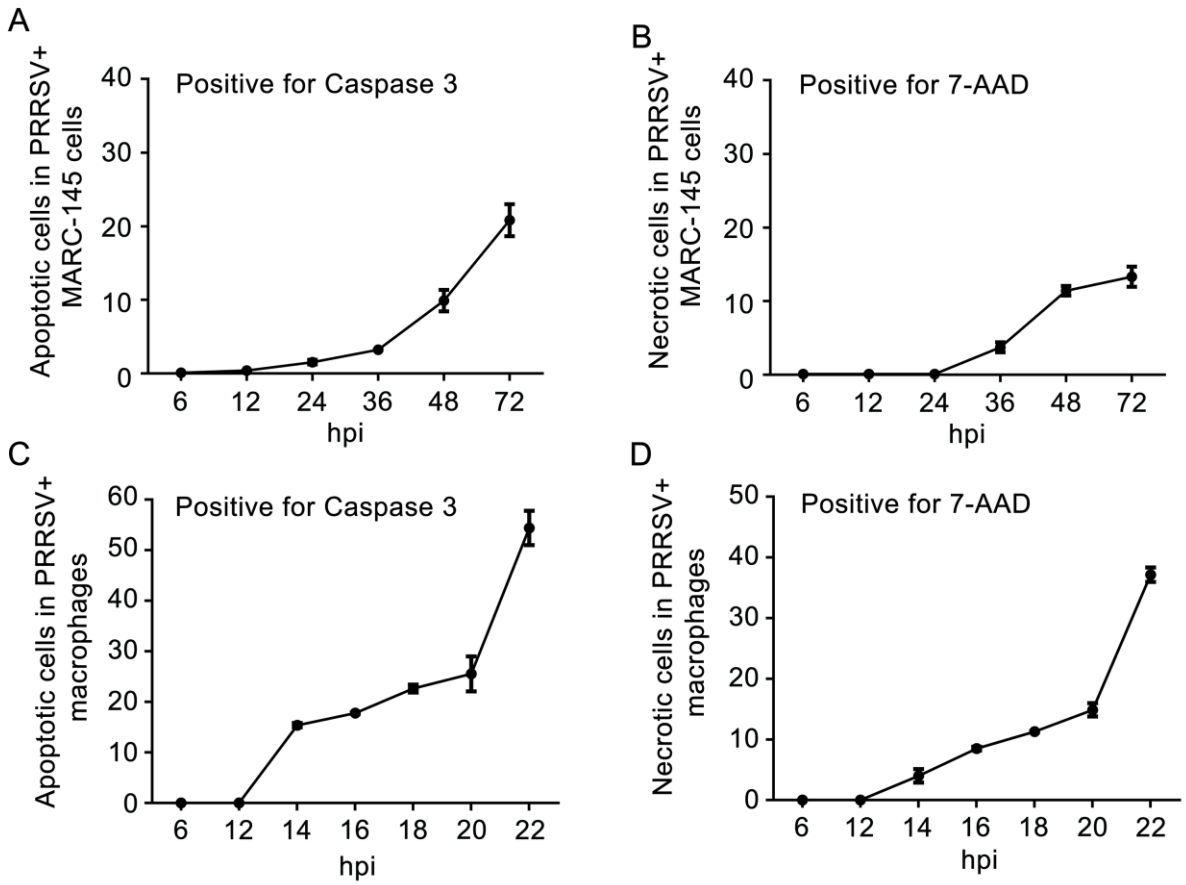

Figure 3.4 Kinetics of cell death in GFP-PRRSV-positive cells. MARC-145 cells (A and B) or PAMs (C and D) were infected with GFP-PRRSV. Samples collected at indicated time points were stained for apoptosis marker (caspase 3) or necrotic marker (7-AAD), and then subjected to flow cytometry analysis. The graphs show the percentages of GFP-PRRSV positive cells with activated caspase 3 or a positive 7-AAD staining. (A and B) Percentages of GFP-PRRSV positive MARC-145 cells underwent apoptosis (A) or necrosis (B). (C and D) GFP-PRRSV positive PAMs underwent apoptosis (C) or necrosis (D). Percentages of data represent the mean ± standard deviation of three independent experiments.

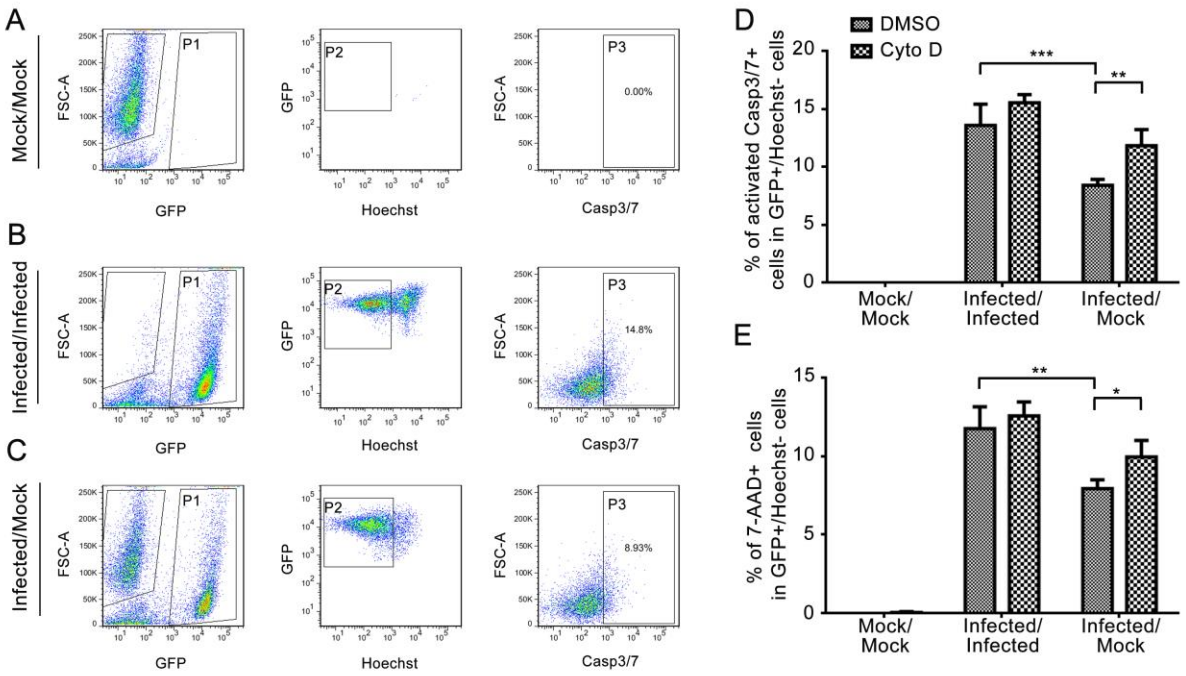

Figure 3.5 Mitochondria transfer through nanotubes rescued necrosis/apoptosis in PRRSV infected cells. MARC-145 cells were initially infected with GFP-PRRSV. At 24 hpi, infected MARC-145 cells were co-cultured with equal numbers of infected or uninfected cells. Hoechst 33342 was used to differentiate the cells from the initially infected cells. After additional 24 hours incubation, cells were stained with an apoptosis marker, caspase 3/7, or a necrosis marker, 7-AAD. To block nanotube formation, cell cultural medium was supplemented with 5μM Cyto D at 1 hour after co-culturing of cells. Representative plots of cell apoptosis analysis of uninfected/uninfected(A), infected/infected(B), infected/uninfected(C) coculture system. . (C) Percentage of GFP-PRRSV+/Hoechst- cells undergoing apoptosis with or without Cyto D treatment. (D) Percentage of GFP-PRRSV+/Hoechst- cells undergoing necrosis with or without Cyto D treatment. Cyto D: cytochalasin D. Percentages of data represent the mean ± standard deviation of three independent experiments.

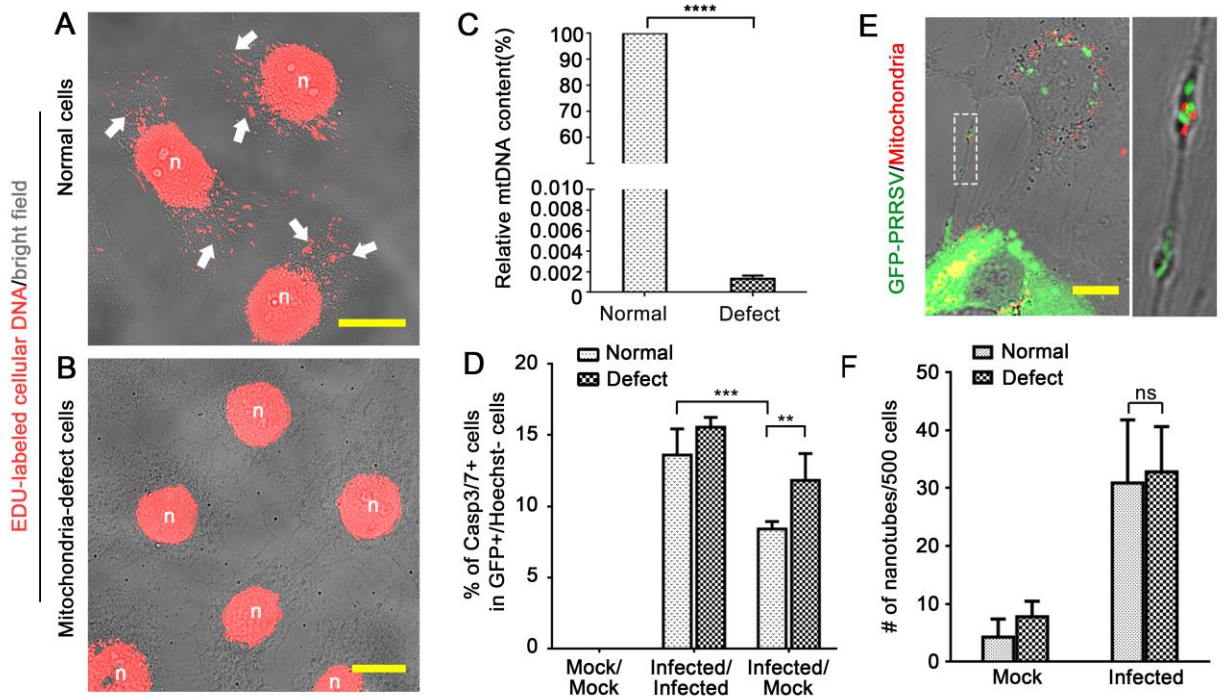
A
Normal cells
B
Mitochondria-defect cells
EDU-labeled cellular DNA/bright field
n
C
Relative mtDNA content(%)
100
90
80
70
60
0.010
0.008
0.006
0.004
0.002
0
****
Normal
Defect
D
Normal
Defect
% of Casp3/7+ cells in GFP+/Hoechst- cells
20
15
10
5
0
***
**
Mock/ Mock
Infected/ Infected
Infected/ Mock
E
GFP-PRRSV/Mitochondria
F
Normal
Defect
# of nanotubes/500 cells
50
40
30
20
10
0
ns
Mock
Infected

Figure 3.6 Ethidium bromide and uridine treated cells carrying defective mitochondria were unable to rescue PRRSV-infected cells from necrosis. (A and B) Detection of mitochondria DNA (mtDNA) in normal MARC-145 cells (A) or MARC-145 cells containing defective mitochondria (B). The mtDNA was detected by using the Click-iT EdU Microplate Assay Kit (ThermoFisher). Scale bar, 10 μm. Arrows in panel A indicate mtDNA. (C) Relative expression level of mtDNA. The cellular DNA from normal or mitochondria defective MARC-145 cells were extracted and subjected to qPCR. The COI copies were normalized with 18s rDNA. (D) Percentage of apoptotic cells in GFP-PRRSV/Hoechst- cells in co-culture system. MARC-145 cells were initially infected with GFP-PRRSV. At 24 hpi, infected MARC-145 cells were co-cultured with normal MARC-145 cells or mitochondria-defect MARC-145 cells. After additional 24 hours incubation, the cells were stained for Casp3/7 and subjected to flow cytometry analysis. Percentages of data represent the mean ± standard deviation of three independent experiments. (E) Mitochondria-defect MARC-145 cells were infected with GFP-PRRSV and then stained by TMRM to visualize mitochondria. Nanotubes connecting infected and uninfected mitochondria-defect MARC-145 cells were observed under a confocal microscope (LSM 880, Zeiss). Scale bar, 10 μm. (F) Normal or mitochondria-defect MARC-145 cells were infected with GFP-PRRSV or mock-infected. Nanotubes were counted from 10 randomly chosen fields of view at 24 hours post co-culture.

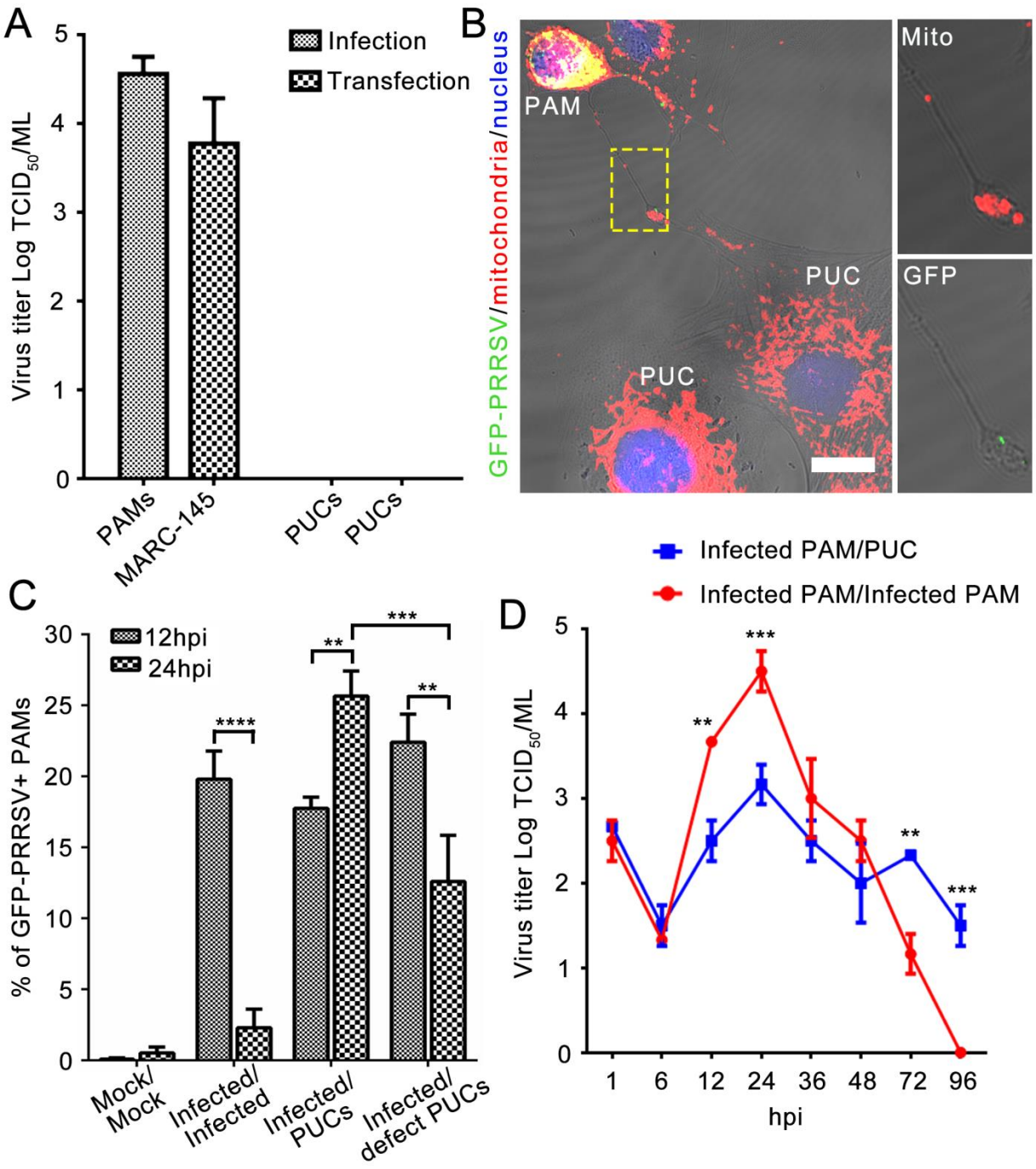
A
Infection
Transfection
Virus titer Log TCID50/ML
PAMs
MARC-145
PUCs
PUCs
B
GFP-PRRSV/mitochondria/nucleus
PAM
PUC
PUC
Mito
GFP
C
12hpi
24hpi
% of GFP-PRRSV+ PAMs
Mock/ Mock
Infected/ Infected
Infected/ PUCs
Infected/ defect PUCs
D
Infected PAM/PUC
Infected PAM/Infected PAM
Virus titer Log TCID50/ML
hpi

Figure 3.7 Co-culture of PUC stem cells rescued GFP-PRRSV infected PAMs from apoptosis. (A) PUC cells were infected by GFP-PRRSV at a moi of 0.1 or transfected with GFP-tagged full-length cDNA clone. PAMs were used as an infection control. MARC-145 cells were used as a transfection control. Cell culture supernatant were subjected to virus titration at 48 hours post infection or transfection. (B) PAMs were infected with GFP-PRRSV, and then co-cultured with normal or mitochondria-defect PUCs at 1 hpi. At 12 hours post co-culture, co-cultured cells were stained with TMRM to visualize mitochondria, and cells were subjected to live cell image. Pictures were taken under a confocal microscope (LSM 880, Zeiss). Scale bar, 10 μm. (C) PAMs were infected with GFP-PRRSV, and then co-cultured with normal or mitochondria-defect PUCs at 1 hpi. After additional 11 or 23 hours incubation, the co-cultured cells were subjected to flow cytometry analysis. Percentages of GFP-PRRSV PAMs in mono-culture or co-culture condition at 12 or 24 hpi were measured. Mock-infected cells were included as a control. Percentages of data represent the mean ± standard deviation of three independent experiments. (D) Cell culture supernantant collected from PAMs/PAMs or PAMs/PUCs condition was used for virus titration.

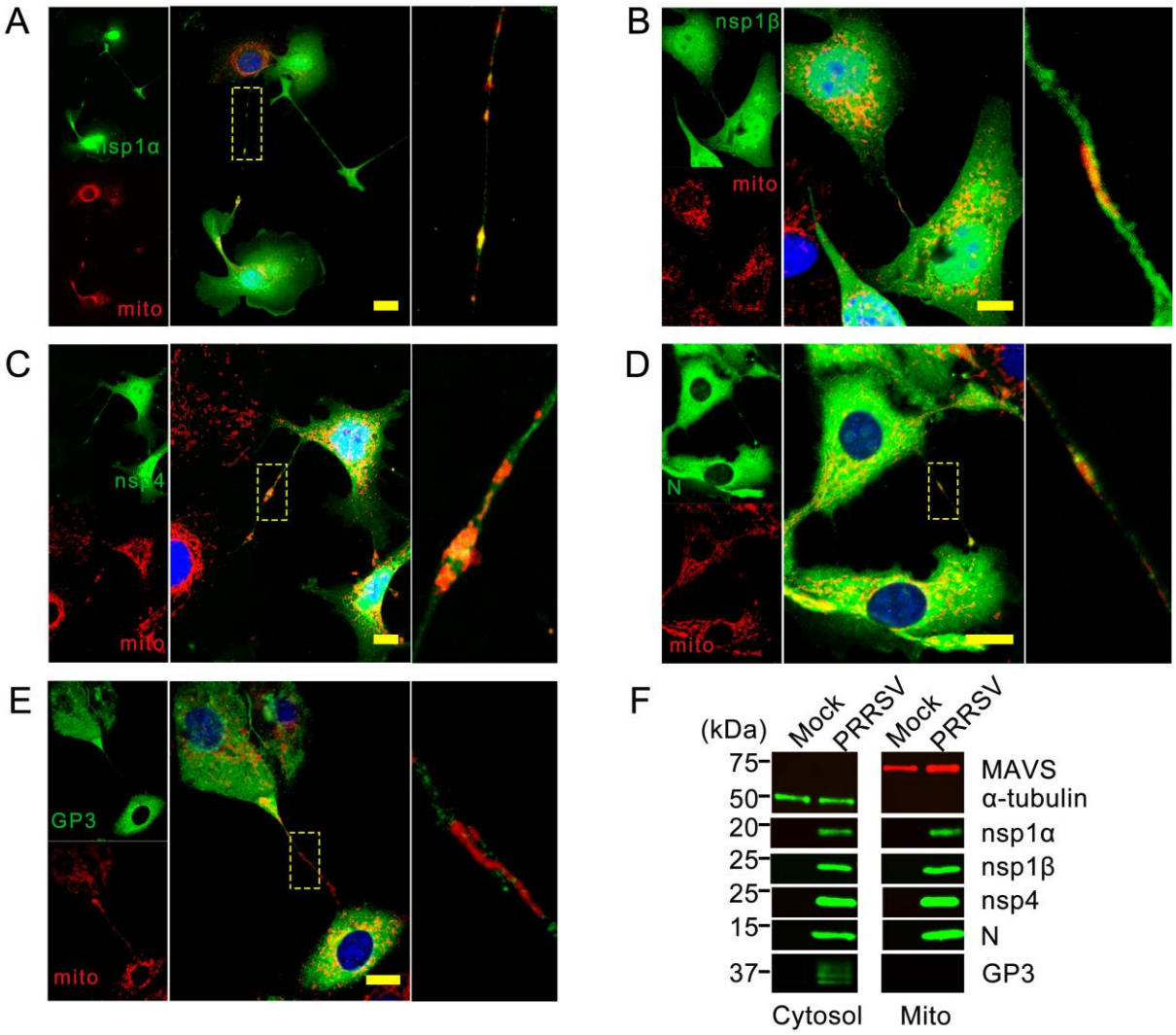
A
nsp1α
mito
B
nsp1β
mito
C
nsp4
mito
D
N
mito
E
GP3
mito
F
(kDa)
Mock
PRRSV
Mock
PRRSV
75
50
20
25
25
15
37
MAVS
α-tubulin
nsp1α
nsp1β
nsp4
N
GP3
Cytosol
Mito

Figure 3.8 Localization of PRRSV proteins and mitochondria in the TNTs. MARC-145 cells were initially infected with PRRSV. At 12 hpi, cells were fixed, permeabilized, and immunostained with a MAb against nsp1α (A), nsp1β (B), nsp4 (C), N (D) protein, or GP3 (E) Mitochondria were visualized by staining with anti-TOM20 PAb. Pictures were taken under a confocal microscope (LSM 880, Zeiss). Boxed area in the middle panels shows a zoomed area of nanotube in the right panels. Scale bar, 10μm. (F) MARC-145 cells were infected with PRRSV or mock-infected. At 24 hpi, the cells were subjected to mitochondria isolation. Viral proteins in cytosolic and mitochondrial fraction were detected by western blot using specific MAbs against nsp1α (A), nsp1β (B), nsp4 (C), N (D) or GP3 (E). MAVS was detected as a mitochondria marker, while α-tubulin was detected as a cytosol marker.

Chapter 4 - Double-stranded viral RNA persists *in vitro* and *in vivo* during prolonged infection of porcine reproductive and respiratory syndrome virus

Rui Guo, Pengcheng Shang, Celena A. Carrillo, Zhi Sun, Yashavanth Shaan Lakshmanappa, Tao Wang, Xingyu Yan, Megan C. Niederwerder, Raymond R.R. Rowland, Gourapura J. Renukaradhya, Jodi McGill, Crystal J. Jaing, Ying Fang

(Submitted to Journal of Virology)

Abstract: Porcine reproductive and respiratory syndrome virus (PRRSV) infection can be divided into at least two distinct stages: acute infection and persistence. Currently, little is known about the mechanism of PRRSV persistence. In this study, a cellular model of persistent infection was established using PRRSV-infected cells that had 109 passages in vitro. Strand-specific quantitative RT-PCR revealed that plus- and minus-strand viral RNAs were present at nearly equivalent levels; and immunofluorescence microscopy and RNAase I treatment analysis showed that double-stranded RNA (dsRNA) conformation existed in persistently infected cells. In contrast, plus- and minus-strand viral RNAs were present at about 69:1 ratio in acute infected cells. Consistent with the data generated from the in vitro cell culture system, there was about 3.3-fold reduction of the plus to minus-strand viral RNAs ratio in lymphoid tissues from PRRSV persistence pigs compared to that in acute PRRSV-infected pigs. Similar results were also obtained from lymphoid tissues collected at 70dpi. Immunohistochemistry analysis showed that viral dsRNAs were detected aggregating inside the germinal centers of tonsil and lymph nodes from PRRSV persistence pigs, while most of the dsRNAs were detected in marginal zones of lymphoid tissues in acute PRRSV-infected pigs. RNA array analysis further showed that dsRNA

in lymphoid tissues had limited ability to stimulate host antiviral responses during persistent infection stage. These results suggest that the PRRSV dsRNA functions as a mediator for viral persistence. The viral dsRNA persistence in germinal centers of lymphoid tissues may reveal a novel mechanism for PRRSV to escape antiviral immune responses.

4.1 Introduction

Porcine reproductive and respiratory syndrome virus (PRRSV) is an enveloped positive-stranded RNA virus, which belongs to the family *Arteriviridae*, order Nidovirales. The virus has a very restricted host range and cell tropism. Pigs are the only known natural host of PRRSV; and the fully differentiated porcine alveolar macrophage serves as a primary cell target for PRRSV infection during acute infection (1). Among many different cell lines tested, only the African green monkey kidney cell line MA-104, and its derivatives, such as MARC-145, are fully permissive for PRRSV replication *in vitro* (2).

PRRSV enters the host cells through standard clathrin-mediated endocytosis, in which CD163 is the major receptor. Following endosome acidification and membrane fusion, the viral genome is released into the cytosol of the infected cell (3, 4). The viral genome is about 15kb in length and contains 5'- UTR, eleven known open reading frames, 3'-UTR. Initial genome translation yields the replicase polyproteins pp1α-nsp2TF, pp1α-nsp2N, pp1a, and pp1ab. These polyproteins are cleaved by viral internal proteinases to generate at least 16 nonstructural proteins, nsp1α/β, nsp2, nsp2TF, nsp2N, nsp3-nsp12 (5, 6). With the exception of the recently discovered nsp2TF and nsp2N, these nonstructural proteins are presumably to be assembled into a replication and transcription complex (RTC). (7). The RTC first synthesizes the full-length minus-strand RNA and subgenomic (sg)-length minus-strand RNAs. The full-length minus-strand RNA is the

template for the synthesis of full-length plus-strand genomes, while the minus-strand sg mRNAs serve as templates for the synthesis of plus-strand sg mRNAs. The sg mRNAs are translated into four membrane-associated glycoproteins (GP2a, GP3, GP4 and GP5), three non-glycosylated membrane proteins (E, ORF5a and M) and the nucleocapsid protein (N) (5, 8). Newly generated full-length plus-strand RNA genomes are packaged into nucleocapsids, which become enveloped by budding through smooth intracellular membranes (5).

After PRRSV infection, initial rapid cytopathic replication in swine macrophages leads to viremia with the release of a large quantity of viral particles into the blood. Within a few weeks, virus disappears from the blood, the result of induction of robust innate and adaptive immune responses. However, after initial acute infection, virus can persist in infected pigs for several months (6, 9-11). RT-PCR can detect viral RNA in lymph nodes for more than 200 days ((10, 12, 13)Molina et al., 2009). PRRSV persistence is defined as the recovery of virus from lymphoid tissues in the absence of viremia (6, 13) . The ability to maintain a long-term nonclinical infection is one of the hallmarks of PRRSV infection. However, PRRSV persistence is not a steady-state infection; the virus decays with time and eventually becomes extinct (6, 9). The mechanism for extinction is unclear but likely results from the disappearance permissive cells. Therefore, persistence during PRRSV infection refers to the period between the disappearance of virus from the blood and extinction in the host (6, 13).

In order to establish a persistent infection, viruses have to meet at least two conditions: (1) evasion of host antiviral responses; (2) the ability to maintain viral genomes within at least a small proportion of infected cells (14, 15)(Randall et al., 2017). Several positive-stranded RNA viruses maintain persistence as double-stranded (ds) RNA; a mechanism to preserve genome stability in the absence of active replication (16-18). For the arteriviruses, dsRNAs are found as

intermediate products of replication (19). In present study, we investigated PRRSV persistence in a cell culture model derived from the serial passage of PRRSV-infected cells. The persistence of viral dsRNA and its association to host immune responses were further analyzed in lymphoid tissues from persistently infected pigs. Our findings revealed a novel PRRSV pathogenic mechanism, in which the dsRNA functions as a potential genomic reservoir for viral persistence.

4.2 Materials and Methods

Cells and viruses. PRRSV-2 isolate SD95-21 (GenBank accession no. KC469618) was used in all *in vitro* assays and pig experiment (trial-1, see below). PRRSV-2 isolate KS62 (GenBank Accession #KM035803) was used in pig experiment (trial-2; see below). MARC-145 cells were used for virus infection and subsequent experiments *in vitro*. These cells were maintained in minimum essential medium (Invitrogen) supplemented with 10% heat-inactivated fetal bovine serum and antibiotics (100 μg/ml of penicillin and streptomycin and 0.25 μg/ml of fungizone) at 37^{o}C with 5% CO_2.

Establishing PRRSV persistent cells: PRRSV persistent cells were established by growing MARC-145 cells that survived in standard acute infection. Initially, ten T-25 flasks of MARC-145 cells were infected with 1 moi of PRRSV strain SD95-21. At 72 hours post infection (hpi), dead cells were washed off by cell culture medium and fresh cell growth medium was added to maintain the cells that survived from acute infection. One flask of cells and medium was harvested each day for 10 days. The cells were trypsinized, stained with 10% Trypan Blue (Sigma), and the number of viable cells was counted using a hemocytometer. Viral RNA copies in the cell culture supernatant were quantified by qRT-PCR assay using the method described previously (24) . A portion of the cells (1/3) in the tenth flask were subcultured up to 109

passages. For each passage, cells were cultured for 3-4 days; and then trypsinized and split in three ways, with 1/3 of the cells placed in a new T-25 flask, another 1/3 of the cells stored in liquid N_2, and the remaining 1/3 cells were used for analysis of viral infection. Passage 109 (P109) cells were designated as MARC/PRRSV-P109, and all P109 cells were initially frozen in liquid N_2 and subsequently used in experiments to study the persistent infection. To determining the growth rates of P109 cells and PRRSV infection, MARC/PRRSV-P109 cells were thawed from liquid N_2 and seeded on 6-well tissue culture plates at the density of 1×10^5/ well. Two wells of cells were harvested each day. One well of cells were trypsinized, stained with 10% Trypan Blue (Sigma), and the number of viable cells was counted using a hemocytometer; another well of cells were fixed for immunofluorescent assay to detect the expression of PRRSV nsp2 and M proteins (see below). Viral RNA copies in the cell culture supernatant were quantified by qRT-PCR assay as described previously (22).

Antibodies. Antibodies for detecting PRRSV proteins, including monoclonal antibody (mAb) SDOW17 (anti-N), and rabbit polyclonal antibodies (pAb) specific to the C-terminal peptide of nsp2 (anti-nsp2C) or the C-terminal peptide of M were described previously (23, 24). The anti-M mAb 120-60 was generated by immunizing BALB/c mice with a synthetic keyhole limpet hemocyanin (KLH) conjugated peptide recognizing the N-terminal of M (aa2 to 14, sequence: GSSLDDFCHDSTA). Experimental procedures for MAb production were described previously(25). Anti-viral dsRNA mAb J2 was purchased from Kerafast. Anti-bcl6 pAb (ab172610) was purchased from Abcam. Alexa-488 conjugated goat anti-mouse IgG and Alexa-594 conjugated goat anti-Rabbit IgG were purchased from Jackson Immunoresearch.

Immunofluorescent assays. For detecting the expression of PRRSV nsp2 and M in MARC/PRRSV-P109, cells seeded on 6-well plates were fixed with 4% paraformaldehyde at 72

hours post seeding (hps) for 10min, permeabilized with 0.5% Triton X-100 for 10 minutes, and then blocked with 1% BSA in 1× PBS for 30 minutes at room temperature.. … Specific mAb (anti-M) or pAb (anti-nsp2) at a concentration of 1:1000 was used as the primary antibody. For detecting the presence of PRRSV protein and dsRNA, naive MARC-145 cells and MARC/PRRSV-P109 cells (3×10^5 cells/dish) were seeded on glass-bottom 35mm cell culture dishes (MatTek). After 2 days incubation, MARC-145 cells were infected with 0.1 moi of PRRSV with the infection medium (Dulbecco's modified Eagle's medium containing 2% horse serum, 100 μg/ml penicillin and streptomycin). At 12 hpi, MARC-145 cells were fixed, permeabilized, and then blockedusing the same method described above. Similarly, at 72 hps, MARC/PRRSV-P109 cells were fixed, permeabilized and blocked using the same method as described above. Specific mAb (anti-dsRNA) or pAb (anti-nsp2 and anti-M) at a concentration of 1:1000 was used as the primary antibody. After 1h incubation at 37˚C, cells were washed with 1× PBS, and a secondary antibody, Alexa Fluor-488 conjugated goat anti-mouse IgG or Alexa Fluor-594 conjugated goat anti-Rabbit IgG, was added at a concentration of 1:250 in 1× PBS. After 1 h incubation in room temperature, cells were washed in 1× PBS, and then counterstained with DAPI (Invitrogen). Cells were imaged with an LSM880 Zeiss confocal microscope (Zeiss). Collected images were processed using Zen 2 (Zeiss) and Adobe Photoshop CS3 (Adobe).

Quantitative RT-PCR. For determining the total amount of viral RNA in infected cells and swine samples, quantitative RT-PCR (qRT-PCR) was performed using the method that we described previously (22)(24). For quantitation of plus- and minus-strand RNA, strand specific qRT-PCR was conducted. Specific primers (forward primer, 5'-CTTCTGTGATAGCCTCCTTCAG-3'; reverse primer, 5'- ACGTGCACCGATCAA

GTATC-3') were designed to target the viral RNA sequence between 5'-end of untranslated region (UTR) and the junction of 5'-UTR and nsp1α-coding region (genome position of nucleotide 95-218 of PRRSV SD95-21); the FAM/TAMRA (6-carboxyfluorescein/ 6-carboxytetramethylrhodamine)-labeled probe (5'-TTGCACTGCTTTACGGTCTCTCCA-3') was designed to target 5'-UTR of PRRSV genomic RNA. Total cellular RNA was extracted using SV Total RNA Isolation System (Promega). Reverse transcription (RT) reaction with 5 μg of total RNA was carried out using SuperScript IV reverse transcriptase, followed the manufacturer's instruction (ThermoFisher). Separate RT reaction included either the reverse primer or forward primer was performed to quantify the number of plus- and minus-strand viral RNA, respectively. Prior to PCR amplification, completed RT reaction mixtures were treated with 1 μl of RNase H (ThermoFisher) to remove RNA complementary to the cDNA. PCR amplification was performed using pre-made PCR Master Mix (ThermoFisher), and quantitative analysis was conducted using a CFX96 Touch™ Real-Time PCR Detection System (Biorad). PCR conditions were carried out at 40 cycles of denaturation at 95 ℃ for 15 s and annealing and extension at 60 ℃ for 30 s. All samples were evaluated in triplicate reactions. A RNA fragment (nucleotide 90-225 of PRRSV genome) synthesized by IDT was used as a template to build the standard curve.

RNase I treatment. To determine whether the RNA samples contain dsRNA, the RNA samples (100ng of total RNA) were treated with 0.5 U of RNase I (Thermofisher) for 30 min at 37 ℃ and inactivated by heating at 100 ℃ for 20 min. The RNase I treated samples were used immediately for one-step RT-PCR using SuperScript™ III One-Step RT-PCR System and Platinum™ Taq DNA Polymerase kit (Thermofisher). Same set of primers for strand specific qRT-PCR was used. RT-PCR was performed following the manufacturer's protocol with minor modifications. Briefly,

samples were denatured at 98˚C for 10 min prior to the one step RT-PCR. The cycling parameters were use as: 60˚C for 30 min; 94˚C for 2 min; 40 cycles of 94˚C for 15 s, 55˚C for 30 s, and 68˚C for 30 s; 68˚C for 5 min; and a 4˚C hold. RT-PCR product was analyzed on a 2% agarose gel.

Pig experiments. Serum and tissue samples from two trials of pig experiments were used in this study. The first pig trial contains 15 specific-pathogen-free (SPF) pigs, which were obtained from the swine farm of The Ohio State University (OSU). Pigs were 5-week-old upon arrival to The OSU animal facility, and they were randomly divided into 3 groups (n = 5). Group 1 pigs were mock-infected, while group 2 and group 3 pigs were inoculated by intramuscular route with 4×10^5 $TCID_{50}$ of PRRSV isolate SD95-21. Pigs were observed daily for clinical signs, and blood samples were collected at 0, 7, 14, 28, 42, and 52dpi. Groups 1 and 2 pigs were euthanized at 52dpi, while group 3 pigs were euthanized at 10 dpi. Tissue samples including tonsil and tracheobronchial lymph node (TBLN) were collected.

In order to confirm the data from the first pig trial, we obtained samples from a previous pig experiment (trial-2) that was originally designed for study the PRRSV persistence and its impact on porcine circovirus (PCV) co-infection (26). Samples used in current study were from a subset of 9 SPF pigs. They were housed in the Kansas State University Large Animal Research Center. The pigs were approximately 4 weeks of age upon arrival to the facility and given 2 weeks of acclimation period. At approximately 6 weeks of age, all 9 pigs were co-infected with PRRSV isolate KS62 (10^5 $TCID_{50}$) and PCV2b ($10^{3.6}$ $TCID_{50}$; Genbank Accession #JQ692110). Pigs were monitored for the clinical signs daily by a veterinarian or veterinary assistant. Blood samples were collected on 0, 4, 7, 11, 14, 21, 28, 35, 42, 56, and 70 dpi. All pigs were humanely

euthanized at 70 dpi and complete necropsies were performed by a board certified pathologist. Tissues samples were collected, included tonsil and TBLN.

The pig experiments were performed according to protocols approved by the Institutional Animal Care and Use Committee (IACUC) of The Ohio State University (pig trial-1) and Kansas State University (pig trial-2).

Immunohistochemistry (IHC) assay: IHC was performed using formalin-fixed paraffin-embedded tissues that were sectioned at 3μm thickness onto positively charged slides. Tissue sections were incubated with the primary antibodies (anti-PRRSV N mAb SDOW17 or anti-dsRNA mAb J2, and anti-bcl6 pAb) at a concentration of 1:1000. After 2 h incubation at room temperature, secondary antibodies, Alexa-488 conjugated goat anti-mouse IgG and Alexa-594 conjugated goat anti-Rabbit IgG, were added at a concentration of 1:500 in 1x PBS. After additional 1h incubation at room temperature, the tissue samples were counterstained with 4',6-diamidino-2-phenylindole (DAPI; Invitrogen) for 10 min. The stained tissue sections were mounted with Fisherfinest™ Premium Cover Glasses (Fisher scientific) by ProLong® Gold antifade reagent (Invitrogen), dried at room temperature overnight, and then visualized with the fluorescent microscope (EVOS FL, Thermofisher)..

Nanostring RNA array analysis. Host cellular immune gene mRNA profiling was performed using the Nanostring nCounter system (Nanostring Technologies, Seattle, WA) and the modified methods described by Geiss et al. (27). A custom-designed code set was used, which contains 189 swine immune genes and 3 housekeeping genes (see Table S1 in the supplemental material). Each reaction mixture contained 100 ng of RNA extracted from tissue samples, hybridization buffer, reporter probes, and capture probes. RNA was hybridized with reporter and capture probes overnight. After 18 h of hybridization at 65 ℃, the excess probes were removed and the

hybridized probe/target complexes were immobilized in an nCounter cartridge using the nCounter Prep Station (Nanostring Technologies, Seatle, WA). Sample cartridges were placed in a Digital Analyzer for data collection. Immune gene targets were counted on the nCounter system, and raw counts were normalized to the geometric mean counts of 3 housekeeping genes (GAPDH, TBP and TUBB). Data were analyzed and unsupervised hierarchical clustering analysis was performed using nSolver Analysis Software (version 3.0; Nanostring Technologies, Seattle, WA). In first pig trial, we used gene expression level in TBLNs of negative control pigs as a reference. In second pig trial, we compared the gene expression levels in TBLNs from non-viremic pigs with that from viremic pigs. Genes with a p-value lower than 0.05 and a fold change greater than 2 or less than 0.5were defined as differentially expressed genes (DEGs). The volcano plots were built with Graphpad Prism 6 (GraphPad Software).

Statistical analysis. Statistical analyses were performed by using one-way analysis of variance (ANOVA) followed by Tukey's post hoc test using GraphPad InStat Prism software (version 6.0). Statistical significance was assessed at p-values of *<0.05, ** <0.01, and ***<0.001.

4.3 Results

***In vitro* model of persistent PRRSV infection.** Persistently infected cells were derived by serially passaging MARC-145 cells. Initially, MARC-145 cells in T-25 flasks (n=10) were infected with 1 moi of PRRSV isolate SD95-21. One flask of cells and medium was harvested each day to determine cell numbers as well as viral growth rates for 10 days. Within three days after the initial infection, increased amount of viral RNA was observed with peak production of virus reached 8.51×10^7 gRNA copies/ml at day 3; on the other hand, the number of viable cells adhering to the flask was decreased more than 11-fold, a result of virus-mediated cytopathic

effect (CPE; **Fig. 4.1A**). The loss of cells correlated with decreased amounts of virus released into the medium (**Fig. 4.1B**). At day 3, the dead cells were washed and fresh culture medium was added to the survival cells in the flask. The monolayer was gradually restored along with a gradual increase in virus (**Figure 4.1A and B**). By day 10, the cell monolayer was only partially restored along with a 10-fold decrease in viral RNA levels compared to that at day 3. Immunofluorescence staining for PRRSV proteins (M and nsp2) showed that 10% of cells were infected. The remaining cells at day 10 were passaged 109 times on a T-25 flask. For each passage, the cells were split in three ways, with 1/3 of the cells placed in a new T-25 flask, another 1/3 of the cells stored in liquid N2, and the remaining 1/3 cells were used for detecting the presence of viral RNA by RT-PCR. The passage 109 cells were designated as MARC/PRRSV-P109 and used for subsequent *in vitro* characterization of PRRSV persistence. Initially, MARC/PRRSV-P109 cells recovered from liquid nitrogen were cultured in 6-well plates ($1x10^5$/well). One well of cells and medium was harvested each day to determine cell numbers as well as viral growth rates for 10 days. The result showed that cells and viruses increased over time (**Fig. 4.1C**); by day 3, the cells had almost reached intact monolayer along with the steady state production of virus.

MARC/PRRSV-P109 cells possess dsRNA in the absence of viral proteins. During PRRSV replication, dsRNA is formed as replicative intermediates needed to copy positive and negative strands of genomic and sgRNAs (19, 28). For this experiment, infected MARC-145 cells were stained with antibodies against dsRNA along with the nonstructural and structural proteins, nsp2 and M. During acute infection, all PRRSV protein positive cells possessed dsRNA (**Fig. 4.2A**). In contrast, for the MARC/PRRSV-P109 culture, a few of dsRNA-positive cells were negative for viral proteins. Interestingly, acutely infected cells showed an intense perinuclear localization

of dsRNA compared to a more diffuse pattern of dsRNA staining in the persistent culture. The number of cells positive for viral proteins and/or dsRNA was counted in acute and persistent infection cultures. The results showed that about 50% of acutely infected cells were positive for both viral proteins and dsRNA at 12 hpi (**Fig. 4.2B and D**). In contrast, only about 20% of the cells were positive for dsRNA in the MARC/PRRSV-P109 cells at 72 hours post seeding (hps); and of these, only half of the cells contained detectable amounts of viral proteins (**Fig. 4.2C and E**). These results confirm the presence of a significant number of cells in the persistent infection culture, which are positive for dsRNA, but negative for viral proteins.

During replication, dsRNA exists in genomic and subgenomic forms. RNase I degradation of single-stranded RNA followed by RT-PCR was used to detect the presence of dsRNA. Viral dsRNA was detected by designing RT-PCR primers that amplified 95-218 nucleotide (nt) region covering the 5'-leader sequence to the beginning of ORF1. (sgRNAs possess a leader sequence followed by ORF2, 3, 4, 5, 6, or 7). Fig. 2F showed positive RT-PCR result that amplified PRRSV nt 95-218 region before and after RNase I treatment, indicating the presence of viral dsRNA in both acutely and persistently infected cells.

For some RNA viruses, increased dsRNA formation correlates to the reduced ratio of plus- to minus-strand viral RNA in infected cells (16-18). In the present study, the amounts of plus- and minus-strand genomic RNA were measured in acute and persistent infection cultures. For acute infection, confluent MARC-145 cells were infected at a moi of 1 with PRRSV. Total RNA was isolated and plus- and minus-strands were amplified using a strand-specific quantitative RT-PCR (qRT-PCR) that incorporates PRRSV primers for amplifying 95-218 nt region. The results showed the predominance of plus genomic strands at 24 hpi (**Fig. 4.2G**). At this time the ratio of plus to minus strands was 59.3/1, and reached the peak value at 48 hpi (ratio

of 68.9/1); by 72 hpi, the ratio was still remained at 45.7/1 (**Fig. 4.2H**), indicating the excess amount of plus-stranded RNA in the acutely infected cells. For the measuring of plus- to minus-strand ratio in persistent infection cells, MARC/PRRSV-P109 cells were seeded on a fresh plate and the amount of plus and minus strands was determined through a time course study. The qRT-PCR results showed an increase in plus and minus strands over time (**Fig. 4.2I**). By 72 hours post seeding, the time when virus production achieves a steady state, that ratio of plus to minus strands was decreased to 1.42/1, indicating the close equal amount of plus and minus strands of viral RNA in the persistently infected cells (**Fig.4. 2J**).

Persistence of dsRNA *in vivo*. During both acute and persistent stages of PRRSV infection in pigs, virus can be detected in lymphoid organs (1, 29-31). In the present study, the different forms of viral RNA were initially evaluated in tonsil and lymph nodes from three groups of pigs. Group 1 was composed of mock-infected pigs, which served as negative controls. Groups 2 and 3 were infected with PRRSV strain SD95-21 and euthanized at 52 and 10 dpi, respectively. Real-time qRT-PCR was performed to measure the viral loads in serum. The result showed that viral RNA (1.32×10^5 copies/ml) was detected in serum from pigs at 10 dpi, but not from pigs at 52 dpi (**Fig. 4.3A**). Consistently, viruses were able to be isolated from 10dpi serum samples, but not from 52dpi serum; the mean titer in 10dpi serum was about 3.33 Log TCID50/ml (**Fig.4.3B**). However, the viral RNA was detected in lymphoid tissues (8.91×10^4 copies/mg of tonsil; 8.32×10^3 copies/mg of TBLN; **Fig. 4.3C**). We further compared the amount of plus- and minus-strand viral RNA in tonsil and TBLN samples from groups 2 and 3 pigs. The results showed that the amount of plus- strand RNA at 52 days was significantly reduced compared to that in acutely infected pigs at 10 dpi (**Fig. 4.3D-E**). Further analysis on the ratio of plus- to minus-strand RNA showed that the RNA ratios (ratios at 13.6/1) in tonsil and (12.5/1) in TBLN of group 2 pigs at

52 dpi were significantly reduced compared to that in group 3 pigs at 10 dpi (2.91-fold lower in tonsil; 5.05-fold lower in TBLN; **Fig. 4.3F**). This result is consistently with that from *in vitro* cell culture system (Fig. 4.2E), indicating reduced ratio of plus- to minus-strand viral RNA presence in lymphoid tissues of PRRSV persistent pigs compared to that in acutely infected pigs.

Next, immunohistochemistry analysis was performed to directly detect the existence of PRRSV dsRNA in the TBLNs. The existence of PRRSV N protein was also detected. The result showed that majority of the viral dsRNA and N protein was located at the interfollicular and marginal zone of the TBLNs from pigs at 10 dpi. Interestingly, in tissue samples from pigs at 52 dpi, viral dsRNA or N protein was detected largely aggregating inside the germinal center (GC) of the TBLNs (Fig. 3G).

To further confirm the persistent nature of viral dsRNA in PRRSV-infected pigs, we analyzed additional set of samples from a different pig experiment, in which pigs were infected with PRRSV (strain KS-62) for 70 days. Serum and TBLN samples were obtained from 6 pigs (designated as non-viremic group), in which qRT-PCR result showed no detectable PRRSV RNA in serum (Fig. 4A), but 2.21×10^3 copies /mg of the viral RNA was detected in TBLNs at 70 dpi. As a comparison, serum and TBLN samples were obtained from additional 3 pigs at 70 dpi (designated as viremic group), in which PRRSV RNA was still detected in serum samples (9.45×10^3 copies/ml; **Fig. 4.4A**) as well as in tissue samples (1.37×10^3 copies /mg of TBLNs; **Fig. 4.4B**). Consistently, plus- and minus-strand viral RNA in TBLN samples was detected by strain-specific qRT-PCR. The non-viremic group of pigs showed 2.1-fold lower ratio of plus- to minus-strand RNA compared to that of viremic group of pigs (**Fig. 4.4C**). RNase I treatment and RT-PCR results further confirmed the existence of genomic dsRNA in the TBLNs from both

groups of pigs, but the average amounts of dsRNA were 79.6% lower in the TBLNs from viremic group of pigs compared to that of non-viremic group of pigs (**Fig. 4.4D**).

The presence of genomic dsRNA in TBLN during persistence fails to stimulate antiviral immune responses. Double stranded RNA is a potent inducer of innate immune responses (32). In the current study, we determined whether the existence of dsRNA in lymphoid tissues was associated with antiviral immune responses. Initially, TBLNs collected from PRRSV-infected pigs at 10 dpi versus 52 dpi were analyzed and compared with those from mock-infected pigs. Swine immune gene mRNA expression profiles were determined in TBLN samples by using NanoString nCounter system to simultaneously analyze the expression of 189 swine immune genes plus 3 housekeeping genes (Table S1). The result showed that the gene expression pattern in TBLNs from the pigs at 52 dpi resembles the one in TBLNs from mock-infected pigs, while a distinct gene expression pattern was observed in TBLNs from the pigs at 10 dpi (**Fig. 4.5A**). Gene expression profiles in TBLNs from pigs at 10 dpi or 52 dpi were compared to that from mock-infected pigs. Swine genes that had a fold change (FC) greater than 2 or less than 0.5 with p-value less than 0.05 were identified as differentiated expressed genes (DEGs). Similar immune gene expression patterns in TBLNs from pigs at 52dpi were detected in comparison to those from mock-infected pigs; IRF7 is the only gene found to be up-regulated DEG in pigs at 52 dpi (FC=2, p-value<0.05) (**Fig. 4.5B**). In contrast, 98 out of 192 genes, including 90 up-regulated and 8 down-regulated genes, were identified as DEGs in TBLNs from pigs at 10 dpi (**Fig. 4.5C**). In comparison to those from pigs at 52 dpi, 89 genes were detected with significantly higher expression levels in TBLNs from pigs at 10dpi (**Fig. 4.5D**). Most of the DEGs were related to innate inflammatory, type I interferon (IFN)-associated anti-viral responses (Table S1).

To confirm the results generated from pigs at 52 dpi versus 10 dpi, we further analyzed immune gene profiles of the TBLN samples collected from those two groups of pigs at 70 dpi. NanoString RNA array analysis classified each group of pigs into a distinct cluster (**Fig. 4.6A**). In comparison to the gene expression profile in TBLNs from the non-viremic group of pigs, total 113 DEGs were identified, in which 109 genes were detected with significantly higher levels in TBLNs from viremic group of pigs (**Fig. 4.6B**). Among the 109 upregulated DEGs, 59 genes were overlapped with the DEGs profile of TBLNs from pigs at 10 dpi (**Fig. 4.6C**; Table S2). Further gene ontology analysis showed that these 59 genes were enriched in innate immunity related RLR-, JAK-STAT, NLR- signaling pathways and adaptive immunity related cytokine-, chemokine-, signaling pathways (**Fig. 4.6D**).

4.4 Discussion

In the current study, an *in vitro* cell culture model of PRRSV persistence was established after the serial passage of infected MARC-145 cells. Similar to other *in vitro* persistent infection models of nidovirus (33-40), the persistent infection culture, MARC/PRRSV-P109, behaved as a carrier culture, which maintained around 10% of cells actively producing virus. When compared to MARC-145 cells acutely infected with PRRSV, the MARC/PRRSV-P109 culture was enriched in cells expressing viral dsRNA, but not the nonstrucutural protein (nsp2) or the structural protein (M). Suppression of viral protein production in the presence of viral nucleic acid is a hallmark of persistent infection of cells. For example, suppressed protein expression of Ebola virus has been shown to contribute to the viral persistence *in vitro* and *in vivo* (41). Since the synthesis of viral proteins results in CPE or being eliminated by the active immune responses, the suppression of viral gene expression becomes an effective mechanism for persistence.

During acute infection, cells contained 68.9-fold higher amount of plus-strand PRRSV RNA compared to minus-strand RNA. In contrast, the ratio of plus-strand versus minus-strand RNA in MARC/PRRSV-P109 persistent cultures was reduced to 1.41:1. RNase I treatment followed by RT-PCR further confirmed the presence of genomic dsRNA during persistence. The *in vitro* data are consistent with observations in lymphoid tissues from PRRSV-infected pigs. During *in vivo* acute infection (at 10dpi), an average of 50.9-fold higher amount of plus-strand RNA compared to minus-strand RNA was found in the TBLN. In contrast, at 52dpi, when virus was no longer detectable in the blood, and the ratio of plus-strand RNA to minus-strand RNA in TBLNs reduced to 10.81. The altered plus- to minus-strand RNA ratio implicates the formation and persistence of dsRNA in lymphoid tissues.

IHC analysis further showed that a larger proportion of PRRSV dsRNA$^+$ cells were observed within germinal centers (GCs) of the lymphoid tissue (TBLN) during persistent infection stage. Interestingly, similar results are found for other viruses, including lactate dehydrogenase-elevating virus (LDV) and human immunodeficiency virus (HIV). LDV, the murine arterivirus, is characterized by being able to establish a life-long, non-clinical infection in mice. During LDV persistence, large quantities of LDV RNA are detected in GCs of lymph nodes and spleen (42). Likewise, in HIV persistently infected individuals, the viral RNA is observed aggregating in GCs of the lymphoid tissues (43) . Recently, germinal center follicular T helper cells (GC Tfh) have been shown highly permissive to HIV infection (44), which suggested that HIV may hide inside GC Tfh cells in order to efficiently modify the reactivity in GC, and in turn to suppress the induction of host immune responses (45). Moreover, CD8$^+$ cytotoxic T lymphocytes are rare in HIV positive GCs, which results in the long-term persistent of HIV$^+$ Tfh cells (46). The exact type of PRRSV persistent cells in GCs remains unknown. In pigs, PRRSV

mainly infects subsets of swine macrophages, present in lungs and lymphoid organs (1, 47); in the lymphoid tissues of PRRSV-1 infected pigs, infected cells were identified as macrophages (1). In our study, we observed a large amount of PRRSV infected cells in the interfollicular regions of lymphoid tissues during acute infection, which are speculated to be the interfollicular macrophages. A similar phenomenon was also reported in a previous study (46). This type of specific macrophages was identified expressing the PRRSV receptor, CD163 (48). Interfollicular macrophages are recruited to germinal centers through the interaction between CX3CL1 and CX3CR1 (49), which are also upregulated during PRRSV acute infections in current study (see Table S1). In the germinal center, the predominant macrophages are tingible body macrophages (TBMs), which are located in the unique microenvironment of germinal centers in close proximity to antigen-retaining follicular dendritic cells (FDC). Although TBMs are CD163 negative macrophages (48), it has extraordinary phagocytotic capability for apoptotic cells (50). Interestingly, it has been shown that CX3CL1 can enhance the apoptotic-cell clearance with TBMs (51). Therefore, it is reasonable to speculate that PRRSV dsRNA containing apoptotic cells may be phagocytized by TBMs, and dsRNA and/or other infectious materials in turn become persistent in TBMs. Moreover, PRRSV dsRNA in debris of infected and lysed cells could be trapped by the follicular dendritic cells of the germinal center. Further studies are needed to identify the exact type of cellular reservoir(s) harboring PRRSV persistence in GCs. Viral dsRNA contains pathogen-associated molecular patterns (PAMPs) that sensed by cellular receptors to activate signaling pathways for anti-viral responses (32). To determine the effect of dsRNA persistence on the host cellular immune responses, we compared the expression levels of 189 selected swine immune genes in TBLNs from mock, acutely (10dpi), and persistently (52dpi) infected pigs. Despite the presence of dsRNA in the TBLNs, few immune genes were activated

in the 52 dpi pigs, in which the gene expression pattern resembles that of mock-infected pigs. To further confirm this result, we analyzed the cellular immune gene expression using additional TBLN samples collected from pigs at 70 dpi. The result of RNA array analysis consistently showed that limited numbers of immune genes were activated in TBLNs from those six pigs without viremia. Interestingly, compared with those pigs without viremia, the three pigs with viremia at 70 dpi showed upregulated gene expression in TBLNs, and the pattern is quite similar to that of acutely infected pigs at 10dpi. When comparing the data set of these two independent animal experiments, 59 overlapped upregulated DEGs were identified in TBLNs from pigs at 10 dpi and pigs with viremia at 70 dpi, which includes a panel of innate immune related genes of IFNA1, IFNB1, typeIII IFN, and IFITM1; and immune genes of adaptive immunity, such as CD40L, CD80, ICOS, IFNg, IL2, IL4, IL5, SLA-II, CTLA4, and IL10 (Table S1). These data indicate that presence of viruses in the blood circulation could be positively associated with immune gene activation in TBLNs.

The limited numbers of immune gene activation in TBLNs from pigs at 52 and 70 dpi (without viremia) suggests that certain mechanisms exist in GC to facilitate the persistence of viral dsRNAs from being detected by host immune system. GCs are dynamic sites within lymphoid organs where mature B cells undergo somatic hypermutation, affinity maturation, and class-switch recombination of the B cell receptor. Inside the GC, Tfh cells interact with GC B cells. Co-receptor interactions between ICOS/ICOSL and CD40L/CD40 have been shown to be absolutely required for Tfh cells development and therefore for GC development (52) . Interestingly, a panel of differential expressed genes involved in T cell and B cells receptor signaling pathway, including ICOS and CD40L, was determined to be unresponsive in TBLNs of persistently infected pigs. Similar results have been obtained from HIV persistent infection, in

which Tfh cells in GCs showed down-regulated ICOS and CD40L expression, resulting in the inhibition of GC activities (53). This would subsequently hamper the clearance of persistently infected cells and allow viruses or viral infectious material to be maintained inside GC for an extended period.

In summary, our study demonstrated that PRRSV dsRNA could function as a mediator for viral persistence. The viral dsRNA persistence in germinal centers of lymphoid tissues may reveal a novel mechanism for PRRSV to escape antiviral immune responses

4.5 References

1. Duan X, Nauwynck HJ, Pensaert MB. 1997. Virus quantification and identification of cellular targets in the lungs and lymphoid tissues of pigs at different time intervals after inoculation with porcine reproductive and respiratory syndrome virus (PRRSV). Vet Microbiol 56.
2. Kim HS, Kwang J, Yoon IJ, Joo HS, Frey ML. 1993. Enhanced replication of porcine reproductive and respiratory syndrome (PRRS) virus in a homogeneous subpopulation of MA-104 cell line. Arch Virol 133:477-83.
3. Nauwynck HJ, Duan X, Favoreel HW, Van Oostveldt P, Pensaert MB. 1999. Entry of porcine reproductive and respiratory syndrome virus into porcine alveolar macrophages via receptor-mediated endocytosis. J Gen Virol 80 (Pt 2):297-305.
4. Kreutz LC, Ackermann MR. 1996. Porcine reproductive and respiratory syndrome virus enters cells through a low pH-dependent endocytic pathway. Virus Research 42:137-147.
5. Snijder EJ, Kikkert M, Fang Y. 2013. Arterivirus molecular biology and pathogenesis. J Gen Virol 94:2141-63.
6. Lunney JK, Fang Y, Ladinig A, Chen N, Li Y, Rowland B, Renukaradhya GJ. 2016. Porcine Reproductive and Respiratory Syndrome Virus (PRRSV): Pathogenesis and Interaction with the Immune System. Annu Rev Anim Biosci 4:129-54.
7. Fang Y, Treffers EE, Li Y, Tas A, Sun Z, van der Meer Y, de Ru AH, van Veelen PA, Atkins JF, Snijder EJ, Firth AE. 2012. Efficient -2 frameshifting by mammalian

ribosomes to synthesize an additional arterivirus protein. Proc Natl Acad Sci U S A 109:E2920-8.

8. Fang Y, Snijder EJ. 2010. The PRRSV replicase: exploring the multifunctionality of an intriguing set of nonstructural proteins. Virus Res 154:61-76.
9. Wills RW, Zimmerman JJ, Yoon KJ, Swenson SL, McGinley MJ, Hill HT, Platt KB, Christopher-Hennings J, Nelson EA. 1997. Porcine reproductive and respiratory syndrome virus: a persistent infection. Vet Microbiol 55:231-40.
10. Allende R, Laegreid WW, Kutish GF, Galeota JA, Wills RW, Osorio FA. 2000. Porcine reproductive and respiratory syndrome virus: description of persistence in individual pigs upon experimental infection. J Virol 74:10834-7.
11. Bierk MD, Dee SA, Rossow KD, Otake S, Collins JE, Molitor TW. 2001. Transmission of porcine reproductive and respiratory syndrome virus from persistently infected sows to contact controls. Canadian Journal of Veterinary Research 65:261-266.
12. Molina RM, Nelson EA, Christopher-Hennings J, Hesse R, Rowland RR, Zimmerman JJ. 2009. Evaluation of the risk of PRRSV transmission via ingestion of muscle from persistently infected pigs. Transbound Emerg Dis 56:1-8.
13. Lopez OJ, Osorio FA. 2004. Role of neutralizing antibodies in PRRSV protective immunity. Vet Immunol Immunopathol 102:155-63.
14. Randall RE, Griffin DE. 2017. Within host RNA virus persistence: mechanisms and consequences. Current Opinion in Virology 23:35-42.
15. Kane M, Golovkina T. 2010. Common threads in persistent viral infections. J Virol 84:4116-23.
16. Tam PE, Messner RP. 1999. Molecular mechanisms of coxsackievirus persistence in chronic inflammatory myopathy: viral RNA persists through formation of a double-stranded complex without associated genomic mutations or evolution. J Virol 73:10113-21.
17. Feuer R, Ruller CM, An N, Tabor-Godwin JM, Rhoades RE, Maciejewski S, Pagarigan RR, Cornell CT, Crocker SJ, Kiosses WB, Pham-Mitchell N, Campbell IL, Whitton JL. 2009. Viral persistence and chronic immunopathology in the adult central nervous system following Coxsackievirus infection during the neonatal period. J Virol 83:9356-69.

18. Klepper A, Eng FJ, Doyle EH, El‐Shamy A, Rahman AH, Fiel MI, Avino GC, Lee M, Ye F, Roayaie S, Bansal MB, MacDonald MR, Schiano TD, Branch AD. 2017. Hepatitis C virus double‐stranded RNA is the predominant form in human liver and in interferon‐treated cells. Hepatology (Baltimore, Md) 66:357-370.
19. Knoops K, Barcena M, Limpens RW, Koster AJ, Mommaas AM, Snijder EJ. 2012. Ultrastructural characterization of arterivirus replication structures: reshaping the endoplasmic reticulum to accommodate viral RNA synthesis. J Virol 86:2474-87.
20. Li Y, Treffers EE, Napthine S, Tas A, Zhu L, Sun Z, Bell S, Mark BL, van Veelen PA, van Hemert MJ, Firth AE, Brierley I, Snijder EJ, Fang Y. 2014. Transactivation of programmed ribosomal frameshifting by a viral protein. Proc Natl Acad Sci U S A 111:E2172-81.
21. Li Y, Zhu L, Lawson SR, Fang Y. 2013. Targeted mutations in a highly conserved motif of the nsp1beta protein impair the interferon antagonizing activity of porcine reproductive and respiratory syndrome virus. J Gen Virol 94:1972-83.
22. Li Y, Shyu DL, Shang P, Bai J, Ouyang K, Dhakal S, Hiremath J, Binjawadagi B, Renukaradhya GJ, Fang Y. 2016. Mutations in a Highly Conserved Motif of nsp1beta Protein Attenuate the Innate Immune Suppression Function of Porcine Reproductive and Respiratory Syndrome Virus. J Virol 90:3584-99.
23. Guo R, Katz BB, Tomich JM, Gallagher T, Fang Y. 2016. Porcine Reproductive and Respiratory Syndrome Virus Utilizes Nanotubes for Intercellular Spread. J Virol 90:5163-75.
24. Nelson EA, Christopher-Hennings J, Drew T, Wensvoort G, Collins JE, Benfield DA. 1993. Differentiation of U.S. and European isolates of porcine reproductive and respiratory syndrome virus by monoclonal antibodies. J Clin Microbiol 31:3184-9.
25. Li Y, Tas A, Snijder EJ, Fang Y. 2012. Identification of porcine reproductive and respiratory syndrome virus ORF1a-encoded non-structural proteins in virus-infected cells. J Gen Virol 93:829-39.
26. Niederwerder MC, Jaing CJ, Thissen JB, Cino-Ozuna AG, McLoughlin KS, Rowland RR. 2016. Microbiome associations in pigs with the best and worst clinical outcomes following co-infection with porcine reproductive and respiratory syndrome virus (PRRSV) and porcine circovirus type 2 (PCV2). Vet Microbiol 188:1-11.

27. Geiss GK, Bumgarner RE, Birditt B, Dahl T, Dowidar N, Dunaway DL, Fell HP, Ferree S, George RD, Grogan T, James JJ, Maysuria M, Mitton JD, Oliveri P, Osborn JL, Peng T, Ratcliffe AL, Webster PJ, Davidson EH, Hood L, Dimitrov K. 2008. Direct multiplexed measurement of gene expression with color-coded probe pairs. Nat Biotechnol 26:317-25.
28. Knoops K, Kikkert M, Worm SH, Zevenhoven-Dobbe JC, van der Meer Y, Koster AJ, Mommaas AM, Snijder EJ. 2008. SARS-coronavirus replication is supported by a reticulovesicular network of modified endoplasmic reticulum. PLoS Biol 6:e226.
29. Rowland RR, Lawson S, Rossow K, Benfield DA. 2003. Lymphoid tissue tropism of porcine reproductive and respiratory syndrome virus replication during persistent infection of pigs originally exposed to virus in utero. Vet Microbiol 96:219-35.
30. Horter DC, Pogranichniy RM, Chang CC, Evans RB, Yoon KJ, Zimmerman JJ. 2002. Characterization of the carrier state in porcine reproductive and respiratory syndrome virus infection. Vet Microbiol 86:213-28.
31. Kawashima K, Narita M, Yamada S. 1999. Changes in macrophage and lymphocyte subpopulations of lymphoid tissues from pigs infected with the porcine reproductive and respiratory syndrome virus (PRRSV). Veterinary Immunology and Immunopathology 71:257-262.
32. Gantier MP, Williams BRG. 2007. The response of mammalian cells to double-stranded RNA. Cytokine & growth factor reviews 18:363-371.
33. Chan PK, To KF, Lo AW, Cheung JL, Chu I, Au FW, Tong JH, Tam JS, Sung JJ, Ng HK. 2004. Persistent infection of SARS coronavirus in colonic cells in vitro. J Med Virol 74:1-7.
34. Mizutani T, Fukushi S, Ishii K, Sasaki Y, Kenri T, Saijo M, Kanaji Y, Shirota K, Kurane I, Morikawa S. 2006. Mechanisms of establishment of persistent SARS-CoV-infected cells. Biochem Biophys Res Commun 347:261-5.
35. Arbour N, Ekande S, Cote G, Lachance C, Chagnon F, Tardieu M, Cashman NR, Talbot PJ. 1999. Persistent infection of human oligodendrocytic and neuroglial cell lines by human coronavirus 229E. J Virol 73:3326-37.

36. Arbour N, Cote G, Lachance C, Tardieu M, Cashman NR, Talbot PJ. 1999. Acute and persistent infection of human neural cell lines by human coronavirus OC43. J Virol 73:3338-50.
37. Chen W, Baric RS. 1996. Molecular anatomy of mouse hepatitis virus persistence: coevolution of increased host cell resistance and virus virulence. J Virol 70:3947-60.
38. Hofmann MA, Sethna PB, Brian DA. 1990. Bovine coronavirus mRNA replication continues throughout persistent infection in cell culture. J Virol 64:4108-14.
39. Stueckemann JA, Holth M, Swart WJ, Kowalchyk K, Smith MS, Wolstenholme AJ, Cafruny WA, Plagemann PG. 1982. Replication of lactate dehydrogenase-elevating virus in macrophages. 2. Mechanism of persistent infection in mice and cell culture. J Gen Virol 59:263-72.
40. Zhang J, Timoney PJ, MacLachlan NJ, McCollum WH, Balasuriya UB. 2008. Persistent equine arteritis virus infection in HeLa cells. J Virol 82:8456-64.
41. Strong JE, Wong G, Jones SE, Grolla A, Theriault S, Kobinger GP, Feldmann H. 2008. Stimulation of Ebola virus production from persistent infection through activation of the Ras/MAPK pathway. Proc Natl Acad Sci U S A 105:17982-7.
42. Anderson GW, Rowland RR, Palmer GA, Even C, Plagemann PG. 1995. Lactate dehydrogenase-elevating virus replication persists in liver, spleen, lymph node, and testis tissues and results in accumulation of viral RNA in germinal centers, concomitant with polyclonal activation of B cells. J Virol 69:5177-85.
43. Fox CH, Tenner-Rácz K, Rácz P, Firpo A, Pizzo PA, Fauci AS. 1991. Lymphoid Germinal Centers Are Reservoirs of Human Immunodeficiency Virus Type 1 RNA. The Journal of Infectious Diseases 164:1051-1057.
44. Kohler SL, Pham MN, Folkvord JM, Arends T, Miller SM, Miles B, Meditz AL, McCarter M, Levy DN, Connick E. 2016. Germinal Center T Follicular Helper Cells Are Highly Permissive to HIV-1 and Alter Their Phenotype during Virus Replication. J Immunol 196:2711-22.
45. Graff-Dubois S, Rouers A, Moris A. 2016. Impact of Chronic HIV/SIV Infection on T Follicular Helper Cell Subsets and Germinal Center Homeostasis. Frontiers in Immunology 7:501.

46. Connick E, Mattila T, Folkvord JM, Schlichtemeier R, Meditz AL, Ray MG, McCarter MD, Mawhinney S, Hage A, White C, Skinner PJ. 2007. CTL fail to accumulate at sites of HIV-1 replication in lymphoid tissue. J Immunol 178:6975-83.
47. Labarque GG, Nauwynck HJ, Van Reeth K, Pensaert MB. 2000. Effect of cellular changes and onset of humoral immunity on the replication of porcine reproductive and respiratory syndrome virus in the lungs of pigs. J Gen Virol 81:1327-34.
48. Lau SK, Chu PG, Weiss LM. 2004. CD163: a specific marker of macrophages in paraffin-embedded tissue samples. Am J Clin Pathol 122:794-801.
49. Truman LA, Ford CA, Pasikowska M, Pound JD, Wilkinson SJ, Dumitriu IE, Melville L, Melrose LA, Ogden CA, Nibbs R, Graham G, Combadiere C, Gregory CD. 2008. CX3CL1/fractalkine is released from apoptotic lymphocytes to stimulate macrophage chemotaxis. Blood 112:5026-36.
50. Davies LC, Jenkins SJ, Allen JE, Taylor PR. 2013. Tissue-resident macrophages. Nature immunology 14:986-995.
51. Miksa M, Amin D, Wu R, Dong W, Ravikumar TS, Wang P. 2007. Fractalkine-Induced MFG-E8 Leads to Enhanced Apoptotic Cell Clearance by Macrophages. Molecular Medicine 13:553-560.
52. Nutt SL, Tarlinton DM. 2011. Germinal center B and follicular helper T cells: siblings, cousins or just good friends? Nat Immunol 12:472-7.
53. Vanham G, Penne L, Devalck J, Kestens L, Colebunders R, Bosmans E, Thielemans K, Ceuppens JL. 1999. Decreased CD40 ligand induction in CD4 T cells and dysregulated IL-12 production during HIV infection. Clin Exp Immunol 117:335-42.

Table 4.1 192 genes in swine immune gene RNA array

Gene Name	Accession #	Gene Name	Accession #
ATG16L1	NM_001190272.1	CD4	NM_001001908.1
ATG5	NM_001037152.1	CD40	NM_214194.1
B2M	NM_213978.1	CD40LG	NM_214126.1
BCL10	NM_001103213.2	CD48	NM_001243714.1
BCL2	XM_003121700.4	CD74	NM_213774.1
BID	NM_001030535.1	CD79A	NM_001135962.1
BLNK	XM_001928233.4	CD79B	NM_001243912.1
BTK	NM_001243576.1	CD80	NM_214087.1
CASP1	NM_214162.1	CD81	NM_001078679.1
CASP10	NM_001161640.1	CD86	NM_214222.1
CASP3	NM_214131.1	CD8A	NM_001001907.1
CASP8	NM_001031779.2	CD8B	NM_213762.2
CCL11	NM_001256774.1	CHUK	NM_001114279.1
CCL16	XM_003131714.4	CIITA	XM_013995652.1
CCL19	NM_001170516.1	CR1	XM_013979663.1
CCL2	NM_214214.1	CSF2	NM_214118.2
CCL20	NM_001024589.1	CTLA4	NM_214149.1
CCL22	NM_001256776.2	CTSS	XM_005663494.2
CCL23	XM_003131712.5	CX3CL1	XM_013988522.1
CCL24	NM_001161434.1	CX3CR1	XM_003358374.3
CCL4	NM_213779.1	CXCL10	NM_001008691.1
CCL5	NM_001129946.1	CXCL11	NM_001128491.1
CCL8	NM_001164515.1	CXCL12	NM_001009580.1
CCR1	NM_001001621.1	CXCL13	XM_003129101.2
CCR10	NM_001044563.1	CXCL2	NM_001001861.2
CCR2	NM_001001619.1	CXCL9	NM_001114289.2
CCR5	NM_001001618.1	CXCR1	XM_003133655.4
CCR6	XM_013992405.1	CXCR2	XM_005672195.2
CCR7	NM_001001532.2	CXCR3	XM_003135179.4
CCR8	XM_003358377.3	CXCR4	NM_213773.1
CD14	NM_001097445.2	CXCR6	NM_001001623.1
CD163	NM_213976.1	CYBB	NM_214043.2
CD19	NM_214377.1	FADD	NM_001031797.1
CD22	XM_013998314.1	FAS	NM_213839.1
CD244	XM_001928325.3	FCER1G	NM_001001265.1
CD247	NM_214155.2	FCGR1A	NM_001033011.1
CD28	NM_001287410.1	FCGR2B	NM_001033013.2
CD3D	NM_213775.2	FCGR3B	NM_214391.1

CD3E	NM_214227.1	FYN	NM_001080206.2
GAPDH	NM_001206359.1	JAK3	XM_003123500.3
GBP1	NM_001128473.1	KIR2DL1	NM_001113218.1
GZMB	NM_001143710.1	KLRK1	NM_213813.2
ICAM1	NM_213816.1	LCK	NM_001143713.1
ICAM2	XM_013980840.1	LCP2	XM_013984858.1
ICOS	NM_001044546.1	LY96	NM_001104956.1
IFI16	XM_013996900.1	MALT1	XM_013993291.1
IFI35	XM_003358024.2	MAP4K1	XM_003127115.5
IFIH1	NM_001100194.1	MAPK14	XM_001929490.5
IFITM1	XM_003124230.2	MYD88	NM_001099923.1
IFNA1	NM_214393.1	NCR1	NM_001123143.1
IFNAR1	NM_213772.1	NFATC1	NM_214161.1
IFNAR2	NM_001204775.2	NFATC2	NM_001113452.1
IFNB1	NM_001003923.1	NFATC3	XM_003481813.3
IFNG	NM_213948.1	NFKB1	NM_001048232.1
IFNGR1	NM_001177907.1	NFKBIA	NM_001005150.1
IFNL1	NM_001142837.1	NLRP3	NM_001256770.1
IFNL3	NM_001166490.1	NOD1	NM_001114277.1
IFNLR1	XM_013999058.1	NOD2	NM_001105295.1
IKBKB	NM_001099935.1	PDCD1	NM_001204379.1
IKBKE	XM_013979630.1	POLR1B	XM_003124801.5
IKBKG	NM_001113053.1	PPBP	NM_213862.2
IL10	NM_214041.1	PRF1	XM_003483492.3
IL12A	NM_213993.1	PRKCD	XM_013981774.1
IL12B	NM_214013.1	PTPN6	XM_003355590.3
IL18	NM_213997.1	PTPRC	XM_003130596.5
IL1B	NM_214055.1	PYCARD	XM_003124468.4
IL2	NM_213861.1	RELA	NM_001114281.1
IL4	NM_214123.1	RPL19	XM_003131509.4
IL5	NM_214205.1	SH2D1A	NM_001078675.1
IL6	NM_214399.1	SLA-1	NM_001097431.1
IL8	NM_213867.1	SLA-2	NM_001113702.1
IRAK1	XM_003135490.3	SLA-3	NM_001097427.1
IRAK4	NM_001112693.1	SLA-DQA1	NM_001114062.2
IRF3	NM_213770.1	SLA-DQB1	NM_001113694.1
IRF5	XM_005657761.2	SLA-DRA	NM_001113706.1
IRF7	NM_001097428.1	SLA-DRB	NM_001113695.1
ITGAL	NM_001044608.1	SPP1	NM_214023.1
ITGB2	NM_213908.1	SRC	XM_001928614.6
JAK1	NM_214114.1	STAT1	NM_213769.1

JAK2	NM_214113.1		STAT2	NM_213889.1
STAT3	NM_001044580.1		TLR8	NM_214187.1
STAT5B	NM_214168.1		TLR9	NM_213958.1
SYK	NM_001104952.1		TMEM173	NM_001142838.1
TAP1	NM_001044581.1		TNF	NM_214022.1
TAP2	NM_001206441.1		TNFAIP3	NM_001267890.1
TAPBP	XM_005665884.2		TNFSF10	NM_001024696.1
TBK1	NM_001105292.1		TOLLIP	NM_001315800.1
TBP	XM_013991786.1		TRAF2	XM_005652719.1
TICAM1	NM_001315738.1		TRAF3	XM_005666443.2
TIRAP	XM_003130060.4		TRAF5	XM_003482755.3
TLR1	NM_001031775.1		TRAF6	NM_001105286.1
TLR2	NM_213761.1		TUBB	NM_001044612.1
TLR3	NM_001097444.1		TYK2	NM_001114670.1
TLR4	NM_001113039.2		XCL1	NM_001134345.1
TLR5	NM_001123202.1		XCR1	NM_001001622.1
TLR7	NM_001097434.1		ZAP70	XM_003481152.3

Table 4.2 DEGs consistently identified in two independent pig studies

		10DPI vs 52DPI		Viremia vs No Viremia
Gene Name	Accession #	Fold Change		Fold Change
ATG16L1	NM_001190272.1	4.32		6.96
ATG5	NM_001037152.1	6.77		9.45
CASP1	NM_214162.1	4.59		15.67
CASP3	NM_214131.1	4.76		4.50
CCL11	NM_001256774.1	6.77		6.36
CCL2	NM_214214.1	5.66		40.22
CCL22	NM_001256776.2	6.92		9.99
CCR1	NM_001001621.1	5.10		8.46
CCR10	NM_001044563.1	5.06		11.39
CCR2	NM_001001619.1	5.06		9.32
CCR5	NM_001001618.1	5.66		15.89
CCR8	XM_003358377.3	5.94		11.00
CD163	NM_213976.1	8.88		9.65
CD40LG	NM_214126.1	7.73		7.67
CD80	NM_214087.1	7.62		11.47
CTLA4	NM_214149.1	6.82		9.71
CTSS	XM_005663494.2	11.08		14.22
CX3CL1	XM_013988522.1	5.46		8.94
CX3CR1	XM_003358374.3	4.79		10.41
CXCL10	NM_001008691.1	5.74		9.99
CXCL12	NM_001009580.1	4.35		23.26
CXCL13	XM_003129101.2	4.89		52.71
CXCL2	NM_001001861.2	6.45		9.92
CXCL9	NM_001114289.2	8.22		78.25
CXCR1	XM_003133655.4	7.57		6.82
CXCR2	XM_005672195.2	6.87		9.71

CYBB	NM_214043.2	4.72		12.55
FCER1G	NM_001001265.1	4.29		16.80
FCGR2B	NM_001033013.2	8.57		21.71
FCGR3B	NM_214391.1	5.58		22.32
ICOS	NM_001044546.1	5.94		6.02
IFITM1	XM_003124230.2	6.77		10.06
IFNA1	NM_214393.1	15.45		8.17
IFNB1	NM_001003923.1	6.87		6.87
IFNG	NM_213948.1	4.11		15.67
IFNL1	NM_001142837.1	10.78		8.06
IFNLR1	XM_013999058.1	6.92		8.63
IKBKG	NM_001113053.1	8.28		8.69
IL10	NM_214041.1	5.28		24.93
IL18	NM_213997.1	5.82		13.55
IL1B	NM_214055.1	7.52		9.99
IL2	NM_213861.1	11.08		8.22
IL4	NM_214123.1	9.19		9.65
IL5	NM_214205.1	5.06		8.75
IL6	NM_214399.1	4.06		14.12
IL8	NM_213867.1	5.06		6.45
KIR2DL1	NM_001113218.1	5.62		9.45
KLRK1	NM_213813.2	7.89		18.00
LY96	NM_001104956.1	7.67		6.82
NOD1	NM_001114277.1	7.46		9.85
NOD2	NM_001105295.1	6.68		14.42
SLA-DRA	NM_001113706.1	4.35		15.67
TBK1	NM_001105292.1	4.66		7.46
TLR1	NM_001031775.1	6.06		12.82
TLR2	NM_213761.1	7.46		15.78
TLR3	NM_001097444.1	8.94		14.42

TLR4	NM_001113039.2	9.25		15.89
TLR8	NM_214187.1	7.89		12.30
TNFSF10	NM_001024696.1	5.39		11.47

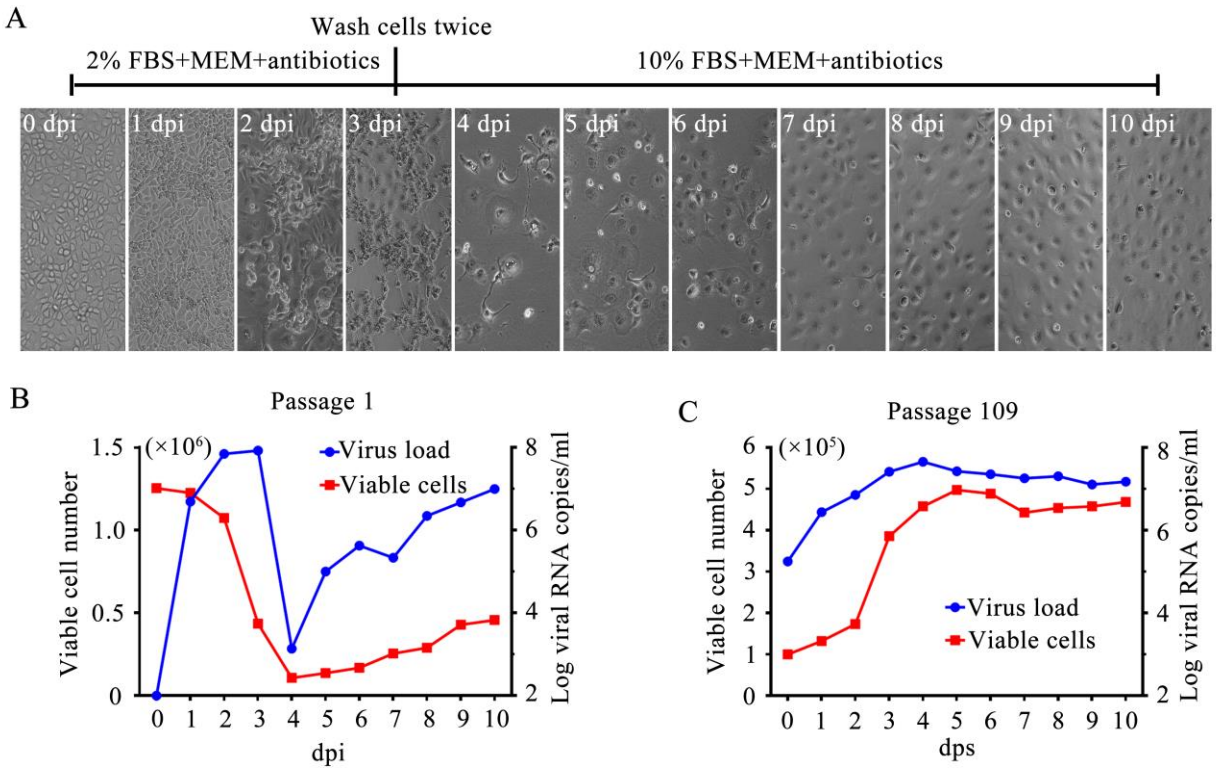

Figure 4.1 Establishment and characterization of the *in vitro* cell model system for PRRSV persistence. (A) MARC-145 cells in T-25 flasks (n=10) were infected with 1 moi of PRRSV isolate SD95-21. At 72 hpi, dead cells were washed off by cell culture medium and fresh cell growth medium was added to maintain the cells that survived from acute infection. One flask of cells and medium was harvested each day to determine cell numbers as well as viral growth rates for 10 days. The remaining cells of the tenth flask were sub-cultured up to 109 passages. Cell morphology was observed daily under a light microscope. (B) Viable cellnumber and viral load in cell culture supernatant during the initial 10 days of establishing PRRSV persistent cells. Cells from each flask were trypsinized, stained with 10% Trypan Blue (Sigma) and then counted with a hemocytometer. Viral load in the medium were quantified by qRT-PCR. (C) Viable cell count and viral load in the cell culture supernatant of MARC/PRRSV-P109 cells were measured using the same methods in (B).

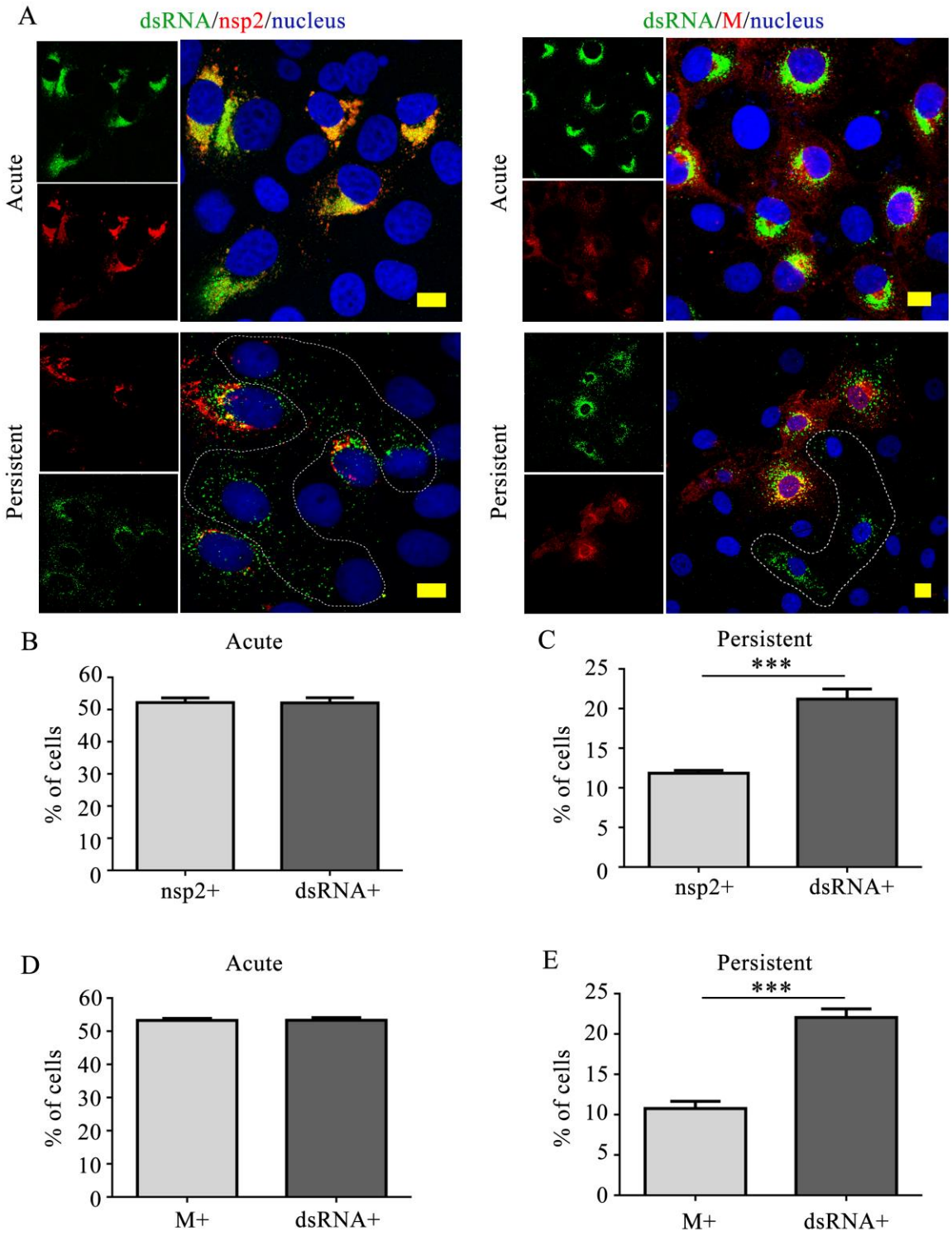
A
dsRNA/nsp2/nucleus
dsRNA/M/nucleus
Acute
Persistent
Acute
Persistent
B
Acute
% of cells
60
50
40
30
20
10
0
nsp2+
dsRNA+
C
Persistent
***
% of cells
25
20
15
10
5
0
nsp2+
dsRNA+
D
Acute
% of cells
60
50
40
30
20
10
0
M+
dsRNA+
E
Persistent
***
% of cells
25
20
15
10
5
0
M+
dsRNA+

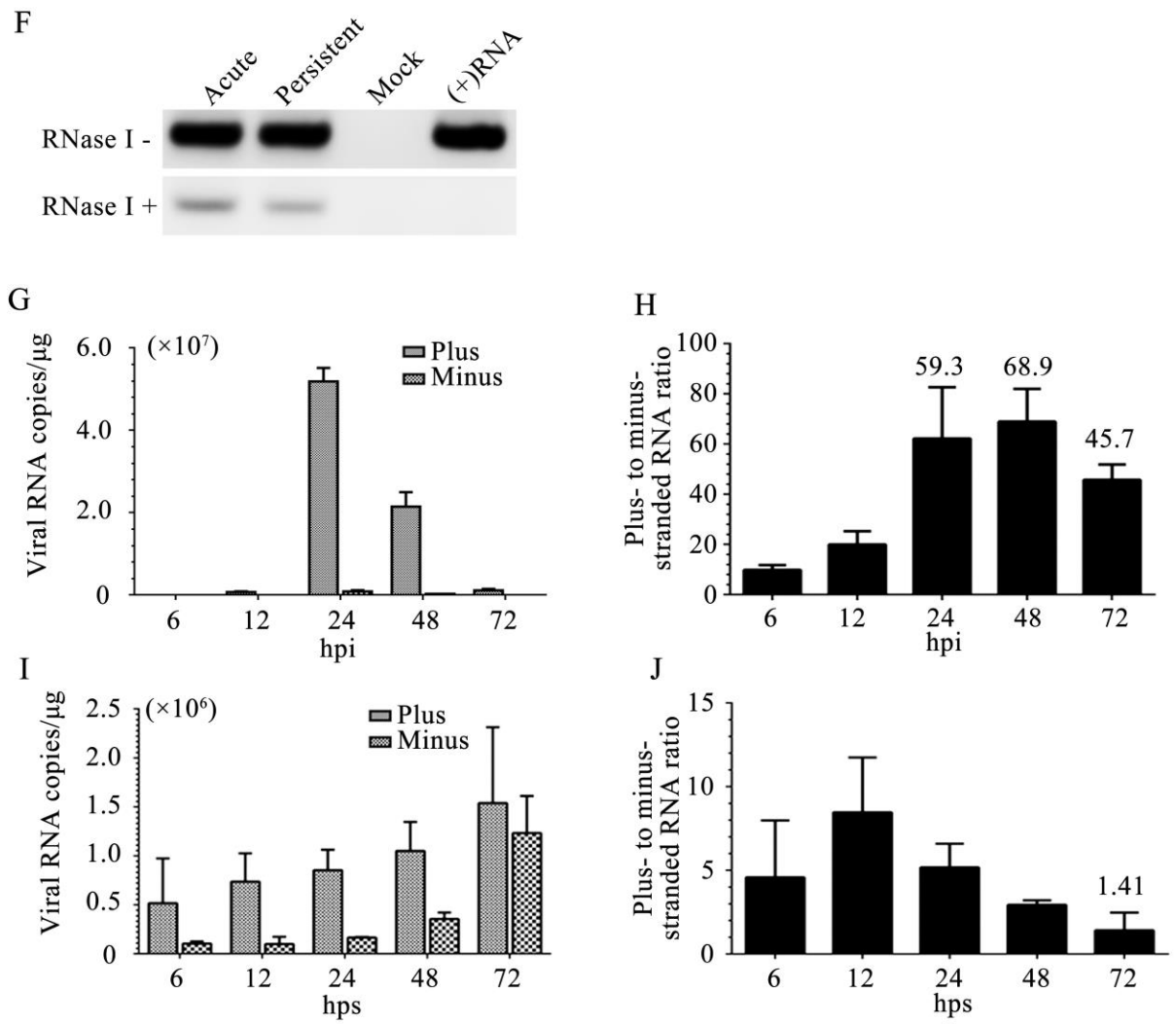

Figure 4.2 PRRSV persistent cells with increased population containing only viral dsRNA.

((A) MARC-145 cells at different infection stages (acute versus persistent) were fixed and stained for PRRSV dsRNA (green) and nsp2 (red) or M protein (red). Pictures were taken under confocal microscope (LSM880, Zeiss). Scale bar, 10 μm. (B and C) Percentages of cells positive with PRRSV nsp2 or dsRNA only determined by counting a total of 2000 cells under the fluorescence microscope. (D and E) Percentages of cells positive with PRRSV M or dsRNA only determined by counting a total of 2000 cells under the fluorescence microscope. (F) Detection of the presence of dsRNA in the acutely and persistently infected cells by RNase I treatment and

one-step RT-PCR. A synthesized single-stranded RNA (+RNA) was used to confirm the RNAase I digestion efficiency. (G and I) Quantification of PRRSV RNA levels in cell at acute (G) and persistent (I) infection stage. Viral RNA was isolated at the indicated time points and subjected for strand specific qRT-PCR. (H and J) Quantification of plus- to minus-strand viral RNA ratio in cells at acute (H) and persistent (J) infection stage.

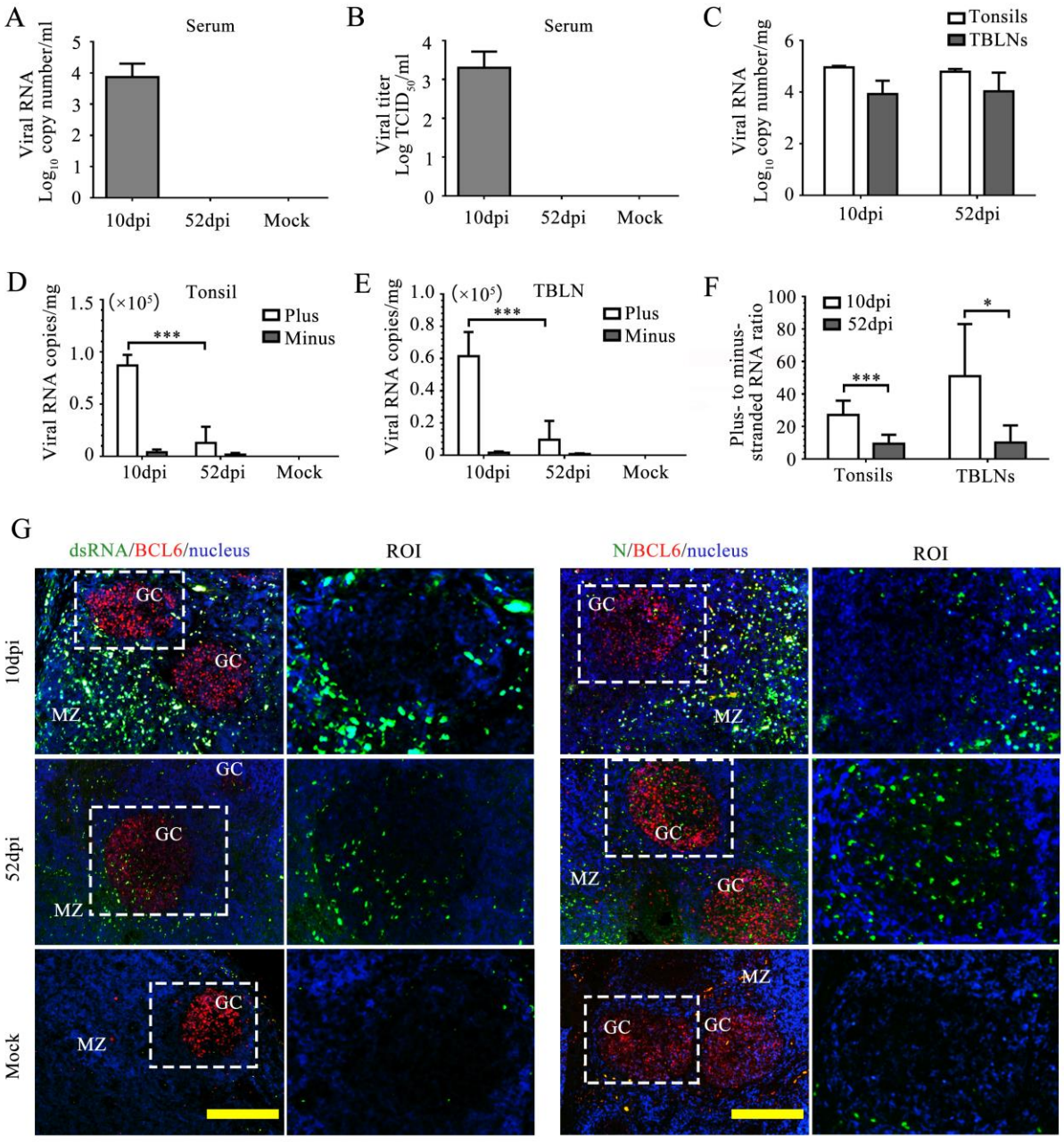
A
Serum
Viral RNA Log10 copy number/ml
10dpi
52dpi
Mock
B
Serum
Viral titer Log TCID50/ml
C
Tonsils
TBLNs
Viral RNA Log10 copy number/mg
D
Tonsil
(×10⁵)
Plus
Minus
Viral RNA copies/mg
***
E
TBLN
F
10dpi
52dpi
Plus- to minus-stranded RNA ratio
*
Tonsils
TBLNs
G
dsRNA/BCL6/nucleus
ROI
N/BCL6/nucleus
GC
MZ

Figure 4.3 Detection of viral dsRNA in serum and lymphoid tissues from PRRSV-infected pigs. (A and B) Quantification of viral RNA in serum samples from pigs at 10dpi,52dpi or mock infected pigs (A).(B)Virus titration of serum samples from10dpi, 52dpi, or mock infected pigs using TCID50 method. (C) Quantification of viral RNA in tonsils and TBLNs of 10dpi or 52dpi pigs. (D) Quantification of plus and minus stranded viral RNA in tonsils of 10dpi, 52dpi or mock infected pigs. (E) Quantification of plus and minus stranded viral RNA in TBLNs of 10dpi or 52dpi pigs. (F) Plus- to minus-strand viral RNA ratio in tonsils or TBLNs of 10 and 52dpi pigs. (G) Immunohistochemistry of TBLN samples. Tissue sections were stained for PRRSV dsRNA or N (green). Bcl6 was used as a marker in germinal center (Red). Nucleus was counterstained by DAPI (blue). Pictures were taken under fluorescent microscope (EVOS FL). Scale bar, 200 μm. Inset in the boxed area of each image showed a zoomed region of interest, in which is shown in column 2 and 4 (region of interest; ROI).TBLN, tracheobronchial lymph node; GC, germinal center; MZ, marginal zone.

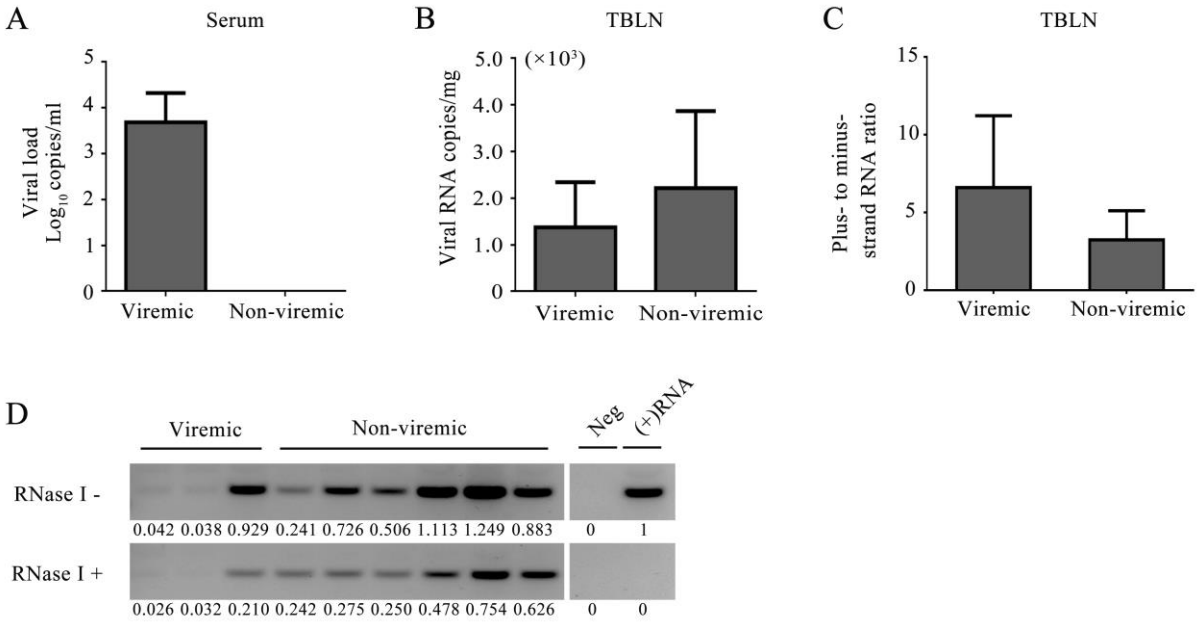

Figure 4.4 Analysis of viral load in serum and TBLN samples from PRRSV-infected pigs at 70 dpi. (A) Viral load in serum collected at 70dpi. Pigs with detectable virus titer at 70 dpi is grouped into viremic group (n = 6); Pigs with no detectable virus titer at 70 dpi is grouped into non-viremic group (n = 3). (B) Viral load in 70dpi TBLNs. (C) Plus- to minus-strand viral RNA ratio in TBLN samples from groups of pigs at 70dpi. (D) Detection of the presence of dsRNA in the TBLN by RNase I treatment and one-step RT-PCR. A synthesized single-stranded RNA (+RNA) was used to confirm the RNase I digestion efficiency.

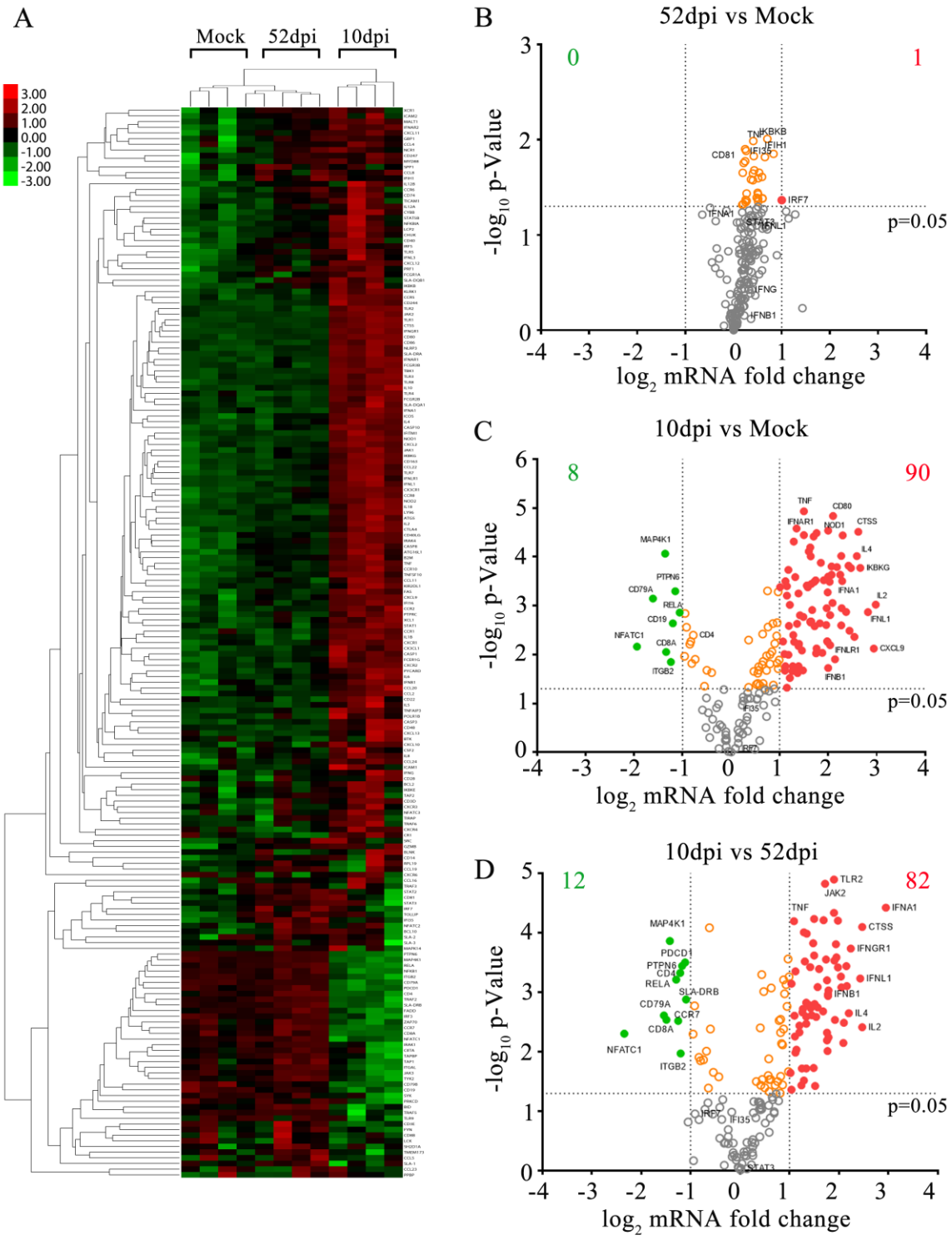
A
Mock
52dpi
10dpi
3.00
2.00
1.00
0.00
-1.00
-2.00
-3.00
B
52dpi vs Mock
0
1
p=0.05
-log10 p-Value
log2 mRNA fold change
TNF
IKBKB
IFIH1
IFI35
CD81
IRF7
IFNA1
STAT3
IFNL1
IFNG
IFNB1
C
10dpi vs Mock
8
90
p=0.05
-log10 p-Value
log2 mRNA fold change
TNF
CD80
IFNAR1
MOD1
CTSS
MAP4K1
IL4
IKBKG
PTPN6
CD79A
IFNA1
IL2
RELA
CD19
IFNL1
NFATC1
CD4
CD8A
IFNLR1
CXCL9
ITGB2
IFNB1
IFI35
IRF7
D
10dpi vs 52dpi
12
82
p=0.05
-log10 p-Value
log2 mRNA fold change
TLR2
JAK2
TNF
IFNA1
MAP4K1
CTSS
PDCD1
IFNGR1
PTPN6
CD4
IFNL1
RELA
SLA-DRB
IFNB1
CD79A
CCR7
IL4
CD8A
IL2
NFATC1
ITGB2
IRF7
IFI35
STAT3

Figure 4.5 RNA array analysis of swine immune gene expression in TBLN samples from PRRSV-infected pigs at 10 dpi versus 52 dpi. (A) Unsupervised hierarchical clustering and heat map analysis of the RNA array data set from TBLN samples: horizontal columns represent individual genes (log2 count of 192 gene codeset), vertical columns stand for individual pig samples Red signals: upregulated genes; Green signals: downregulated genes. (B-D) Volcano plot built for comparing gene expression levels in TBLNs from different groups of pigs. The X axis of the plots was expressed as the log2 fold changes of gene expression. The Y axis of the plots was expressed as the –log10 p-values. (B) Comparison between groups of PRRSV-infected pigs at 10 dpi and mock-infected pigs. (C) Comparison between groups of PRRSV-infected pigs at 52 dpi and mock-infected pigs. (D) Comparison between groups of PRRSV-infected pigs at 10 dpi and 52 dpi. Genes that had a fold change (FC) $\geqslant$2 and p-value <0.05 were identified as differentiated expressed genes (DEGs). The up-regulated DEGs were shown as red circles; the red numbers indicate the number of upregulated DEGs. The down regulated DEGs were shown as green circles; the green numbers indicate the number of upregulated DEGs.

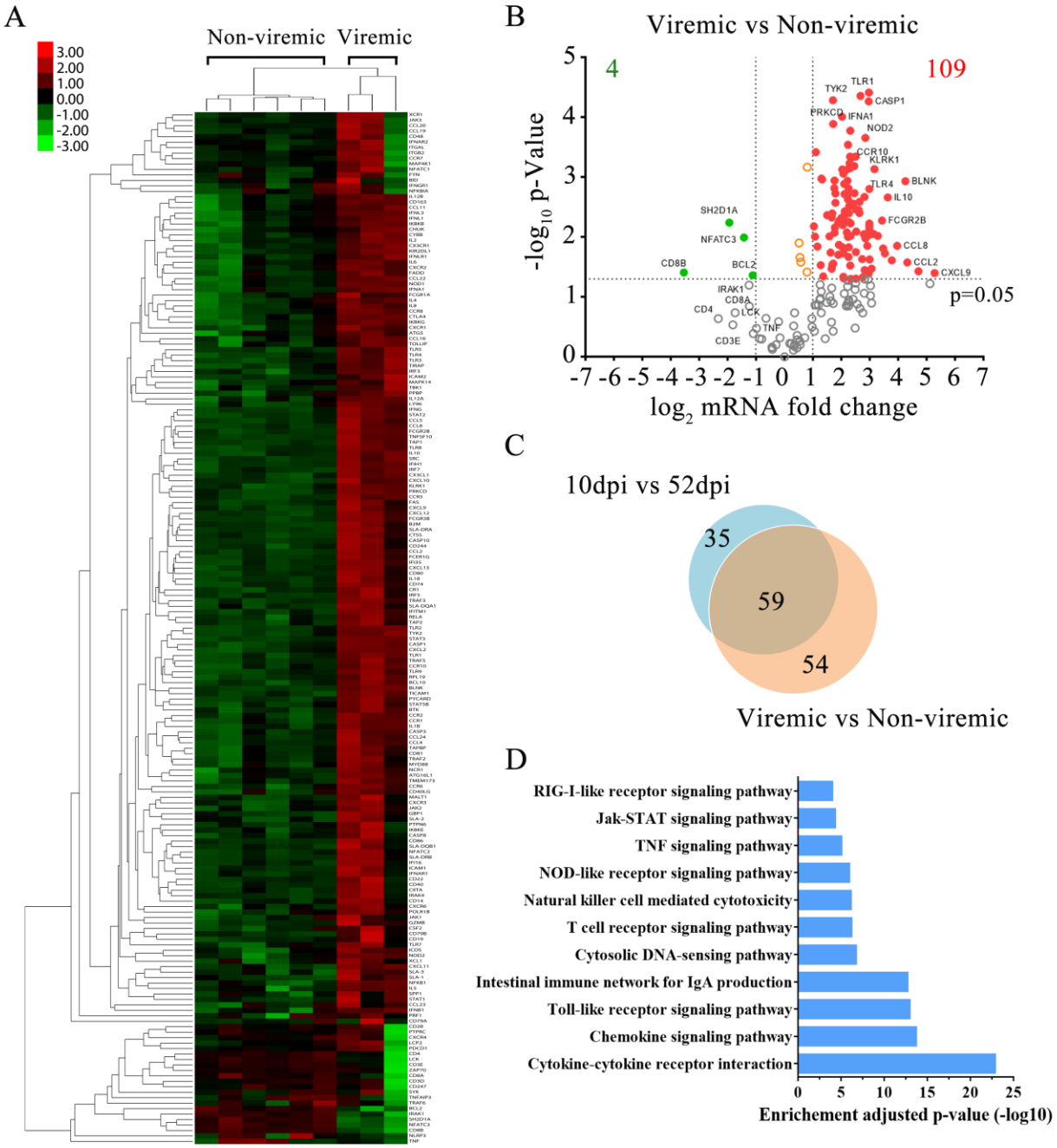
A
Non-viremic
Viremic
3.00
2.00
1.00
0.00
-1.00
-2.00
-3.00
B
Viremic vs Non-viremic
4
109
-log10 p-Value
log2 mRNA fold change
p=0.05
TLR1
TYK2
CASP1
PRKCD
IFNA1
NOD2
CCR10
KLRK1
TLR4
BLNK
IL10
FCGR2B
CCL8
CCL2
CXCL9
SH2D1A
NFATC3
CD8B
BCL2
IRAK1
CD8A
CD4
LCK
TNF
CD3E
C
10dpi vs 52dpi
35
59
54
Viremic vs Non-viremic
D
RIG-I-like receptor signaling pathway
Jak-STAT signaling pathway
TNF signaling pathway
NOD-like receptor signaling pathway
Natural killer cell mediated cytotoxicity
T cell receptor signaling pathway
Cytosolic DNA-sensing pathway
Intestinal immune network for IgA production
Toll-like receptor signaling pathway
Chemokine signaling pathway
Cytokine-cytokine receptor interaction
Enrichement adjusted p-value (-log10)

Figure 4.6 Comparison of immune gene expression profiles in TBLN samples from different treatment groups of pigs. (A) Unsupervised hierarchical clustering and heat map analysis of the entire RNA array data set of TBLN samples from pigs at 70 dpi; horizontal columns represent individual genes (log2 count of 192 gene codeset), vertical columns stand for individual pig samples. Red signals: upregulated genes; Green signals: downregulated genes. (B) Volcano plot built for comparing gene expression levels in TBLN samples from viremic group of pigs versus non-viremic group of pigs at 70dpi. The X axis of the plots was expressed as the log2 gene expression fold changes. The Y axis of the plots was expressed as the –log10 p-values. The up-regulated DEGs were shown as red circles; the red numbers indicate the number of upregulated DEGs. The down regulated DEGs were shown as green circles; the green numbers indicate the number of upregulated DEGs. (C) Venn diagram built for comparing the common and unique upregulated DEGs from pigs at 10 dpi versus 52 dpi to the DEGs from viremic versus non-viremic pigs. (D) Enriched functional categories of the 59 overlapped DEGs shown in panel C. KEGG Pathway Enrichment analysis was performed using DAVID program. P-values adjusted by Benjamini-Hochberg correction, in which less than 0.05 were defined as significant enrichment. The x-axis is the -log10 of p-value.

Chapter 5 - Conclusion

PRRSV is known to be one of the most economically important pathogens in the swine industry worldwide. In this dissertation, we investigated two novel mechanisms associated with PRRSV intercellular transmission and persistence. Understanding the pathogenic mechanisms of PRRSV will be helpful on the development of effective control programs.

In the chapter 2 and 3, we demonstrated that PRRSV could utilize intercellular tunneling nanotubes (TNTs) as an alternative pathway for cell to cell transmission. PRRSV infectious materials including viral proteins and RNAs could be transported from the cell to cell through the TNTs. Using co-culture system, we further confirmed that PRRSV can spread infection intercellularly through the TNTs. Importantly, viruses could utilize TNTs to escape the host immune response, especially the neutralizing antibodies. We further demonstrated that PRRSV infection can induce increased number of TNTs formation in a ROS dependent manner and mitochondria transferring through this TNT pathway could rescue cell death during the early stage of viral infection. In fact, previous studies presumed that PRRSV may evolve certain strategies to attenuate apoptosis to complete sufficient viral replication during the early infection. TNT-mediated mitochondria transferring could be one of the mechanisms for PRRSV to attenuate cell death at the early infection stage. Moreover, this TNT pathway was determined to be hijacked by PRRSV for their intercellular transmission; PRRSV proteins were observed transporting in the opposite directions of the mitochondria movement and also, mitochondria were observed to act as cargos to transport some of the PPRSV proteins. Based on these findings, we therefore proposed a model for TNT associated intercellular transmission of PRRSV (**Fig. 5.1**). Like most of the viruses, PRRSV can be transmitted by cell free dissemination through the receptor-dependent primary entry pathway. Additionally, PRRSV infection can be transmitted

through a receptor-independent transmission pathway mediated by intercellular tunneling nanotubes. The initial PRRSV infection in the local cells can trigger the increased level of reactive oxygen species (ROS) and distribution of "call for help signals" including S100A4 in the surrounding space. These signals were further received by the neighboring uninfected cells and mediated the nanotubes formation. During the early stage of infections, nanotubes predominantly connected between uninfected cells and infected cells. Mitochondria transferring from the uninfected cells through these nanotubes could attenuate virus induced cell death of the infected cells, which is beneficial for PRRSV to complete sufficient replication. However, at the same time, PRRSV could utilize this intercellular transferring pathway to spread its infectious core materials including viral proteins and RNA to the neighboring uninfected cells. At the late infection stage, all the cells were infected and eventually killed by exaggerated infections. More questions were also raised in this study which will be future research directions, including: are there other cellular components which can be transported through PRRSV-induced nanotubes? How to differentiate experimentally between intercellular transfer and communication phenomena based on TNTs and those mediated by gap junctions or extracellular vesicles, such as exosomes? How to prove functional TNTs existed in contiguous tissue or inside the body?

In the chapter 4, we investigated the molecular mechanism underlying PRRSV persistence. The capability to establish persistence is one of the hallmark features of PRRSV infection. To study the mechanisms of PRRSV persistence, we established an *in vitro* model of PRRSV persistently infected MARC-145 cells. Using this *in vitro* model system, we identified that viral dsRNA could act as mediator for PRRSV persistence. Consistent with the data obtained from the *in vitro* cell culture system, PRRSV dsRNA was also detected persisting in pig lymphoid tissues for a longterm after the initial infections. Importantly, viral dsRNAs were

observed aggregating inside the germinal centers of tonsils and lymph nodes from PRRSV persistence pigs. By contrast, most of the dsRNA+ cells were detected in marginal and interfollicular zones of lymphoid tissues in acute PRRSV-infected pigs. Further RNA array data showed that dsRNA in lymphoid tissues of persistently infected pigs had limited ability to stimulate host antiviral responses. We demonstrated that PRRSV dsRNA functions as a mediator for viral persistence. The viral dsRNA persistence in germinal centers of lymphoid tissues may reveal a novel mechanism for PRRSV to escape antiviral immune responses. However, a number of questions also need to be answered, including: how the cells maintain PRRSV dsRNAs? What are the exact subsets of dsRNA+ cells in the germinal centers? How those dsRNA+ cells evade from host immune surveillance? What is the link between virus reactivation and dsRNA persistence *in vivo*? Answering these questions in the future will help us better understand the PRRSV persistence and improve PRRSV controlling system.

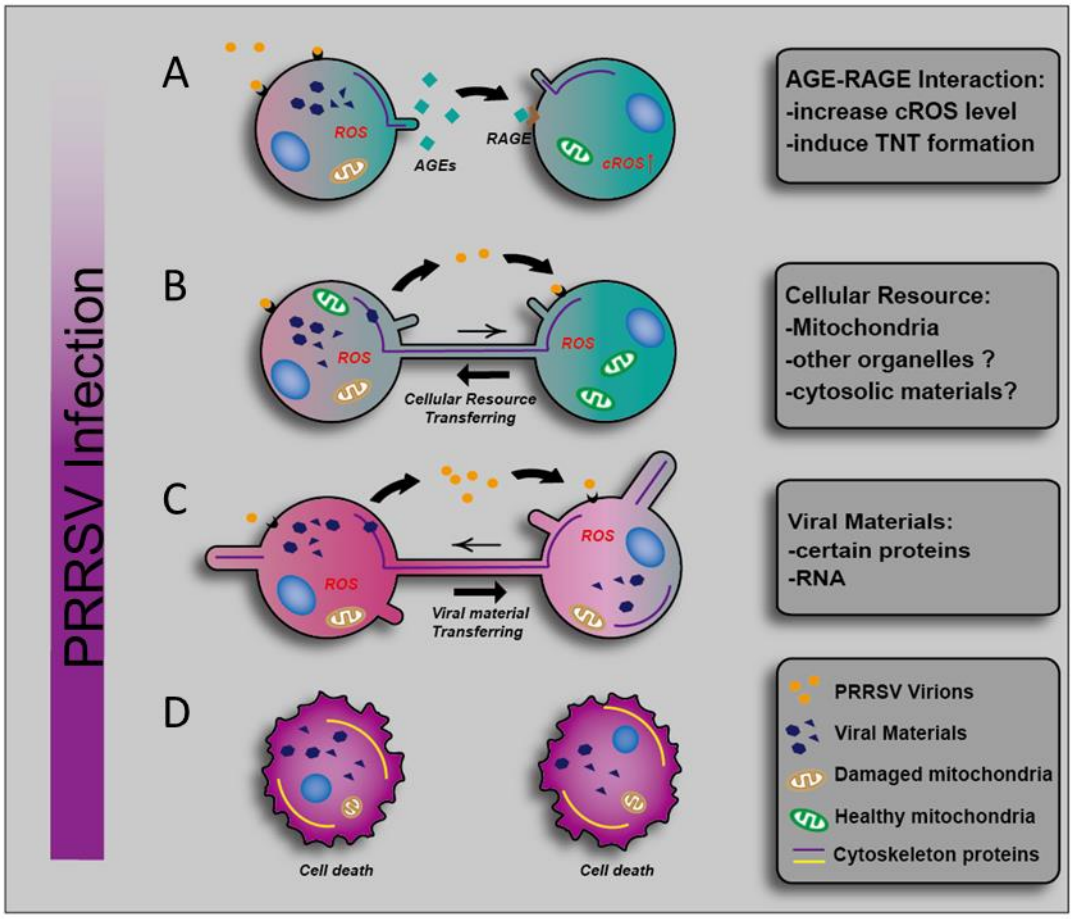

Figure 5.1 A proposed model for PRRSV intercellular spread. (A) A PRRSV-infected cell neighboring an uninfected cell in the beginning stages of establishing an intercellular connection. (B) The cellular extension connects and fuses to the plasma membrane of the uninfected cell, allowing exchange of cellular components including mitochondria. (C) Viral infectious materials (eg. viral RNAs and RTC components) spread through TNTs. (D) Cells eventually die from exaggerated PRRSV infection.

Publisher's Permission for Reproducing Published Materials

Chapter 1 related:

http://jvi.asm.org/content/90/10/5163.full.pdf+html

Journal of Virology-Permissions Request

Authors in ASM journals retain the right to republish discrete portions of his/her article in any other publication (including print, CD-ROM, and other electronic formats) of which he or she is author or editor, provided that proper credit is given to the original ASM publication. ASM authors also retain the right to reuse the full article in his/her dissertation or thesis. For a full list of author rights, please see: http://journals.asm.org/site/misc/ASM_Author_Statement.xhtml

Chapter 2 related:

https://www.sciencedirect.com/science/article/pii/S0042682217304233?via%3Dihub

Virology- Permissions Request

Please note that, as the author of this Elsevier article, you retain the right to include it in a thesis or dissertation, provided it is not published commercially. Permission is not required, but please ensure that you reference the journal as the original source. For more information on this and on your other retained rights, please visit: https://www.elsevier.com/about/our-business/policies/copyright#Author-rights